AD-A058 086 MINNESOTA UNIV MINNEAPOLIS DEPT OF AEROSPACE ENGINE--ETC F/G 20/11
STRUCTURAL INELASTICITY XXI. FINITE ELEMENT MODELS WITH VELOCIT--ETC(U)
MAY 78 H M RIJ, P G HODGE N00014-75-C-0177
UNCLASSIFIED AEM-H1-21 NL

1 OF 2
ADA
058086




Report AEM-H1-21

LEVEL II

12

STRUCTURAL INELASTICITY XXI

Finite Element Models with Velocity Discontinuities

Hendrik M. van Rij, Research Assistant

and

Philip G. Hodge Jr., Professor of Mechanics

Department of Aerospace Engineering and Mechanics
University of Minnesota
Minneapolis, Minnesota 55455

May 1978

Technical Report

Prepared for

OFFICE OF NAVAL RESEARCH
Arlington, VA 22217

OFFICE OF NAVAL RESEARCH
Chicago Branch Office
536 South Clark St.
Chicago, IL 60605

DISCLAIMER NOTICE

THIS DOCUMENT IS BEST QUALITY PRACTICABLE. THE COPY FURNISHED TO DDC CONTAINED A SIGNIFICANT NUMBER OF PAGES WHICH DO NOT REPRODUCE LEGIBLY.

SECURITY CLASSIFICATION OF THIS PAGE (When Data Entered)

REPORT DOCUMENTATION PAGE	READ INSTRUCTIONS BEFORE COMPLETING FORM
1. REPORT NUMBER (14) AEM-H1-21	2. GOVT ACCESSION NO. / 3. RECIPIENT'S CATALOG NUMBER
4. TITLE (and Subtitle) (6) STRUCTURAL INELASTICITY XXI. Finite Element Models with Velocity Discontinuities.	5. TYPE OF REPORT & PERIOD COVERED (9) Technical Report, / 6. PERFORMING ORG. REPORT NUMBER
7. AUTHOR(s) (10) Hendrik M. van Rij, ~~Research Assistant~~ / Philip G. Hodge, Jr. ~~Prof. of Mechanics~~	8. CONTRACT OR GRANT NUMBER(s) (15) N00014-~~NR~~-75-C-0177
9. PERFORMING ORGANIZATION NAME AND ADDRESS: University of Minnesota, Minneapolis, Minnesota 55455	10. PROGRAM ELEMENT, PROJECT, TASK AREA & WORK UNIT NUMBERS: NR 064-429
11. CONTROLLING OFFICE NAME AND ADDRESS: OFFICE OF NAVAL RESEARCH, Chicago Branch Office, 536 South Clark St. - Chicago, IL 60605	12. REPORT DATE: ~~July 1978~~ May 78 / 13. NUMBER OF PAGES: (12) 109p. ~~215~~
14. MONITORING AGENCY NAME & ADDRESS (if different from Controlling Office)	15. SECURITY CLASS. (of this report): Unclassified / 15a. DECLASSIFICATION/DOWNGRADING SCHEDULE

16. DISTRIBUTION STATEMENT (of this Report)

~~Qualified requesters may obtain copies of this report from DDC.~~

DISTRIBUTION STATEMENT A
Approved for public release;
Distribution Unlimited

17. DISTRIBUTION STATEMENT (of the abstract entered in Block 20, if different from Report)

18. SUPPLEMENTARY NOTES

19. KEY WORDS (Continue on reverse side if necessary and identify by block number)

Plasticity, perfectly-plastic, finite-elements, plane strain, Prandtl punch, slip, velocity discontinuities, notched bar.

20. ABSTRACT (Continue on reverse side if necessary and identify by block number)

Conventional finite-element models are based on displacement or velocity fields which are at least continuous. However, it is known that perfectly plastic materials may involve discontinuities of the tangential velocity component along certain lines. In this investigation, two two-dimensional finite element models are proposed which will allow for such discontinuities.

A regular pattern of triangular elements is assumed. In the first model, the elements are assumed to be rigid, and in the second model, we have a linear

DD FORM 1 JAN 73 1473 EDITION OF 1 NOV 65 IS OBSOLETE S/N 0102-014-6601 | (COVER)

405395 78 07 12 065

SECURITY CLASSIFICATION OF THIS PAGE (When Data Entered)

displacement field in each element. Across the line separating any two adjoining elements the normal displacement component is continuous, but a discontinuity may exist in the tangential component. The defining equations - compatibility, equilibrium, and constitutive - are developed with the aid of the Principle of Virtual Work.

Prandtl's punch problem and tension in notched bars are solved under plane strain conditions. Comparison is made with existing analytical and other numerical solutions, in order to evaluate the merits of allowing for discontinuities.

Chapter I Introduction

The basic concept of the finite element method is that a given structure or continuum is modeled by a finite assemblage of individual components or elements. Within each element and in the reactions between the elements simplifying assumptions are made in the static, kinematic, or constitutive equations.

Two of the first such methods were the "framework-method" of Hrennikoff [1]* and the "lattice analogy" of McHenry [2]. Their plane stress system was represented by an assemblage of one dimensional elements along the edges of triangles as in Fig. 1.

In a pioneering paper in 1956, Turner, Clough, Martin and Topp [3] proposed a finite element model for two dimensional problems which we shall refer to as the classical model. The elements are triangles and the model has the following properties: the displacement field is linear in each triangle and continuous over the whole domain; the strain and stress fields are constant in each triangle; if the given body and surface forcefield is approximated by concentrated forces acting only at the nodes, then these forces must be in equilibrium at each node.

*Numbers in square brackets refer to items listed in the bibliography.

A general approach to any finite element model for an elastic material is to assume a particular form for the displacement field. The unknowns are then determined by constitutive equations (Hooke's law) and the Principle of Minimum Potential Energy. Alternatively, an equilibrium stress field can be assumed. The constitutive equations and the Principle of Minimum Complementary Energy will determine the unknowns. More general fields, which include both static and kinematic parameters, can be used in conjunction with a variational principle of Reissner [4], which permits a simultaneous variation of both displacement and stress. These variational approaches all lead to the set of equations proposed by Turner et al [3] applied to the classical model.

All previously mentioned methods are based on elastic constitutive relations, but similar approaches can be used for inelastic materials. In this case all defining equations must be rederived, using the appropriate minimum or variational principle, for each specific material. A more general method, applicable to any material, is to use the Principle of Virtual Work [5]. Starting with an assumed form for the kinematic variables, we can use this principle to derive generalized variables, equilibrium equations, and constitutive relations.

Hodge [6] showed that when this method is applied to the constant-strain triangle model for two-dimensional

problems with piecewise constant loading, the resulting equations agree with those first obtained by Turner et al [3], thus demonstrating that these equations are applicable to any material and loading.

Since the classical model and other models to be considered here are all based on a field which is kinematically admissible for the original continuum, the results will satisfy any kinematic minimum principle for the material involved. For example, for an elastic material the total potential energy of a model solution will be an upper bound on the total potential energy of the continuum. Further, as might be expected, if the number of elements is increased in a suitable systematic fashion, the upper bound will decrease and, in all known cases, will approach the true potential energy for the continuum.

Similarly, for an elastic/perfectly-plastic material the model yield-point will be an upper bound on that of the continuum [7]. However, as first pointed out by Nagtegaal, Parks, and Rice [8] under plane strain conditions this upper bound is often infinite regardless of how many elements are used. This phenomenon, also called locking up of degrees of freedom, can be explained as follows. At any load, the finite element solution must satisfy the incremental virtual work principle

$$\int_S \dot{T}_i \, \dot{u}_i \, dS = \sum_{elem} \int_{V_{elem}} \dot{\sigma}_{ij} \, \dot{\epsilon}_{ij} \, dV \qquad (1\text{-}1)$$

precisely, where $\dot{\sigma}_{ij}$ is the stress rate following from the prescribed constitutive law in terms of the current stress σ_{ij} and strain rate $\dot{\epsilon}_{ij}$ within each element. Separating the right-hand side into a deviatoric and a dilatational part we observe that the deviatoric part will vanish pointwise in the vicinity of the limit load, but, as follows from plastic normality, will never be negative. Therefore Eq. (1-1) shows that

$$\int_S \dot{T}_i \, \dot{u}_i \, dS \geq \sum_{elem} \int_{V_{elem}} K(\dot{\epsilon}_{kk})^2 \, dV \qquad (1\text{-}2)$$

where K is the bulk modulus. As Nagtegaal et al concluded: "In order for a limit load to exist for the discretized finite element model of an elastic/plastic problem, it is necessary that the elements be capable of deforming so that $\dot{\epsilon}_{kk} = 0$ pointwise throughout the elements. Otherwise Eq. (1-2) requires that the load-deflection curve be steadily rising - i.e., no limit load exists."

The constraint $\dot{\epsilon}_{kk} = 0$ is not easily satisfied. Indeed, in a large field of 4N triangles, there will be approximately 2N nodes and two degrees of freedom per node so that there is an average of one degree of freedom per triangle. Therefore, one incompressibility constraint per triangle will leave essentially no degrees of freedom in the total domain, regardless of the number of elements.

Nagtegaal et al resolved this dilemma by requiring the triangles to be grouped in quadrilaterals such as the squares in Fig. 1. It is easily shown that if three of the four triangles in a quadrilateral undergo any incompressible deformation, the fourth will necessarily satisfy $\dot{\epsilon}_{kk} = 0$. Thus there are only 3N constraints, which leaves one degree of freedom for each four triangles.

The velocity field associated with the yield-point load of many continuum problems exhibits another phenomenon which is not well modelled by the classical finite element model, namely, discontinuity of certain tangential velocity components. For example, let us consider the identation of a semi-infinite domain by a rigid beam under conditions of plane strain. For the simple case of a rigid/perfectly plastic material, Prandtl [9,10] presented a yield-point incipient flow field (see Fig. 17) which involved part of the domain (the triangles) moving as rigid bodies, and part of it (the quarter circle) deforming with zero volume change. We observe that the deforming part of the material moves relative to the non-deforming part with a finite tangential velocity discontinuity across the boundary separating the regions.

Therefore, in view of the facts that any continuous finite element model has difficulty representing incompressible flow, and that tangential velocity discontinuities actually exist in continuum solutions, it

appears worthwhile to investigate a finite element model which will allow for such discontinuities.

In the next three chapters we present a <u>slip model</u> in which these discontinuites are the only permissible motion, i.e. we consider an array of triangular elements which are internally rigid, but can slip relative to each other. In Chap. II we derive the basic equations based on the Principle of Virtual work, and discuss the boundary conditions. In doing this, we visualize the edge between two triangles as a rectangle of small thickness and ignore second-order effects. Also, it is shown that we have one degree of freedom per node for this incompressible model. In Chap. III we discuss the Prandtl punch problem referred to above, where we assumed rough material contact between the punch and the material. The results are compared with known exact and numerical solutions as well as with solutions of a kinematically admissible approximation model and a statically admissible approximation model.

In Chap. IV we apply the model to several other examples: the Prandtl smooth punch, the deep double notched tensile bar, and the single edge notched tensile bar. In all cases a limit load is found.

In the second half of the thesis the classical model, i.e. constant strain triangles, and the slip-model are combined to obtain the <u>combined model</u>.

It is shown that the combined model separates into classical and slip parts with only very limited coupling between the two. The (reaction) forces on the boundary are the same for both parts, and the boundary displacements are obtained by super-position of the displacements of the two parts. In this combined model nonzero slip can only occur if a collection of yielding edge elements form a yielding mechanism. Therefore, during the elastic and early plastic stages, the combined model will have the same solution as the classical model. At the other extreme, in all examples considered, the limit load and the yielding mechanism will be the same as the slip model.

The general theory of the combined model is presented in Chap. V. Then, in Chap. VI we discuss in some detail the Prandtl rough punch whose slip model was presented in Chap. III. Chapter VII then gives combined model solutions for the problems discussed in Chap. IV.

Finally, in Chap. VIII we formulate some conclusions with regard to the value of the slip and combined models, and indicate some possible directions for future research in this area.

The thesis also includes three appendices. Appendix A extends the kinematics to an arbitrary arrangement of triangles, Appendix B gives details of the computer programs used, and Appendix C computes the yield point load for the classical model using the upper-bound theorem of limit analysis.

Chapter II Slip Model

A. Interior Domain

Although the theory can be developed for any regular or irregular arrangement of triangles, we shall consider only the case of a regular array of isosceles right triangles illustrated in Fig. 1. In this two-dimensional finite element model the triangles are considered as rigid bodies which can slip relative to each other but must not become separated. Therefore, the only "strains" in the model will be measured by the relative motion or slip between the two adjacent triangles.

Let d_{ik} be the slip along a generic edge ik joining nodes i and k. It is positive when, from the viewpoint of an observer at node i and facing edge ik, the triangle on the right moves towards the observer with respect to the triangle on the left. Evidently $d_{ik} = d_{ki}$. A dimensionless strain is then defined by

$$\omega_{ik} = d_{ik}\ \ell_{ik}/\ell_o^2 \qquad (2\text{-}1)$$

where ℓ_{ik} is the length of the edge and ℓ_o is a reference length for the domain.

If we ignore boundary effects, then in a large domain with N nodes, there will be 2N triangles and 3N edges, hence there will be 3N generalized strains. The requirement that triangles do not separate will introduce several compatibility constraints among these strains. In the first place, there can obviously be no relative rotation of triangles so that at most we need consider only two degrees of translational freedom per triangle, or a total of 4N for the field. However, since even a uniform separation is prohibited, there will be an additional constraint on each of the 3N edges, so that we are left with only N degrees of freedom, i.e. one degree of freedom per node. It follows that, if one elementary mechanism is associated with each node, all possible infinitesimal motions in a large field may be expressed as linear combinations of these mechanisms.

Figures 2 and 3 show respectively the elementary mechanisms associated with a generic "small" node, where four triangles intersect, and a generic "large" node with eight triangles. Evidently Fig. 3 may be obtained from Fig. 2 by a change of scale and a rotation so that the mechanisms are essentially the same.

Let ℓ be the length of the side of the square in Fig. 2 and d the displacement of the triangle AOD along

side AD. We define the generalized displacement θ_O at a small node by

$$\theta_O = d\ell/\ell_o^2 \tag{2-2a}$$

In view of (2-1), the strains along the horizontal and vertical edges are

$$\omega_{AD} = \omega_{DB} = \omega_{BC} = \omega_{CA} = \theta_O \tag{2-2b}$$

The displacements across diagonal edges AO and OB must be equal, so that we can refer to AB as a single diagonal edge with strain ω_{AB}, and similarly for edge CD. In view of the definition (2-1), these strains are

$$\omega_{AB} = \omega_{CD} = -2d\ell/\ell_o^2 = -2\theta_O \tag{2-2c}$$

The generalized displacement at the large node mechanism in Fig. 3 is defined by

$$\theta_B = -d\ell/\ell_o^2 \tag{2-3a}$$

where d is the relative displacement across AB. Evidently

$$\omega_{AE} = \omega_{EF} = \omega_{FG} = \omega_{GA} = \theta_B \tag{2-3b}$$

$$\omega_{AB} = \omega_{EB} = \omega_{FB} = \omega_{BG} = -\theta_B \tag{2-3c}$$

We note that each of the edges in Fig. 3 may also be

involved with different small node mechanisms, so that none of the resultant strains are necessarily equal.

The total strain in any edge will be the resultant of several mechanisms. For example, along a horizontal edge such as AB in Fig. 3, strain will occur under the large node mechanisms centered at A and B and the small node mechanisms at C and D. Therefore, the total strain in AB may be written:

$$\omega_{AB} = \theta_C + \theta_D - \theta_A - \theta_B \qquad (2\text{-}4a)$$

with a similar result for a vertical edge. The strain in a diagonal edge such as AB of Fig. 2 is caused by mechanisms at C, O and D, hence

$$\omega_{AB} = -2\theta_O + \theta_C + \theta_D \qquad (2\text{-}4b)$$

To find the virtual internal work [5] of an edge we expand the edge to a narrow rectangle as shown in Fig. 4. The basic assumption is made that the height $\ell_o\delta$ of the rectangle is the same for all expanded edges. Let v' be the common normal displacement of the two triangles separated by edge PQ, u' the tangential displacement of the triangle below PQ in Fig. 4, and $u'' = u' + d_{PQ}$ the tangential dis-

placement of the triangle above PQ. Then

$$u = (u'+u'')/2 + y\, d_{PQ}/\ell_o\delta;\ v = v' \qquad (2\text{-}5)$$

is a continuous displacement field in the rectangle. In view of (2-1), the only non-zero strain is the constant

$$\gamma_{xy} = \omega_{PQ}\, \ell_o/\ell_{PQ}\delta \qquad (2\text{-}6)$$

The dimensionless virtual work done in the edge is

$$W_{int} = W_{int}/k\ell_o^2 = \lim_{\delta\to o} (1/k\,\ell_o^2)\int q\cdot\xi\, dA$$
$$= \tau_{PQ}\,\omega_{PQ} \qquad (2\text{-}7)$$

where k is the yield stress in shear, and

$$\tau_{PQ} = \lim_{\delta\to o} \left[\int (\sigma_{xy}/k)\, dA\right]/\ell_o\ell_{PQ}\delta \qquad (2\text{-}8a)$$

is the averaged dimensionless stress. For any reasonable constitutive behavior a constant strain will imply a constant stress so that (2-8a) may be replaced by

$$\tau_{PQ} = \sigma_{xy}/k \qquad (2\text{-}8b)$$

In view of (2-7), τ_{PQ} and ω_{PQ} satisfy Prager's

criterion [11] for generalized stress and strain respectively.

It follows from Eqs. (2-2) and (2-7) that the dimensionless virtual work due to the small node mechanism of Fig. 2 is:

$$W_{int} = \theta_O (\tau_{AD} + \tau_{DB} + \tau_{BC} + \tau_{CA} - 2\tau_{AB} - 2\tau_{CD}) \quad (2\text{-}9)$$

If there are no body forces and if node O is sufficiently far from the boundary, then the external work is zero and the equilibrium equation associated with a small node O is

$$\tau_{AD} + \tau_{DB} + \tau_{BC} + \tau_{CA} - 2\tau_{AB} - 2\tau_{CD} = 0 \quad (2\text{-}10a)$$

Similarly, the equilibrium equation associated with the large node B in Fig. 3 is

$$\tau_{AE} + \tau_{EF} + \tau_{FG} + \tau_{GA} - \tau_{BA} - \tau_{BE} - \tau_{BF} - \tau_{BG} = 0 \quad (2\text{-}10b)$$

The constitutive behavior within the edges of the model must reflect that of the material to be modeled, and we consider here the case of an elastic/perfectly-plastic material. Since some unloading will be found to occur in the examples to be considered, the equations must be written in rate form. At a generic time t_o, the state of stress and strain is assumed known, and the rates must satisfy

$$\text{IF } |\sigma_{xy}| < k \text{ THEN } \dot{\sigma}_{xy} = G\,\dot{\gamma}_{xy} \quad (2\text{-}11a)$$

$$\text{ELSE IF } \sigma_{xy}\,\dot{\gamma}_{xy} \geq 0 \text{ THEN } \dot{\sigma}_{xy} = 0 \quad (2\text{-}11b)$$

$$\text{ELSE } \dot{\sigma}_{xy} = G\,\dot{\gamma}_{xy} \quad (2\text{-}11c)$$

Evidently the third branch, unloading from a yielding stage will occur only if both $|\sigma_{xy}| = k$ and $\sigma_{xy}\,\dot{\gamma}_{xy} < 0$. In view of (2-6) and (2-8b), Eq. (2-11) may be written immediately in terms of generalized variables

$$\text{IF } |\tau_{PQ}| < 1 \text{ THEN } \dot{\tau}_{PQ} = G'\dot{\omega}_{PQ}\,\ell_o/(k\,\ell_{PQ}) \quad (2\text{-}12a)$$

$$\text{ELSE IF } \tau_{PQ}\,\dot{\omega}_{PQ} \geq 0 \text{ THEN } \dot{\tau}_{PQ} = 0 \quad (2\text{-}12b)$$

$$\text{ELSE } \dot{\tau}_{PQ} = G'\dot{\omega}_{PQ}\ell_o/(k\,\ell_{PQ}) \quad (2\text{-}12c)$$

where we have defined

$$G' = G/\delta \quad (2\text{-}13)$$

Equation (2-12) may be viewed in two ways. If G is the shear modulus of the real material, then since $\dot{\tau}_{PQ}$ is bounded, $\dot{\omega}_{PQ}$ must tend to zero with δ so that there can be no slip in the edge elements less than yield. However, even in this case useful information can be obtained from Eq. (2-12) as will be illustrated in Chapter V.

An alternative viewpoint, which is more useful for the model considered in this chapter, is to regard the edge as made of a fictitious material whose shear modulus tends to zero with δ so that G' remains finite. For such a model non-zero slips can be found even in the elastic range, but they will all be expressed in terms of the single unknowable modulus G'.

To summarize, we have defined a model with one generalized displacement variable θ_i for each interior node. For N sufficiently large, a model with N nodes will have as kinematic variables approximately N generalized displacements θ_i. Since slip is continuous through a small node, there will be 2N generalized strains ω_{ij}. The static variables will be 2N stresses τ_{ij}. To determine these 5N unknowns, we have 2N strain-displacement equations (2-4), N equilibrium equations (2-10), and 2N constitutive equations (2-12).

However, for any finite number N, the number of variables and equations may vary slightly from these numbers due to some nodes and edges being on the boundaries. We consider some of these variations in the next section.

B. Boundary Value Problem

In the examples to be considered later, all domains

are rectangular with vertical and horizontal boundaries which pass through large nodes. Boundaries at 45° could also be considered, but more general domains would require more general triangle arrangements.

The general approach is to introduce fictitious rigid triangles on the outside of the domain and apply boundary conditions to these fictitious triangles. Figure 5 shows a small rectangular domain which exemplifies most of the features to be found in later examples. The only non-homogeneous boundary conditions are prescribed normal displacements on the left edge AB and part ED on the top edge; homogeneous boundary conditions are force or displacement as indicated in Fig. 5.

We first derive the strain-displacement relation for boundary edges. In Fig. 5, all of the small nodes and the large nodes 7 and 12 are interior and their mechanisms are shown in Figs. 2 and 3. However, the large nodes on the boundary are less constrained than nodes 7 or 12 and will have simpler mechanisms. Figure 6 shows the mechanism for node 13 (point E). Comparison with Fig. 3 shows that the slip along EF or ED is half that along an interior edge. Since there is no mechanism at the fictitious point G, it follows that (2-4a) must be replaced by

$$\omega_{FE} = \theta_C - 1/2\ (\theta_F + \theta_E) \qquad (2\text{-}14)$$

Next we observe that in any finite rectangle the total number of degrees of freedom is one less than the total number of nodes. Indeed, if each interior and boundary node is given an equal motion θ, the result in view of (2-4) and (2-14) will be to leave the entire domain in its original position. Therefore, we may arbitrarily assign one node the value of zero and eliminate the corresponding equilibrium equation as being a linear combination of the other equilibrium equations. In the following discussion, we set $\theta_{16} = 0$.

In the interior of the domain in Fig. 5, there are 2 large nodes and 6 small ones so that there are 8 unknowns θ_i and 8 homogeneous equilibrium equations. In the interior, there are 19 unknown slips ω_{ij} and 19 unknown shear stresses τ_{ij}. Consequently, there are 19 constitutive relations (2-12) and an equal number of strain-displacement relations (2-4). Therefore, there are a total of 46 interior unknowns and an equal number of equations.

Consider next the boundary segment AE in Fig. 5. Since the fictitious elements are free to move and no shear forces are transmitted across segment AE, the

stress in the boundary edges is zero, and the strain is irrelevant. However, at node 8 a mechanism motion of the form shown in Fig. 6 is possible, so that θ_8 must be added to the list of unknowns. Evidently the only work will be along edges 3-7, 7-13, and 7-8, so that Eq. (2-10b) reduces to

$$\tau_{3.7} + \tau_{7.13} - \tau_{8.7} = 0 \qquad (2\text{-}15)$$

The situation is somewhat different on edge BC. Since $\theta_{16} = 0$ by definition, and since the fictitious triangle below edge 11-16 cannot move vertically, it follows from Fig. 6 that $\theta_{11} = 0$. The same reasoning shows $\theta_6 = \theta_1 = 0$, so that no displacements are introduced along BC. Since $T_t = 0$, the shear stresses all vanish along BC and the strains are irrelevant. Thus BC does not add to either the equations or unknowns of the problem. The same conclusion obviously applies to side CD.

On edge AB the prescribed normal displacement is u_0. Rotating Fig. 6 90°, we see that since $\theta_1 = 0$, we must have

$$\theta_2 = 2\ u_0\, \ell/\ell_0^2 \qquad (2\text{-}16a)$$

to meet the conditions along edge 1-2. This mechanism produces a displacement $-u_0$ along edge 2-3 so that in order to satisfy the boundary condition on that edge

$$\theta_3 = 2\theta_2 \qquad (2\text{-}16b)$$

Note that if the edge were longer the next node would have a magnitude $3\theta_2$, the next $4\theta_2$ etc. However, for the domain in Fig. 5, since the triangle above edge 3-8 may move without constraint, θ_3 causes no problem on that edge. As on the other boundary edges considered, $\tau_{1.2} = \tau_{1.3} = o$, and the strains are irrelevant. Thus we have added one independent new equation by equating internal and external work for the motion of Eqs. (2-16)

$$\tau_{1.7} + \tau_{3.7} - \tau_{2.7} + 2\tau_{2.8} = T_2 \qquad (2\text{-}17)$$

The corresponding unknown T_2 is, of course, the averaged force divided by the yield stress k exerted across edge AB.

Finally, on edge ED a mechanism motion with

$$\theta_{13} = 2v_o\ell/\ell_o^2 \qquad (2\text{-}18)$$

will satisfy the prescribed boundary motion of ED. Since the fictitious triangle above ED is constrained against horizontal motion $\tau_{13.18}$ and $\omega_{13.18}$ are unknowns related by the constitutive relation (2-12). The strain-displacement equation is obtained from Eq. (2-14) with $\theta_{18} = 0$. Equating the internal and external work we obtain finally the equilibrium equation

$$\tau_{8.12} + \tau_{12.18} - \tau_{13.12} - 1/2\tau_{13.18} = 1/2\ T_1 \qquad (2\text{-}19)$$

where T_1 is the averaged dimensionless vertical force along the boundary ED necessary to produce the prescribed v_o.

In summary then, the edge variables at the boundary are the generalized displacement θ_8, the unknown forces T_1 and T_2, and the stress and strain $\tau_{13.18}$ and $\omega_{13.18}$ along edge ED. The edge equations are the equilibrium equations (2-15), (2-17), and (2-19), a strain-displacement relation (2-14), and a constitutive relation (2-12) for edge ED. Since we have added 5 each of unknowns and equations the problem balances at 51 equations and unknowns.

The extension of the method used to larger domains with the same boundary conditions is obvious. The extension to different specific boundary conditions is not difficult and will be indicated where it occurs in particular applications.

C. Computation

For simplicity of exposition, we refer to the specific problem in Sec. B. However, we find it convenient to temporarily shift our viewpoint and regard T_1 and T_2 as given with θ_2 and θ_{13} taken as unknowns. Equations (2-16a) and (2-18) then serve merely as definitions of

u_o and v_o. The basic method is to regard the displacements at nodes 13, 2, 4, 5, 7, 8, 9, 10, 12, 14, 15 as fundamental unknowns and to reduce the problem to 11 equations for these 11 θ_i. To this end we first introduce a column-vector $\underline{\theta}$ with the 11 components θ_i ordered as above.

Next, we have 20 strain-displacement relations, of which a generic one can be written

$$\omega_{PQ} = \underline{v}_{PQ}\,\underline{\theta} \tag{2-20}$$

where each of the 20 $\underline{v}_{PQ}$ is a row vector whose components are determined from the appropriate (2-4) or (2-14) and where θ_3 has been replaced by (2-16b).

We consider first the case where all edges are elastic whence (2-12a) reduces to 20 equations of the form

$$\tau_{PQ} = G'\omega_{PQ}\,\ell_o/k\,\ell_{PQ} \tag{2-21}$$

Rather than substitute (2-21) and (2-20) in the equilibrium equations (2-10), etc, we find it convenient to rederive them in the above notation. To this end, let $\underline{\delta\theta}$ be a virtual displacement row vector independent of $\underline{\theta}$. Then the internal work along edge PQ is

$$w_{int} = \delta\omega_{PQ}\tau_{PQ} = \underline{\delta\theta}\,\underline{\underline{A}}_{PQ}\,\underline{\theta}\,G'/k \tag{2-22a}$$

The elastic stiffness matrix $\underline{\underline{A}}$ for the entire domain can be found by summation of the elastic stiffness matrices

$$\underline{\underline{A}}_{PQ} = \underline{v}^T_{PQ}\,\underline{v}_{PQ}\,\ell_o/\ell_{PQ} \tag{2-22b}$$

of all the elastic edges in the domain. $\underline{\underline{A}}$ is positive definite and symmetric. The total internal work can be written

$$w_{int} = \underline{\delta\theta}\,\underline{\underline{A}}\,\underline{\theta}\,G'/k \tag{2-23}$$

The corresponding dimensionless external work is

$$w_{ext} = (\ell_{ED}T_1\delta v_o + \ell_{AB}T_2\delta u_o)/\ell_o^2 \tag{2-24a}$$

We use Eqs. (2-16a) and (2-18) and define a column force vector $\underline{F}$ whose only non-zero components correspond to $\delta\theta_{13}$ and $\delta\theta_2$ to write

$$w_{ext} = \underline{\delta\theta}\,\underline{F} \tag{2-24b}$$

whence the Principle of Virtual Work produces the equilibrium equations in the form

$$\underline{F} = \underline{\underline{A}}\,\underline{\theta}\,G'/k \tag{2-25}$$

In the computation method we used the contribution of an edge is computed and added to the overall stiffness matrix. This process is called the "direct stiffness method" [12].

In the examples which follow we have a maximum of two non-homogeneous equations so we find it convenient to express Eq. (2-25) as follows:

$$\begin{Bmatrix} \underline{F}_1 \\ \underline{0} \end{Bmatrix} = \begin{Bmatrix} \underline{\underline{A}}_{11} & \underline{\underline{A}}_{21}^T \\ \underline{\underline{A}}_{21} & \underline{\underline{A}}_{22} \end{Bmatrix} \cdot \begin{Bmatrix} G'\underline{\theta}_1/k \\ G'\underline{\theta}_2/k \end{Bmatrix} \qquad (2\text{-}26)$$

where $\underline{F}_1$ is the force vector of the two non-homogeneous equilibrium equations, $\underline{\theta}_1$ the generalized displacement variables associated with v_o and u_o (θ_{13} and θ_2 in the example of Fig. 5) and $\underline{\theta}_2$ the remaining 9 displacement variables. The 4 parts of matrix $\underline{\underline{A}}$ are subdivisions of the stiffness matrix. It is readily seen that we can write

$$\underline{F}_1 = (\underline{\underline{A}}_{11} - \underline{\underline{A}}_{21}^T \underline{\underline{A}}_{22}^{-1} \underline{\underline{A}}_{21}) \; (G'\underline{\theta}_1/k) \qquad (2\text{-}27a)$$

$$(G'\underline{\theta}_2/k) = - \underline{\underline{A}}_{22}^{-1} \underline{\underline{A}}_{21} \; (G'\underline{\theta}_1/k) \qquad (2\text{-}27b)$$

Equations (2-27) enable us to handle either force-prescribed or displacement-prescribed problems within the same framework. If $\underline{F}_1$ is prescribed, $\underline{\theta}_1$ is first determined from (2-27a); if $\underline{\theta}_1$ is given, (2-27a) serves simply to compute the reaction forces $\underline{F}$. In either case, the bulk of computation consists of finding $\underline{\theta}_2$ from (2-27b) with $\underline{\theta}_1$ being known. Finally, of course, the strains ω_{ij} and stresses τ_{ij} can now be computed with (2-20) and (2-21).

We consider for definiteness a problem with a single monotonically increasing deformation parameter v. Since the elastic solution is linear, a solution with v=1 can immediately be used to obtain any elastic solution. In particular, we can find the value v_e and the corresponding solution for which the first edge, PQ say, reaches the yield limit $\tau_{PQ} = \pm 1$. For simplicity of exposition we take PQ to be a single edge, but no essential complication is introduced if several edges reach yield at v_e.

During some finite time interval v_e to v_1, say, only edge PQ will be plastic. During this time, edge PQ will require Eq. (2-12b), $\dot{\tau}_{PQ} = 0$, but all other edges will continue to be governed by (2-12a) as they were during the elastic solution. It follows that the only modification necessary to solve the problem is to subtract the elastic contribution of the edge PQ from the stiffness matrix (2-23). Since we inverted a part of the stiffness matrix (2-27), it is convenient to use a modification of the Sherman-Morrison formula [13], i.e.

$$(\underline{\underline{A}}_{22} - \underline{v}_{PQ}^T \underline{v}_{PQ} \, \ell_o/\ell_{PQ})^{-1} = \underline{\underline{A}}_{22}^{-1} + \beta \, \underline{\underline{A}}_{22}^{-1} \underline{v}_{PQ}^T \underline{v}_{PQ} \underline{\underline{A}}_{22}^{-1} \qquad (2\text{-}28a)$$

$$\beta = 1/(\ell_{PQ}/\ell_o - \underline{v}_{PQ} \underline{\underline{A}}_{22}^{-1} \underline{v}_{PQ}^T) \qquad (2\text{-}28b)$$

The left hand side is the adjusted inverted matrix for the next stage, while $\underline{\underline{A}}_{22}$ and $\underline{\underline{A}}_{22}^{-1}$ are the matrices for the present stage. The coefficients in $\underline{v}_{PQ}$ related with $\underline{\theta}_1$

are deleted in Eqs. (2-28) because, according to Eq. (2-26), the matrix $\underline{\underline{A}}_{22}$ is a part of the stiffness matrix $\underline{\underline{A}}$.

With the revised stiffness matrix, and a prescribed increment δv, the solution is obtained as before, and is linear in δv. Therefore, we can immediately obtain the value v_1 at which some other edge P'Q' becomes plastic, and repeat the process by deleting the elastic contribution of P'Q' to $\underline{\underline{A}}$.

Consider now a generic displacement v_k for which a collection of edges E_1 are at yield. The method just outlined assumes that $\dot{\tau}_{ij} = 0$ for all edges in E_1. According to Eq. (2-12b) this statement is true only if $w_{ij} = \tau_{ij}\dot{\omega}_{ij} \geq 0$. This criterion is easily checked, once the complete solution is found. If it is valid for each edge in E_1, the solution is accepted, v_{k+1} is found, and the next stage solved. This compliance is, in fact, the usual situation in the examples considered.

However, if one or more edges predict a negative w_{ij}, the solution must be rejected. Instead, the edge RS with the numerically largest negative w_{ij} is assumed to follow Eq. (2-12c), i.e., to unload elastically. According to this hypothesis, the elastic contribution of edge RS must be added back into $\underline{\underline{A}}$. The new solution is now checked against the requirement that $w_{RS} \leq 0$ and

that $w_{ij} \geq 0$ for all edges in E_1 other than RS. Since unloading turns out to be a relatively rare occurence, no attempt was made to maximize the efficiency of this adjustment process, but it is continued until all requirements are satisfied.

D. Singular Solutions

At the end of each stage, the complete solution of θ_k, ω_{ij}, τ_{ij}, and v is known. Since we are concerned with an elastic/perfectly-plastic material, the limit load will be reached at the end of some stage. This phenomenon causes no difficulty. The rate solution for the next stage will simply predict that $\dot{\tau}_{ij} = 0$ with all kinematic rates being expressed in terms of $\dot{v}$.

However, in some of the examples to be considered, a complication occurs in that the stiffness matrix becomes singular before the yield point load is reached. To discuss this situation, we consider the small domain in Fig. 7 with the boundary conditions as shown. This problem is similar to that considered in Sec. B.

Each of the 5 interior nodes has one displacement variable and one homogeneous equilibrium equation as follows:

$$\tau_{2.7} + \tau_{6.7} - 2(\tau_{1.7} + \tau_{2.6}) = 0 \qquad (2.29a)$$

$$\tau_{2.7} + \tau_{7.8} - 2(\tau_{2.8} + \tau_{3.7}) = 0 \qquad (2.29b)$$

$$\tau_{2.6} + \tau_{6.12} + \tau_{12.8} + \tau_{2.8} - (\tau_{2.7} + \tau_{6.7} + \tau_{12.7} + \tau_{8.7}) = 0 \qquad (2.29c)$$

$$\tau_{6.7} + \tau_{7.12} - 2(\tau_{6.12} + \tau_{7.11}) = 0 \qquad (2.29d)$$

$$\tau_{8.7} + \tau_{7.12} + \tau_{8.13} - 2(\tau_{7.13} + \tau_{8.12}) = 0 \qquad (2/29e)$$

There are 12 interior edges and one relevant boundary edge, 8-13. The 13 strain-displacement relations are obtained from (2-4), (2-14), (2-16), and (2-18) and written in the rate form:

$$\dot{\omega}_{2.6} = -2\dot{\theta}_4 + \dot{\theta}_7 \qquad (a)$$

$$\dot{\omega}_{1.7} = -2\dot{\theta}_4 - \dot{d}/4 \qquad (b)$$

$$\dot{\omega}_{2.7} = \dot{\theta}_4 + \dot{\theta}_5 - \dot{\theta}_7 + \dot{d}/4 \qquad (c)$$

$$\dot{\omega}_{3.7} = -2\dot{\theta}_5 - 5\dot{d}/4 \qquad (d)$$

$$\dot{\omega}_{2.8} = -2\dot{\theta}_5 + \dot{\theta}_7 - \dot{d}/2 \qquad (e)$$

$$\dot{\omega}_{6.7} = \dot{\theta}_4 - \dot{\theta}_7 + \dot{\theta}_9 \qquad (f)$$

$$\dot{\omega}_{7.8} = \dot{\theta}_5 - \dot{\theta}_7 + \dot{\theta}_{10} + \dot{d} \qquad (g) \qquad (2\text{-}30)$$

$$\dot{\omega}_{7.11} = -2\dot{\theta}_9 \qquad (h)$$

$$\dot{\omega}_{6.12} = \dot{\theta}_7 - 2\dot{\theta}_9 \qquad (i)$$

$$\dot{\omega}_{7.12} = -\dot{\theta}_7 + \dot{\theta}_9 + \dot{\theta}_{10} \qquad (j)$$

$$\dot{\omega}_{8.12} = \dot{\theta}_7 - 2\dot{\theta}_{10} \qquad (k)$$

$$\dot{\omega}_{7.13} = -2\dot{\theta}_{10} - \dot{d} \qquad (l)$$

$$\dot{\omega}_{8.13} = \dot{\theta}_{10} + \dot{d}/2 \qquad (m)$$

The elastic problem is easily solved, as are the first few elastic-plastic stages. Figure 8 shows the

sequence of stages, the circled numbers denoting the order in which edges become plastic. Stage 5 ends when edges 6-7 and 7-12 simultaneously reach their yield values.

If all six edges at yield behave plastically, stage 6 must be solved with

$$\dot{t}_{6.7} = \dot{t}_{7.8} = \dot{t}_{7.11} = \dot{t}_{6.12} = \dot{t}_{7.12} = \dot{t}_{8.12} = 0 \qquad (2\text{-}31)$$

For the other seven edges, $\dot{t}_{ij}$ is proportional to $\dot{\omega}_{ij}$ as given by (2-21). Substitution for $\dot{t}_{ij}$ in (2-29) shows that (2-29d) is identically satisfied, and the other four equations with Eqs. (2-30) become

$$\dot{\theta}_4 + \dot{\theta}_5 - \dot{\theta}_7 + \dot{d}/4 - \sqrt{2}(-4\dot{\theta}_4 + \dot{\theta}_7 - \dot{d}/4) = 0$$

$$\dot{\theta}_4 + \dot{\theta}_5 - \dot{\theta}_7 + \dot{d}/4 - \sqrt{2}(-4\dot{\theta}_5 + \dot{\theta}_7 - 7\dot{d}/4) = 0$$

$$(4 + \sqrt{2})(-\dot{\theta}_4 - \dot{\theta}_5 + \dot{\theta}_7 - \dot{d}/4)/2 = 0$$

$$(1/2 + \sqrt{2})(2\dot{\theta}_{10} + \dot{d}) = 0 \qquad (2\text{-}32)$$

We see that $\dot{\theta}_9$ is undetermined and

$$\dot{\theta}_5 = 3\dot{\theta}_4 = -9\dot{d}/16 \quad \dot{\theta}_7 = \dot{\theta}_{10} = -\dot{d}/2 \qquad (2\text{-}33)$$

The stress rates are all uniquely determined as are the strain rates in the elastic edges, but combination of

(2-33) and (2-30) shows that the plastic strain rates are

$$\dot{\omega}_{6.7} = 5\dot{d}/16 + \dot{\theta}_9 \geq 0 \qquad \dot{\omega}_{6.12} = -\dot{d}/2 - 2\dot{\theta}_9 \leq 0$$

$$\dot{\omega}_{7.8} = 7\dot{d}/16 \geq 0 \qquad \dot{\omega}_{7.12} = \dot{\theta}_9 \leq 0$$

$$\dot{\omega}_{7.11} = -2\dot{\theta}_9 \geq 0 \qquad \dot{\omega}_{8.12} = \dot{d}/2 \geq 0 \qquad (2\text{-}34)$$

The inequalities in (2-34) are required by the condition $\tau_{ij}\dot{\omega}_{ij} \geq 0$ at a yielding edge. Evidently they will be satisfied for any $\dot{\theta}_9$ satisfying

$$-\dot{d}/4 \leq \dot{\theta}_9 \leq 0 \qquad (2\text{-}35)$$

so that the kinematic solution is not unique, but it is bounded.

According to Fig. 8, all of the edges involved in a mechanism motion about node 9 have yielded. Thus, there is no internal work and hence $\dot{\theta}_9$ can not be determined. However, this configuration is not a mechanism since a mechanism motion in either direction would require unloading in some edges. Indeed, if the motion about node 9 were the only contribution to edges 6-7 and 7-12 for example, $\dot{\theta}_9$ would have to be zero. The freedom allowed by (2-35) is due to the fact that other mechanisms have produced strains and that only the total strain rate is subjected to the inequalities (2-34).

Now we consider the computational aspects of this singularity. $\underline{\underline{A}}_{22}^{-1}$ must be adjusted for the yielding in edges 6-7 and 7-12. The first adjustment causes no difficulty, but the second leads to zero value of the denominator in (2-28b). The adjustment of $\underline{\underline{A}}_{22}^{-1}$ is hence not completed. The program then observes that all the edges of the elementary mechanism at node 9 are at yield, hence the associated equilibrium equation is an identity and $\dot{\theta}_9$ becomes indeterminate. Computationally it is the simplest to set $\dot{\theta}_9 = 0$, by adding an appropriate component to the matrix $\underline{\underline{A}}_{22}^{-1}$ and then using the Sherman-Morrison formula (2-28) to adjust $\underline{\underline{A}}_{22}^{-1}$ for the yielding in edge 7-12.

During subsequent stages we assume that no unloading occurs in the edges of the elementary mechanism at node 9. At the end of each stage we determine the range of $\dot{\theta}_9$ using the appropriate Eqs. (2-30). If at least one value of $\dot{\theta}_9$ exists which satisfies all the strain rate inequalities, the solution is accepted. If these inequalities do not have a solution, then unloading must occur in one or more of the edges in the node 9 mechanism. Thus, $\dot{\theta}_9$ and Eq. (2-29d) are returned to the problem and unloading is allowed as described at the end of Sec. C.

Since the present investigation was more concerned with the predictions of the slip model than with computational aspects, the ranges for $\dot{\theta}_9$ were determined by examination of the output, rather than by the program.

Although it would not be difficult to incorporate this procedure in the program for one undetermined displacement unknown related to an elementary mechanism, it would be quite complicated in case two or more undetermined displacement unknowns contribute to the strain of one edge.

Singularities can also be caused by a combined mechanism involving more than one node. The procedure here is similar but more complicated and will be described in an example in Chapter IV where it first occurs.

Chapter III Example of Slip Model

Prandtl investigated the incipient plastic flow of the identation of a semi-infinite body by a flat rigid rough punch under conditions of plane strain [9,10]. To model this problem we place an elastic/perfectly-plastic material in a lubricated box as shown in Fig. 9. Because of symmetry, we need to consider only the left half of the material. The symmetry boundary conditions on CD and the perfect-lubrication conditions on the box sides AB and BC all prescribe zero shear force and zero normal displacement. There are no tractions across AE. Finally, the fictitious triangle above DE is subject to zero horizontal and prescribed downward vertical motion. Evidently this problem is the same as the one described in Chapter II, Sec. B with $u_o = 0$, $v_o = -i_o v^*$.

The first stage of our solution is the fully elastic range. This stage is terminated when edge pq of Fig. 1 reaches positive yield for $v^* = 2.27\ G'/k$ and an averaged compressive stress under the punch of 2.50, i.e. $T_1 = -2.50$. Figure 10 pictures the elastic displacement field by showing the averaged vertex displacements at representative small nodes.

As v^* is increased above its maximum elastic value, there will be a succession of elastic-plastic stages. The

sequence in which edges become plastic is indicated in Fig. 11, and the load-deflection curve for the punch is shown in Fig. 12.

No difficulties with the solution are encountered until stage 10. The first rate solution at this stage shows that edge pv which reached positive yield at the end of stage 6, now has a negative strain rate ω_{pv} and violates the inequality of the constitutive equation (2-12b). Therefore, this rate solution must be rejected and edge pv assumed to be elastic again for stage 10. It remains elastic during all subsequent stages. The maximum unloading occurs at the end of stage 15 and is about 2% less than the yield stress.

Edge hi alternates being elastic and plastic. At the end of stage 10 this edge reaches positive yield and remains at yield until the beginning of stage 15. Here the first rate solution predicts a negative strain rate, hence the edge is taken to be elastic. The strain rate is negative through stage 15, but the total decrease in stress is less than one percent. In stage 16, the elastic strain rate is positive and the stage terminates when this edge again reaches positive yield. It yields during stage 17 but becomes elastic again in stages 18 through 21 with a stress always within one percent of yield. Finally, it yields a third time to terminate

stage 21 and remains at yield up to the limit load. The possible physical significance of this alternating loading and unloading will be discussed in Chapter VIII.

At the end of stage 19 we see in Fig. 11 that the edges of the elementary large node mechanism of node p are all at yield. Therefore, the stiffness matrix $\underline{A}_{22}$ becomes singular and $\dot{\theta}_p$ is undetermined, subject to the inequalities of Eq. (2-12b). These inequalities reduce to

$$-.179\dot{v}^* \geq \dot{\theta}_p \geq -.189\dot{v}^* \qquad (3\text{-}1)$$

for stages 20 and 21.

Fig. 11 also shows that at the end of stage 21 all of the edges associated with the elementary mechanism of small node k are also at yield so there is a further singularity in the stiffness matrix. The rate solution for stage 22 puts the following bounds on $\dot{\theta}_k$ and $\dot{\theta}_p$:

$$\begin{aligned} -.114\dot{v}^* &\geq \dot{\theta}_k \geq -.121\dot{v}^* \\ .055\dot{v}^* + 2\dot{\theta}_k &\geq \dot{\theta}_p \geq -.190\dot{v}^* \end{aligned} \qquad (3\text{-}2)$$

At the end of stage 22, four edges simultaneously reach yield, $T_1 = -6.00$, and $v^* = 25.05\, G'/k$. An attempt to adjust the stiffness matrix for these yielding edges causes a zero in the denominator of Eq. (2-28b), but no additional elementary mechanism can be found whose edges are all at yield. Therefore, the program is stopped and

the results analyzed manually. It is evident from Fig. 11 that sufficient edges have yielded to permit any of the combined mechanism motions shown in Fig. 13, with all inequalities (2-12b) being satisfied. Since all stresses in the non-homogeneous equilibrium equation corresponding to (2-19) are at yield and hence constant, the load is constant, and $T_1 = -6.00$ represents the yield-point load.

It is of some interest to note that each of the mechanisms a, b, d, g in Fig. 13 involve yielding of only one of the four edges which reach yield at the end of stage 22. The other mechanisms in Fig. 13 are linear combinations of these four and the interior mechanisms at nodes *k* or *p*.

In order to evaluate this method of velocity-discontinuities we compare the results in the fully elastic range and at the limit load condition with analytical and other numerical results.

Green and Zerna [14], as well as Milne Thomson [15], describe the analytical solution of the Prandtl punch in the fully elastic range for the semi-infinite domain. The displacement field for an incompressible material is given by

$$G(u+iv) = \Omega(z) - \overline{\Omega}(\overline{z}) - (z-\overline{z})\overline{\Omega}'(z) + C$$

$$\Omega(z) = \frac{iy}{4\pi} \ln \left(re^{i\theta} + \sqrt{r_1 r_2}\, e^{i(\theta_1+\theta_2)/2}\right) \qquad (3\text{-}3)$$

Where G is the shear modulus, y is the total force of the punch, and C is a complex constant which we define in such a way that the point corresponding node C in the finite domain (Fig. 9) remains in position and the remaining variables are defined by Fig. 14. In Fig. 15, we show the analytical results in the same fashion as we did for the velocity discontinuity model (Fig. 10).

Using the same domain and element arrangement as the velocity discontinuity model, we solved the problem with the classical finite element model with constant strain triangles, under plane strain conditions, and a Poisson ratio of $\nu = .49$ (Appendix B). In Fig. 16, we show the displacement field in the fully elastic range where the displacement at each small node is the average of the four surrounding large nodes. We also note that the fully elastic range is terminated when $T_1 = -3.87$ and $v^* = .25\ G/k$ because the element bounded by the nodes *t*, p, and q of Fig. 1 reaches yield.

Figures 10 and 16 show surprisingly good agreement for the elastic solution. It must, of course, be emphasized that the dimensionless displacements in Fig. 16 are defined in terms of known physical constants, whereas in Fig. 10 they include the essentially unknowable modulus G'. However, by choosing the constant $G' = 14.05\ G$ so that the over-all slopes match in Fig. 12, we obtain agreement over the entire field.

The agreement of both numerical solutions with the analytical solution in Fig. 15 is quite good near the punch and along most of the free boundary. The poor agreement along the edges suggests that the size of the box in the model was too small to give a good approximation to a semi-infinite domain.

Little information is available for comparison of the various elastic-plastic stages, but a partial solution at the yield-point load was first given by Prandtl [9,10] and was later shown by Shield and Drucker to be complete [16]. Fig. 17 shows the resulting kinematic pattern. The yield point stress is:

$$T_1 = -(2 + \pi) = -5.14 \qquad (3\text{-}4)$$

compared with our value of -6.00.

We conclude this chapter by discussing an alternative triangle arrangement which uses the fan of long thin triangles shown in Fig. 18. Hodge [17] analyzed this problem from the viewpoint of statically admissible discontinuous stress fields. The yield load point is in this case reached for

$$T_1 = -2\left[1 + (N-1)\sin\frac{\pi}{2(N-1)}\right] \qquad (3\text{-}5)$$

which is less than the Prandtl load (3-4) but approaches it as N tends to infinity.

The similar, but slightly different, triangle arrangement of Fig. 19 can be used to define a kinematically admissible field involving slip of rigid triangles. Along each edge with slip the tangential stress is 1, hence a recursion relation for the total normal force on each edge is easily obtained from overall equilibrium (insert to Fig. 19):

$$R_{\phi+\Delta\phi} - R_{\phi} = 4\sqrt{2}\tan(\Delta\phi/2) \qquad (3\text{-}6)$$

If there are N-1 discontinuities between triangles, Eq. (3-6) may be successively applied from the free boundary to obtain

$$T_1 = -4(N-2)\tan\frac{\pi}{4(N-2)} - 2 \qquad (3\text{-}7)$$

Figure 20 shows the limit load as a function of N according to (3-5) and (3-7). As expected, as N increases they converge towards the true limit load (3-4) from below and above, respectively.

It is interesting to note that for N=3 we obtain precisely the value $T_1 = -6.00$ in accord with our earlier analysis. Indeed, the mechanism in Fig. 13b is exactly the same as that of Fig. 19 with N=3.

Chapter IV Other Examples Of The Slip Model

In this chapter we discuss three additional problems using the slip model: the Prandtl punch problem with a lubricated punch material contact, the deep double edge notched tensile specimen, and the single edge notched tensile specimen.

A. Prandtl Smooth Punch

The Prandtl smooth punch problem differs from the rough punch only in the boundary condition along DE, where $u_o = 0$ must be replaced by zero tangential stress. As a consequence, edge gw of Fig. 1 can be omitted from the list of equations and unknowns.

This difference turns out to have very little effect on the numerical solution method or on the results. Indeed, to the scale used, the differences in the load deflection diagram and the elastic displacement field are imperceptible, so that Fig. 10 and the curve in Fig. 12 are immediately applicable to this problem also. However, there are some slight differences in the yielding pattern so that the points marked on the curve in Fig. 12 must be modified. Figure 21 shows the sequence in yielding edges. It is identical with Fig. 11 for the rough punch through the first three stages, and the only difference up through stage 15 is that stages 4, 5, and 6 are permuted. Edge pv still unloads at stage 10 and remains elastic, edge hi unloads and reloads once instead of twice, and edge bc becomes plastic at the end of stage 15 instead of stage 17.

However, the only significant difference in the two examples is that edge pw becomes plastic at the end of stage 16 whereas in the rough punch problem the stress in edge pw was only 80% of negative yield at the limit load. This has the effect of introducing an earlier singularity due to a mechanism at node s. θ_k and θ_p also became indeterminate as in the rough punch example. However, at each stage a range of admissible values exist for the undetermined rates. For example, during stage 21 they must satisfy:

$$\begin{aligned} -.114\dot{v}^* \geq \dot{\theta}_k \geq -.121\dot{v}^* \\ 2\dot{\theta}_k + .055\dot{v}^* \geq \dot{\theta}_p \geq \dot{\theta}_k - .074\dot{v}^* \\ \dot{\theta}_k \geq 2\dot{\theta}_s \geq -.333\dot{v}^* \end{aligned} \qquad (4\text{-}1)$$

which has, as one possible solution,

$$\dot{\theta}_k = -.120\dot{v}^*;\ \dot{\theta}_p = -.190\dot{v}^*;\ \dot{\theta}_s = -.150\dot{v}^* \qquad (4\text{-}2)$$

The Prandtl smooth punch problem reached the limit load at the end of stage 21 with $T_1 = -6.00$, $v^* = 25.05G'/k$, the same values as the rough punch. Obviously, all of the limit load mechanisms in Fig. 13 are still possible. In addition, because edge pw is also at yield, the mechanisms in Fig. 22 are also possible yield modes as are various combinations of Figs. 13 and 22.

Comparisons of the slip model with other solutions are similar to those for the rough punch. Indeed, Green and Zerna's solution [14,15] for the rough punch on an infinite incompressible half-space predicts $\sigma_{xy} = 0$ under the punch,

so that it is equally applicable to the smooth punch problem. Similarly, numerical differences in the classical finite element method are too slight to be detected on the scale used in Fig. 16. Therefore, the same general comparative conclusions apply here as in the previous chapter.

At the limit load, Hill [10,18] pointed out that the alternative slip line field shown in Fig. 23 was equally acceptable with Fig. 17. Indeed, Fig. 22a may be regarded as a simple approximation to Fig. 23 in the same sense that Fig. 13b approximates Fig. 17.

This alternative mechanism can also be approached by the triangular fan models used at the end of the previous chapter. Indeed, it follows from Fig. 24 that the averaged stress under the punch as function of the number of discontinuities is again defined by Eqs. (3-5) and (3-7). However, since nodes t and s are not directly connected by an edge, there is no fan model which coincides exactly with any of the possible slip models.

B. Double Notched Tensile Specimen

A bar with deep symmetrical slits is gripped between rigid jaws at its ends and stretched at a uniform rate $2v_o$. Because of symmetry, it is sufficient to consider only the lower left quadrant as shown in Fig. 25. If the dimensions of the quarter-bar are the same as the half box in Fig. 9, then the problem is very simular to the Prandtl smooth problem. Indeed, except for a change in sign of v_o, the

only difference between the two problems is the boundary conditions along AB. However, the replacement of $u_o = 0$ by $T_n = 0$ on this boundary turns out to have a significant effect on many features of the solution. Physically, this difference can be expected, since the indentation forces material up along the top edge AE, whereas material for the bar elongation can come from side AB. Figure 26 for the elastic solution shows this phenomenon quite dramatically. Indeed, the particles along AB move primarily horizontally, whereas in Fig. 10 such motion is primarily vertical.

Figure 27 shows the elastic displacement for the classical finite element model with $\nu = 0.49$. As in the Prandtl punch problems, the agreement between the two models is excellent.

Figures 28 and 29 show respectively the yielding sequence of the edges and the load-deflection curve. As expected, the load-deflection curve for this problem lies below that for the punch problems, since the problem is less constrained.

Just as in the punch problem, plastic flow starts near DE. Indeed, comparison of Figures 21 and 28 shows that the first 7 edges to become plastic here are among the first 8 for the smooth punch. However, the 8th edge here is the 14th in Fig. 21, and the 11th here never does become plastic under the punch. Later stages differ even more as plastic behavior spreads down the bar, and the bar passes through more than twice as many elastic-plastic stages before the limit load is reached.

Figure 28 shows that many edges have histories of unloading from the plastic state. For example, edge bg reaches positive yield at the end of stage 25, remains there for the next 21 stages, but unloads just before the yield point load is reached. Other edges, such as pv, yield and unload twice before finally yielding again at the yield-point load.

For stage 22, neither the first nor the second rate solution is accepted since it turns out that both edges mu and ov unload during this stage. Similarly, four trials are necessary to get the correct solution for stages 29 or 40. The stress in edge ae drops to 85% of positive yield point load. However, all other bars which ever yielded never fall to less than 97% of the yield stress value.

In the earlier examples, any singularities which occurred before the yield-point load was reached were related to elementary mechanisms. It was easy to handle this phenomenon within the computer program, since the corresponding row and column of $\underset{=}{A}_{22}$ contained only zero elements and hence were easily recognized.

However, at the end of stage 41 in the present example when edges go, fm, and mt all become plastic, the revision of $\underset{=}{A}_{22}^{-1}$ breaks down, but no zero rows or columns are found in $\underset{=}{A}_{22}$. Instead, the singularity is due to the linear dependence of a combination of rows which corresponds to a combined mechanism. Rather than program a search for such combinations, the program

was stopped and the combined mechanism shown in Fig. 30 was recognized from the output. Since this mechanism involved $\dot{\theta}_j$, $\dot{\theta}_m$, and $\dot{\theta}_r$ we arbitrarily replaced the equilibrium equation for node m by the constraint $\dot{\theta}_m = 0$, modified $\underset{=}{A}_{22}$ accordingly, and restarted the program by inverting $\underset{=}{A}_{22}$ and continuing as usual.

Before the limit load was reached, $\dot{\theta}_j$ and $\dot{\theta}_s$ also became elastically undetermined. It is interesting to note that although $\dot{\theta}_s$ became undetermined in stage 43, its bounds

$$.167\ \dot{v}^* \geq \dot{\theta}_s \geq .166\ \dot{v}^* \qquad (4\text{-}2)$$

are very close together and they remained close for all of the remaining stages 44-49.

As is shown in Fig. 31, a great many limit load mechanisms are possible. Cases a through e form a series where each one can be obtained from the previous case and an undertermined mechanism. A similar series is formed by cases a, f, and g. The difference between cases f and h is a large node mechanism at the top and the mechanism of Fig. 30 at the bottom. Case i is a combination of f and h and the difference between cases i and j is a small node mechanism. Case k, a combination of a and f, differs from case i by a large node mechanism. A modification of the top of cases g and f is shown in m and n. Case o is based on cases n and g plus an additional undetermined mechanism.

The limit load mechanisms are larger in number and in all cases different from the Prandtl punch problem, even though the present problem is frequently viewed as the tensile analogue of the Prandtl punch. We also observe that the magnitude of the limit load in the present problem is 5.00 as opposed to 6.00 for the Prandtl punch. This relatively large difference shows that the notch problem is more sensitive than the punch one to the choice of a relatively small finite domain as an approximation to the theoretical infinite one.

C. Single Notched Tensile Specimen.

The final example with the slip model is the least complicated. The bar of the previous section is replaced by a bar with one slit, Fig. 32. Due to symmetry it is sufficient to consider the lower half of the domain on side CD, the boundary condition $u = 0$ of the previous section is replaced by $T_n = 0$. A horizontal rigid body motion is avoided by setting θ at corner node D equal to zero.

The incompressible classical model and the slip model in the fully elastic range are again in good agreement, Figs. 33 and 34. The yielding sequence of the edges and the load-deflection curve are respectively shown in Figs. 35 and 36. The unique limit load mechanism of Fig. 37 is the same as we find for the totally consistent field of a rigid perfectly-plastic material [10].

Chapter V Combined Model

A. Classical Model

Traditionally finite element models are based on certain assumptions on strain within the elements and continuity between the elements. In particular, the original finite element model proposed by Turner et al [3] is based on triangular elements with constant strain in each element. Since the geometry of this classical model is identical with the slip model considered here, it is of obvious interest to compare the two models and then to construct a new combined model. In the present section we briefly review the classical model.

Since displacements are continuous in the classical model, the displacements of all vertices which meet at a node are equal and may be referred to as nodal displacements $\ell_o u_C$ and $\ell_o v_C$, where ℓ_o is again a reference length of a domain. The extensional strains in the triangle edges, also called the natural strains [19], are for the edges of Fig. 38a

$$\begin{aligned} \varepsilon^C_{AB} &= (u_B - u_A)\ \ell_o/\ell \\ \varepsilon^B_{AC} &= (u_C + v_C - u_A - v_A)\ \ell_o/\ell \\ \varepsilon^A_{BC} &= (-u_C + v_C + u_B - v_B)\ \ell_o/\ell \end{aligned} \qquad (5\text{-}1)$$

and the strains in the remaining edges of Fig. 38 are obtained in similar fashion. The relations between the natural strains and the cartesian strains are [19]

cases a,b	cases c,d
$\varepsilon_{xx} = \varepsilon^C_{AB}$	$\varepsilon_{xx} = \varepsilon^B_{AC}+\varepsilon^A_{BC}-\varepsilon^C_{AB}$
$\varepsilon_{yy} = \varepsilon^B_{AC}+\varepsilon^A_{BC}-\varepsilon^C_{AB}$	$\varepsilon_{yy} = \varepsilon^C_{AB}$
$\gamma_{xy} = \varepsilon^B_{AC}-\varepsilon^A_{BC}$	$\gamma_{xy} = \varepsilon^B_{AC}-\varepsilon^A_{BC}$

(5-2)

The dimensionless virtual internal work for each of the triangles of Fig. 38 is

$$W_{int} = (1/k\ell_o^2) \int \underline{\sigma}\cdot\underline{\varepsilon}\, dA = (\ell/\ell_o)^2 (\varepsilon^C_{AB}Q^C_{AB}+\varepsilon^B_{AC}Q^B_{AC}+\varepsilon^A_{BC}Q^A_{BC}) \quad (5-3)$$

where Q^C_{AB}, Q^B_{AC} and Q^A_{BC} are the dimensionless stresses of triangle ABC. The subscripts refer to the edge and the superscript to the opposite vertex of the triangle. For example, in case a or b

$$Q^C_{AB} = (2/\ell)^2/k \int (\sigma_{xx}-\sigma_{yy})\,dA = (\sigma_{xx}-\sigma_{yy})/k \quad (5-4)$$

where the last step is justified since constant strain implies constant stress for any reasonable material. Similarly the generalized stresses for all cases in Fig. 38 are

cases a,b	cases c,d
$Q^C_{AB} = (\sigma_{xx}-\sigma_{yy})/k$	$Q^C_{AB} = (\sigma_{yy}-\sigma_{xx})/k$
$Q^B_{AC} = (\sigma_{yy}+\sigma_{xy})/k$	$Q^B_{AC} = (\sigma_{xx}+\sigma_{xy})/k$
$Q^A_{BC} = (\sigma_{yy}-\sigma_{xy})/k$	$Q^A_{BC} = (\sigma_{xx}-\sigma_{xy})/k$

(5-5)

Next, we derive an equilibrium equation with the principle of virtual work for a horizontal displacement of node O of Fig. 2. It follows from (5-1) that a virtual displacement u_o produces the virtual strains

$$\varepsilon_{OA} = \varepsilon_{OC} = -\varepsilon_{OB} = -\varepsilon_{OD} = u_o\ell_o/\ell \quad (5-6)$$

The resulting virtual work is

$$W_{int} = u_o\,(-Q^C_{OB}+Q^B_{OC}+Q^A_{OC}+Q^C_{OA}+Q^D_{OA}-Q^A_{OD} -Q^B_{OD}-Q^D_{OB})\,(\ell/4\ell_o) \quad (5-7)$$

In the absence of body forces, the external work is zero and hence we obtain the equilibrium equation

$$-Q^C_{OB}+Q^B_{OC}+Q^A_{OC}+Q^C_{OA}+Q^D_{OA}-Q^A_{OD}-Q^B_{OD}-Q^D_{OB} = 0 \quad (5-8a)$$

The vertical equilibrium equation at a small node and two equations at a large node (Fig. 3) are obtained similarly:

$$-Q^C_{OB}-Q^B_{OC}-Q^A_{OC}+Q^C_{OA}+Q^D_{OA}+Q^A_{OD}+Q^B_{OD}-Q^D_{OB}=0$$

$$Q^G_{BC}+Q^A_{BC}+Q^C_{BA}+Q^D_{BA}+Q^A_{BD}+Q^E_{BD}$$
$$-Q^E_{BH}-Q^F_{BH}-Q^H_{BF}-Q^I_{BF}-Q^F_{BI}-Q^G_{BI}=0$$

$$-Q^C_{BG}-Q^G_{BC}-Q^A_{BC}+Q^A_{BD}+Q^E_{BD}+Q^D_{BE}$$
$$+Q^H_{BE}+Q^E_{BH}+Q^F_{BH}-Q^F_{BI}-Q^G_{BI}-Q^I_{BG}=0 \qquad (5\text{-}8b)$$

The constitutive equations, expressed for an elastic/perfectly-plastic material in plane strain, are [10]

$$f=[(\sigma_{xx}-\sigma_{yy})/2k]^2+(\sigma_{xy}/k)^2\le 1 \qquad \dot\lambda\ge 0$$

$$2G\dot\varepsilon_{xx}=\dot\sigma_{xx}-\nu(\dot\sigma_{xx}+\dot\sigma_{yy})+\dot\lambda(\sigma_{xx}-\sigma_{yy})/2k^2$$

$$2G\dot\varepsilon_{yy}=\dot\sigma_{yy}-\nu(\dot\sigma_{xx}+\dot\sigma_{yy})+\dot\lambda(\sigma_{yy}-\sigma_{xx})/2k^2$$

$$G\dot\gamma_{xy}=\dot\sigma_{xy}+\dot\lambda\sigma_{xy}/k^2 \qquad (5\text{-}9)$$

Substitution of Eqs. (5-2) and (5-5) into Eqs. (5-9) leads to the uniform results for all triangles in Fig. 38:

$$f=(Q^C_{AB}/2)^2+[(Q^A_{BC}-Q^B_{AC})/2]^2\le 1 \qquad \dot\lambda\ge 0$$

$$(2G/k)\dot\varepsilon_{AB}=\dot Q^C_{AB}/2+(1-2\nu)(\dot Q^C_{AB}+\dot Q^B_{AC}+\dot Q^A_{BC})/2+\dot\lambda Q^C_{AB}/2k^2$$

$$(2G/k)\dot\varepsilon_{AC}=(\dot Q^B_{AC}-\dot Q^A_{BC})/2+(1-2\nu)(\dot Q^C_{AB}+\dot Q^B_{AC}+\dot Q^A_{BC})/2$$
$$+\dot\lambda(Q^B_{AC}-Q^A_{BC})/2k^2$$

$$(2G/k)\dot\varepsilon_{BC}=-(\dot Q^B_{AC}-\dot Q^A_{BC})/2+(1-2\nu)(\dot Q^C_{AB}+\dot Q^B_{AC}+\dot Q^A_{BC})/2$$
$$-\dot\lambda(Q^B_{AC}-Q^A_{BC})/2k^2 \qquad (5\text{-}10)$$

Eqs. (5-10) can be solved for the stress rates and $\dot\lambda$ to obtain

$$\dot Q^C_{AB}=(2G/k)\{2\dot\varepsilon_{AB}-\dot\varepsilon_{AC}-\dot\varepsilon_{BC}\}-\dot\lambda Q^C_{AB}/k^2$$

$$\dot Q^B_{AC}=(2G/k)\{-\dot\varepsilon_{AB}+[1.5+\nu/(1-2\nu)]\dot\varepsilon_{AC}+[.5+\nu/(1-2\nu)]\dot\varepsilon_{BC}\}$$
$$+\dot\lambda(Q^C_{AB}-Q^B_{AC}+Q^A_{BC})/2k^2$$

$$\dot Q^A_{BC}=(2G/k)\{-\dot\varepsilon_{AB}+[.5+\nu/(1-2\nu)]\dot\varepsilon_{AC}+[1.5+\nu/(1-2\nu)]\dot\varepsilon_{BC}\}$$
$$+\dot\lambda(Q^C_{AB}+Q^B_{AC}-Q^A_{BC})/2k^2$$

IF $f<1$ OR $\dot f<0$, THEN $\dot\lambda=0$ ELSE

$$\dot\lambda=(2Gk/f)\{Q^C_{AB}[\dot\varepsilon_{AB}-(\dot\varepsilon_{AC}+\dot\varepsilon_{BC})/2]/2+(Q^B_{AC}-Q^A_{BC})(\dot\varepsilon_{AC}-\dot\varepsilon_{BC})/4\} \qquad (5\text{-}11)$$

Now we consider the boundary value problem of Fig. 5. For every unknown strain there will be a strain-displacement relation, an unknown stress, and a constitutive equation. Therefore, the problem must contain one equilibrium equation for each displacement unknown. For each of the eight interior nodes, we have already found two equilibrium equations for the two displacement unknowns, Eqs. (5-8). If we take only the terms of Eqs. (5-8) which are inside the domain, then we can use these equilibrium equations also for the boundary displacement unknowns v_2, v_3, u_6, u_8, v_8, u_{11}, v_{17}.

On edge AB, a single horizontal motion is allowed, with $u_1=u_2=u_3=u_0$. Equating the internal and external work associated with a virtual u_0 we obtain

$$-8T_2 = Q^4_{1.6}+Q^6_{1.4}+Q^2_{1.4}+Q^1_{2.4}+Q^7_{2.4}+Q^4_{2.7}+Q^5_{2.7}$$

$$+Q^7_{2.5}+Q^3_{2.5}+Q^2_{3.5}+Q^8_{3.5}+Q^5_{3.8} \qquad (5\text{-}12)$$

If T_2 is given, Eq. (5-12) provides an equation for the unknown u_0; if u_0 is given, it defines the necessary force T_2. Similarly, setting $v_{13} = v_{18} = v_0$ we obtain,

$$4T_1 = Q^8_{10.13}+Q^{12}_{10.13}+Q^{10}_{12.13}+Q^{15}_{12.13}+Q^{12}_{13.15}$$

$$+Q^{18}_{13.15}+Q^{13}_{15.18}+Q^{17}_{15.18}+Q^{15}_{17.18} \qquad (5\text{-}13)$$

Finally, the remaining boundary displacements v_1, v_6, v_{11}, u_{13}, u_{16}, v_{16}, u_{17}, and u_{18} are all prescribed to be zero. Therefore, equilibrium equations based on them are not part of the main problem, although they could be used to compute reaction forces if desired.

B. Interior Domain For Combined Model

We now consider a combined model in which we allow for both a constant strain in each triangle and for slip across each edge. The kinematical slip variables d_{ij}, ω_{ij}, and θ_i are defined as in Chapter II, but in defining the conventional variables we must use the vertex displacements for each triangle, since these may be different for each vertex at a node.

However, it is still convenient to define

quantities u_i and v_i at each node as follows. At a generic large node B, let vertex displacements $\bar{u}_k$ (k = 1, ..., 16) be defined as indicated in Fig. 39 and define two numbers u_B and v_B by

$$\bar{u}_3 = [\ell\, u_B + \ell_o(\theta_I - 1/2\theta_B - 1/2\theta_F)]\ell_o/\ell$$

$$\bar{u}_4 = [\ell\, u_B + \ell\, v_B + \ell_o(\theta_I - \theta_F)]\ell_o/(\ell\sqrt{2}) \qquad (5\text{-}14)$$

The normal displacements at B across the edges BF and BI are, according to Eq. (5-14) and Fig. 39:

$$\bar{v}_1 = \bar{u}_4\sqrt{2} - \bar{u}_3 = [\ell\, v_B + \ell_o(\theta_B - \theta_F)/2]\ell_o/\ell \qquad (5.15a)$$

$$\bar{v}_2 = \bar{u}_3\sqrt{2} + \bar{u}_4 = [-\ell\, u_B + \ell\, v_B + \ell_o(\theta_B - \theta_I)]\ell_o/(\ell\sqrt{2}) \qquad (5.15b)$$

Using the slip d_{ij} across edges BF and BI, the slip-strain relation Eq. (2-1), and the strain-displacement relations Eqs. (2-4) and (2-14) we obtain with Eq. (5-14):

$$\bar{u}_2 = [\ell\ \ u_B - \ell_o(\theta_H - 1/2\theta_B - 1/2\theta_F)]\ell_o/\ell$$

$$\bar{u}_5 = [\ell\ \ u_B + \ell_o\, v_B + \ell_o(\theta_G - \theta_I)]\ell_o/(\ell\sqrt{2}) \qquad (5\text{-}16)$$

Next, we can use Eqs. (5-15) and (5-16) to find $\bar{u}_1$ and $\bar{u}_6$:

$$\bar{u}_1 = (\bar{u}_2 - \bar{v}_1)/\sqrt{2} = [\ell\, u_B - \ell\, v_B + \ell_o(\theta_F - \theta_H)]\ell_o/(\ell\sqrt{2})$$

$$\bar{u}_6 = (\bar{u}_5 + \bar{v}_2)/\sqrt{2} = [\ell\, v_B - \ell_o(\theta_I - 1/2\theta_B - 1/2\theta_G)]\ell_o/\ell \qquad (5\text{-}17)$$

Continuation of this procedure leads to

$$\bar{u}_1 = [\ell\, u_B - \ell\, v_B + \ell_o(\theta_F-\theta_H)]\ell_o/(\ell\sqrt{2})$$

$$\bar{u}_2 = [\ell\, u_B - \ell_o(\theta_H-1/2\theta_B-1/2\theta_F)]\ell_o/\ell$$

$$\bar{u}_3 = [\ell\, u_B + \ell_o(\theta_I-1/2\theta_B-1/2\theta_F)]\ell_o/\ell$$

$$\bar{u}_4 = [\ell\, u_B + \ell\, v_B + \ell_o(\theta_I-\theta_F)]\ell_o/(\ell\sqrt{2})$$

$$\bar{u}_5 = [\ell\, u_B + \ell\, v_B + \ell_o(\theta_G-\theta_I)]\ell_o/(\ell\sqrt{2})$$

$$\bar{u}_6 = [\ell\, v_B - \ell_o(\theta_I-1/2\theta_B-1/2\theta_G)]\ell_o/\ell$$

$$\bar{u}_7 = [\ell\, v_B + \ell_o(\theta_C-1/2\theta_B-1/2\theta_G)]\ell_o/\ell$$

$$\bar{u}_8 = [-\ell\, u_B + \ell\, v_B + \ell_o(\theta_C-\theta_G)]\ell_o/(\ell\sqrt{2}) \qquad (5\text{-}18)$$

$$\bar{u}_9 = [-\ell\, u_B + \ell\, v_B + \ell_o(\theta_A-\theta_C)]\ell_o/(\ell\sqrt{2})$$

$$\bar{u}_{10} = [-\ell\, u_B - \ell_o(\theta_C-1/2\theta_B-1/2\theta_A)]\ell_o/\ell$$

$$\bar{u}_{11} = [-\ell\, u_B + \ell_o(\theta_D-1/2\theta_B-1/2\theta_A)]\ell_o/\ell$$

$$\bar{u}_{12} = [-\ell\, u_B - \ell\, v_B + \ell_o(\theta_D-\theta_A)]\ell_o/(\ell\sqrt{2})$$

$$\bar{u}_{13} = [-\ell\, u_B - \ell\, v_B + \ell_o(\theta_E-\theta_D)]\ell_o/(\ell\sqrt{2})$$

$$\bar{u}_{14} = [-\ell\, v_B - \ell_o(\theta_D-1/2\theta_B-1/2\theta_E)]\ell_o/\ell$$

$$\bar{u}_{15} = [-\ell\, v_B + \ell_o(\theta_H-1/2\theta_B-1/2\theta_E)]\ell_o/\ell$$

$$\bar{u}_{16} = [\ell\, u_B - \ell\, v_B + \ell_o(\theta_H-\theta_E)]\ell_o/(\ell\sqrt{2})$$

Eqs. (5-18) were derived from Eq. (5-14) by using the slip relations. However, they could also be written down by symmetry considerations. It follows that although u_B and v_B do not have any simple physical interpretation, their definition is independent of the particular triangle with vertex at B, so that they are logical variables to be associated with the vertex B. Equations (5-18) then provide explicit expressions for all vertex displacements at a large node in terms of nodal displacements u_B and v_B and nodal rotations θ_i at B and surrounding nodes.

In a similar fashion at a generic small node (Fig. 40):

$$\bar{u}_{17} = [\ell\, u_o - \ell\, v_o + \ell_o(\theta_D-\theta_O)]\ell_o/(\ell\sqrt{2})$$

$$\bar{u}_{18} = [\ell\, u_o + \ell\, v_o + \ell_o(\theta_O-\theta_C)]\ell_o/(\ell\sqrt{2})$$

$$\bar{u}_{19} = [\ell\, u_o + \ell\, v_o + \ell_o(\theta_A-\theta_O)]\ell_o/(\ell\sqrt{2})$$

$$\bar{u}_{20} = [-\ell\, u_o + \ell\, v_o + \ell_o(\theta_O-\theta_D)]\ell_o/(\ell\sqrt{2}) \qquad (5\text{-}19)$$

$$\bar{u}_{21} = [-\ell\, u_o + \ell\, v_o + \ell_o(\theta_B-\theta_O)]\ell_o/(\ell\sqrt{2})$$

$$\bar{u}_{22} = [-\ell\, u_o - \ell\, v_o + \ell_o(\theta_O-\theta_A)]\ell_o/(\ell\sqrt{2})$$

$$\bar{u}_{23} = [-\ell\, u_o - \ell\, v_o + \ell_o(\theta_C-\theta_O)]\ell_o/(\ell\sqrt{2})$$

$$\bar{u}_{24} = [\ell\, u_o - \ell\, v_o + \ell_o(\theta_O-\theta_B)]\ell_o/(\ell\sqrt{2})$$

Therefore the kinematics of the combined model are fully defined by the three variables u_i, v_i, and θ_i at each node.

In the notation of Fig. 39 and Eqs. (5-18) and (5-19) we see that typical elongational strains in edges BF and BI of triangle BIF are

$$\epsilon^{I}_{BF} = (u_F - u_B)\ell_o/\ell$$
$$\epsilon^{F}_{BI} = (u_I + v_I - u_B - v_B)\ell_o/\ell \qquad (5\text{-}20)$$

Since all the other natural strains are also independent of θ_i, this part of the combined model is the same as the classical model.

As already noted, the slips d_{ij}, the strains ω_{ij}, and the displacements θ_i in this combined model are the same as in the slip model. However, we need to show that the variables τ_{ij} and ω_{ij} of Chap. II are also proper generalized variables in this model. The displacement field for the expanded edge of Fig. 4 is now

$$u = \ell_o(\bar{u}_P + \bar{u}_Q)/2 + \ell_o(\bar{u}_Q - \bar{u}_P)x/\ell_{PQ} + d_{PQ}y/\ell_o\delta$$
$$v = \ell_o(\bar{v}_P + \bar{v}_Q)/2 + \ell_o(\bar{v}_Q - \bar{v}_P)x/\ell_{PQ} \qquad (5\text{-}21)$$

with $\bar{u}_P$, $\bar{v}_P$, $\bar{u}_Q$, $\bar{v}_Q$ being the averaged displacements of the two adjacent triangle vertices at nodes P and Q respectively. The slip d_{PQ} across the edge is the same as in Eq. (2-5). Using Eq. (2-1) we find the constant strains in the expanded edge:

$$\epsilon_{xx} = \ell_o(u_Q - u_P)/\ell_{PQ} \qquad \epsilon_{yy} = 0$$
$$\gamma_{xy} = \ell_o(v_Q - v_P)/\ell_{PQ} + \omega_{PQ}\ell_o/\ell_{PQ}\delta \qquad (5\text{-}22)$$

Substitution of Eqs. (5-22) in Eq. (2-7) leads directly to the conclusion that also here τ_{PQ} and ω_{PQ} are proper generalized dimensionless stress and strain variables.

Generalized stress and strain are interrelated through the constitutive relation Eqs. (2-12) and (5-11). The shear modulus G is a well defined material property for the classical model. Using the same G in the slip model we can eliminate G' from Eq. (2-12) with Eq. (2-13). This procedure immediately leads to the result that no slip can occur in an edge less than yield. Further, slip can not occur in an isolated edge even if it is at yield, since surrounding edges would force the slip to be zero. Even elastically undetermined displacement unknowns are, due to their bounds, forced to be zero. Therefore, the kinematical variables d_{ij}, ω_{ij}, θ_i will all be zero unless sufficient edges have reached yield stress with the proper sign to form a mechanism as the term is used in Chap. II.

We find it convenient to define new quasi-kinematic variables $\bar{\theta}_i$, etc. by

$$d_{ij} = \bar{d}_{ij}\delta, \quad \omega_{ij} = \bar{\omega}_{ij}\delta, \quad \theta_i = \bar{\theta}_i\delta \qquad (5\text{-}23)$$

Although the barred variables have no direct physical significance, they are related by the kinematic equations (2-1) and (2-4). Further, the constitutive Eqs. (2-12) can be written

IF $|\tau_{PQ}| \le 1$ THEN $\dot{\tau}_{PQ} = G\,\dot{\bar{\omega}}_{PQ}\ell_o/(k\ell_{PQ})$ (5-24a)

ELSE IF $\tau_{PQ}\,\dot{\bar{\omega}}_{PQ} \ge 0$ THEN $\dot{\tau}_{PQ} = 0$ (5-24b)

ELSE $\dot{\tau}_{PQ} = G\,\dot{\bar{\omega}}_{PQ}\ell_o/(k\ell_{PQ})$ (5-24c)

Therefore, the edge stresses τ_{ij} can be computed even though the strains ω_{ij} are zero. In particular, a record can be kept as to which edges are plastic.

C. Boundary Value Problem

We saw in Sec. IIB that if all θ_i in a finite domain were equal, the entire domain would remain unchanged, so that one θ_i could be arbitrarily assigned the value zero. Evidently the same reasoning applies to the combined model. In addition, we can establish two other identities among the kinematic variables.

To this end, we first observe that if we start with a small node mechanism of unit magnitude in Fig. 2, and add large node mechanisms $\theta_B = \theta_C = 2$, the result is to shift square ADBC to the right, but leave it internally undeformed. Applying this same reasoning to the finite domain in Fig. 5, we see that the motion

$$\begin{aligned} &\theta_1 = \theta_6 = \theta_{11} = \theta_{16} = 0 \\ &\theta_4 = \theta_9 = \theta_{14} = 1 \\ &\theta_2 = \theta_7 = \theta_{12} = \theta_{17} = 2 \\ &\theta_5 = \theta_{10} = \theta_{15} = 3 \\ &\theta_3 = \theta_8 = \theta_{13} = \theta_{18} = 4 \end{aligned} \qquad (5\text{-}25)$$

will shift the entire domain as a rigid body to the right. If we then combine (5-25) with a uniform horizontal vertex motion $\dot{u}_i = -\ell_0/\ell$, the net result is that all vertex displacements and strains are zero. Therefore, we can arbitrarily set $u_{16} = 0$, because its associated equilibrium equation can be expressed as a linear combination of the equilibrium equations associated with θ_i and the remaining u_i. Using the same reasoning in the vertical direction we can also arbitrarily set $v_{16} = 0$. Notice that these three arbitrary conditions are inherent in our choice of kinematical variables and are not related to a rigid-body motion of the entire domain. For example, if the boundary conditions in Fig. 5 consisted entirely of prescribed loads, then we could also take, say, $u_1 = v_1 = u_3 = 0$ to suppress an overall rigid-body motion.

Equations (5-18) must be modified if the node B is on the boundary. For example, consider the case where BF in Fig. 39 is part of the top boundary of the domain. Then triangle BHF is part of the domain, BFI is a fictitious triangle as defined in Chap. II and BIG does not exist. It follows that $\bar{u}_1$ and $\bar{u}_2$ are still given by the first two Eqs. (5-18), but that the next two equations for $\bar{u}_3$ and $\bar{u}_4$ must be replaced.

If d_{BF} denotes the boundary slip, then $\bar{u}_3 = \bar{u}_2 + d_{BF}$. In view of Eqs. (2-1) and (2-14) for the slip, this leads to the relation

$$\bar{u}_3 = \ell_0 u_B \tag{5-26}$$

Therefore, at a boundary point B, the variable u_B has an immediate physical interpretation as the dimensionless tangential motion of the boundary. However, the normal displacement $\bar{v}_1$ is still given by (5-15a) which relates it to both v_B and $\theta_B - \theta_F$.

Let us now express the boundary conditions of Fig. 5 in terms of displacement variables. Since $v = 0$ along BC, we can apply Eq. (5-15a) to the two boundary vertices of triangle 11-14-16 to obtain

$$\ell v_{16} + 1/2\, \ell_0(\theta_{11}-\theta_{16}) = 0 \tag{5-27a}$$

$$\ell v_{11} + 1/2\, \ell_0(\theta_{11}-\theta_{16}) = 0 \tag{5-27b}$$

Therefore, since we have set $\theta_{16} = v_{16} = 0$, it follows that $\theta_{11} = v_{11} = 0$. Continuation of this reasoning leads to $\theta_i = v_i = 0$ along BC, and a similar consideration shows that $\theta_i = u_i = 0$ along CD.

Since $u = u_0$ along AB, it follows that

$$u_0 = [\ell u_1 + 1/2\, \ell_0(\theta_2-\theta_1)]\, \ell_0/\ell \tag{5-28a}$$

$$u_0 = [\ell u_2 + 1/2\, \ell_0(\theta_2-\theta_1)]\, \ell_0/\ell \tag{5-28b}$$

$$u_0 = [\ell u_2 + 1/2\, \ell_0(\theta_3-\theta_2)]\, \ell_0/\ell \tag{5-28c}$$

$$u_0 = [\ell u_3 + 1/2\, \ell_0(\theta_3-\theta_2)]\, \ell_0/\ell \tag{5-28d}$$

Equations (5-27) show that $u_1 = u_2 = u_3$ just as in the classical model. Therefore, we find it convenient

to define a new variable

$$u_{0c} = \ell_0 u_1 = \ell_0 u_2 = \ell_0 u_3 \tag{5-29a}$$

Further, with $\theta_1 = 0$, Eq. (2-16) for the slip must hold, and we define

$$u_{0s} = \ell_0{}^2\theta_2/2\ell = \ell_0{}^2\theta_3/4\ell \tag{5-29b}$$

Finally, then, Eq. (5-28) reduces to the constraint

$$u_0 = u_{0c} + u_{0s} \tag{5-29c}$$

A similar argument applied to DE leads to

$$v_{0c} = \ell_0 v_{13} = \ell_0 v_{18} \tag{5-30a}$$

$$v_{0s} = \ell_0{}^2\, \theta_{13}/2\ell \tag{5-30b}$$

$$v_0 = v_{oc} + v_{os} \tag{5-30c}$$

Since the tangential boundary displacements along DE are zero, it follows directly from Eq. (5-26) that $u_{13} = u_{18} = 0$. We note that $u_{18} = 0$ is consistent with the result we obtained along boundary CD.

We can now divide the solution of the combined model problem into two parts, i.e. a slip part for the unknown θ_i and related ω_{ij} and τ_{ij}, and a classical part for u_i, v_i and related stresses and strains.

The slip part of the combined model is almost identical with the slip model of Chap. II, the only difference being that Eqs. (2-16) and (2-18) with u_0 and v_0 are replaced by Eqs. (5-29b) and (5-30b) with

u_{0s} and v_{0s}. The slip model can be solved in terms of the boundary forces T_1 and T_2, or in terms of the displacements $\bar{u}_{0s} = u_{0s}/\delta$ and $\bar{v}_{0s} = v_{0s}/\delta$. Of course a combination of displacements and forces is also possible.

For the classical part, let the displacements u_i and v_i be formally identified with the nodal displacements of the classical model. Then this part is the same as the classical model of Sec. A except that u_{0c} and v_{0c} as given by Eqs. (5-29a) and (5-30a) replace u_0 and v_0 of Sec. A. This part can be solved in terms of the displacements u_{0c} and v_{0c}, in terms of the forces T_1 and T_2, or in terms of a combination of displacements and forces.

If T_1 and T_2 are both prescribed, the two parts of the combined model are completely uncoupled and the displacement solution is simply the sum of the displacement solutions of the slip model and classical model. However, if u_0 and v_0 are prescribed, Eqs. (5-29) and (5-30) must be used to determine u_{0c}, u_{0s}, v_{0c}, v_{0s}, T_1, and T_2 in terms of the given u_0 and v_0, thus coupling the two parts of the problem. We shall discuss a method of doing this in the next section.

D. Solution of the combined model

To allow for progressive plastic behavior we discuss this problem in terms of rates with prescribed velocities $\dot{u}_0$ and $\dot{v}_0$. In the fully elastic range velocity discontinuities are not allowed. In view of Eqs. (5-29) and (5-30) this implies that as δ tends to

zero $\dot{u}_{0s}$ and $\dot{v}_{0s}$ can remain finite. Therefore we can solve the classical model by using Eqs. (5-29) and (5-30). $\dot{T}_1$ and $\dot{T}_2$ are computed from Eqs. (5-12) and (5-13) and used as prescribed quantities to solve the slip model.

The end of a stage is determined by either an edge or triangle. If an edge reaches yield, the stiffness matrix in the slip model is adjusted. Since this does not affect the stiffness matrix of the classical model, the classical rate solution remains unchanged and we need solve only a new slip part.

A triangle may determine the end of a stage for either of two reasons. Obviously a stage must end if any elastic triangle reaches $f = 1$. However, even if no new triangle reaches yield, a stage may still have to be terminated because of excessive stress changes in an already plastic triangle. Since the yield function f in Eq. (5-10) is quadratic, the rate equation $\dot{f} = 0$ corresponds to motion along a tangent to the surface $f = \text{const}$, rather than motion along the surface itself. Large stress changes would therefore lead to values of f much greater than 1 and hence would substantially change the yield criterion. To avoid this occurence, a stage is terminated if f increases by 0.001 in any plastic triangle.

When the end of a stage is caused by a triangle, for either reason, the triangle stiffness matrix must be adjusted. For a previously elastic triangle which

has just reached yield, the adjustment is similar to the Sherman-Morrison formula. However, because all three stress components are involved, the Woodbury formula [13] must be used in place of (2-28). Details may be found in Appendix B.

In addition, the constitutive equation in each plastic triangle depends upon the existing stress state which is, in general, different than at the beginning of the previous stage. Therefore, further adjustments in the stiffness matrix must be made for each plastic triangle.

These changes in the triangle stiffness matrix will, in general, lead to different values of $\dot{T}_1$ and $\dot{T}_2$ and hence to a different problem for the slip rates. Therefore, the classical and slip rate solutions will be different in the next stage.

The solution will continue in this fashion until either a slip mechanism is formed or the yield-point load of the classical model is reached. During this uncoupled range, the solution for the triangle variables is exactly the same as in the classical model and the slip variables are obtained as a simple additional problem at each stage.

Assume that at a certain point during loading the edges at yield are able to form a yielding mechanism. This mechanism is formed as a linear combination of the elementary interior and allowable boundary mechanisms of Figs. 2, 3, and 6. The yielding mechanism

will, of course, be independent of δ so that at least one $\dot{u}_{0s}$ or $\dot{v}_{0s}$ can now be different from zero. In general, it will have one degree of freedom and hence will lead to a relation of the form

$$\dot{u}_{0s} = \alpha \dot{v}_{0s} \tag{5-31}$$

No net external work rate will be associated with this yielding mechanism. Therefore the total external work rate on the domain of Fig. 5 must satisfy

$$\dot{W}_{ext} = 0 = (2/3 \dot{T}_2 \dot{u}_{0s} + 1/3 \dot{T}_1 \dot{v}_{0s})/\ell_0 \tag{5-32}$$

hence

$$2\alpha \dot{T}_2 + \dot{T}_1 = 0 \tag{5-33}$$

The classical part can now be solved with $\dot{u}_{0s}$ and $\dot{v}_{0s}$ as additional variables and with Eqs. (5-31) and (5-33) as additional equations. A necessary condition to maintain the yielding mechanism is that no unloading occurs in edges that make up this mechanism. If $\dot{v}_{0s}$ must be, say, positive in order to have no unloading in the initial mechanism, then no unloading will occur as long as $\dot{v}_{0s}$ remains positive in subsequent stages.

Obviously Eq. (5-33) is automatically satisfied in the slip model. Therefore the slip model can be solved by taking for example $\dot{T}_1$ as an interaction force between the slip part and the classical part, and we can set $\dot{u}_{0s}$ equal to zero.

The yielding edges can now be divided into two

groups. The first group contains all the yielding edges that are part of the yielding mechanism, and the second group contains the remaining yielding edges. The verification that no unloading occurs in the first group is done in the classical part, as described above. The no unloading check for the edges of the second group is, of course, done in the slip part.

We continue solving the new stages in this partly-coupled range with one interacting force rate until either the expanded classical part reaches limit load conditions or the yielding edges are able to form a second yielding mechanism. In the latter case this mechanism is also formed as a linear combination of the elementary interior and boundary mechanisms. This second yielding mechanism is also independent of δ, and the two mechanisms are also independent of each other. Therefore we now have two degrees of freedom so that both $\dot{u}_{0s}$ and $\dot{v}_{0s}$ can be different from zero. Since neither of these displacement rates will cause a net external work rate we must necessarily have

$$\dot{T}_1 = \dot{T}_2 = 0 \qquad (5\text{-}33)$$

Hence the model has reached the limit load.

As previously mentioned, either the uncoupled range or the partly-coupled range could terminate with the formation of a limit-load mechanism in the classical model. However, this contingency did not occur in any of the examples considered herein.

Chapter VI Example of Combined Model

The Prandtl rough punch problem was solved in Chap. II according to the slip model. In this chapter the same problem is solved for both the classical and the combined model, taking $\nu = 0.3$. The same arrangement is used as before (Fig. 9). Obviously, we have the same boundary conditions as in the slip model. Therefore, the present problem is a special case of the one described in Sec. VC with $u_0 = 0$ and $v_0 = -\ell_0 v^*$.

The load deflection curves are shown in Fig. 41. The yielding sequence of the edges and the triangles for the 76 stages of the uncoupled range is shown in Fig. 42. In this range the classical part of the solution is exactly the same for the classical and combined models. However, the slip part of the solution with the combined model is not identical with that of the slip model, since the stress solution interacts with the reaction forces of the classical part, even in the absence of slip. As might be expected, these differences grow as the load increases. A comparison of Figs. 11 and 42 shows that the first three edges to yield in the slip model are the first three to yield in the same order in the slip part of the combined model. The first eight edges to yield in the slip model are among the first nine, but in different order, to reach the yield stress in the slip part of the combined model.

However, in the slip model edge pv yields at the end of stage six and unloads at the beginning of stage ten to remain elastic, whereas it reaches and leaves the yield stress several times in the slip part of the combined model. Further, the ninth edge to yield in the slip model is only the 14th to reach yield in the slip part of the combined model, and the tenth yielding edge in the slip model is the 23rd in the slip part of the combined model.

As in the slip model solution, more than one edge may reach yield at the same time, as in stages 72, 73, and 76. In this example we never find two triangles reaching yield at the same time, although the phenomenon could certainly occur. However, at the end of stage 68 we find both one triangle and one edge reaching yield. None of the above cause any difficulty; the adjustment formulas are just applied for each yielding domain.

We also find that several stages are ended by an 0.001 increase in f. Specifically, this happens to end stages 19, 25, 29, 34, 38, 47, 50, 55, 57, and 69.

It is interesting to note that even though edge yielding in the uncoupled range does not influence the load deflection curve, the elastic limit of the combined model occurs at $T_1 = -2.52$, $v^* = 0.32\ G/k$ when edge pq reaches yield, whereas the fully elastic range in the classical model is terminated when triangle Δpq

yields at $T_1 = -2.76$ and $v^* = .35G/k$.

Actually, except for a change of sign, Fig. 42a compares more favorable with Fig. 28, i.e. the yielding sequence of the double edge notched tensile bar solved with the slip model, than it does with Fig. 11. The difference between the two problems is the boundary condition along the outside edge AB. For the notched bar the force is prescribed zero and the displacements along AB are not restricted, whereas $u_0 = 0$ in the punch problem. However, in the combined model this constraint is on the total displacement $u_0 = u_{0c} + u_{0s}$, Eq. (5-29c), which allows for certain freedom in $\bar{u}_{0s}$.

As evidence of this agreement we note that we need only to interchange stages 3 and 4, stages 8 and 10, and stages 11 and 12 to obtain the same yielding sequence in the edges during the first twelve stages with the punch problem solved with the combined model and the double edge notched bar solved with the slip model.

At the end of stage 73 in the punch problem an undetermined slip mechanism becomes possible in the lower right corner. This mechanism is identical with the mechanism of the notched bar at stage 41 as is shown in Fig. 30. However, since no boundary motions are involved in the mechanism, there is still no coupling between the triangle and the slip parts of the model.

Stage 76 marks the end of the uncoupled range as seven edges yield simultaneously and produce a situation similar to the multiple collapse mode for the slip model of the double edge notched bar. Indeed, with a change of direction any of the mechanisms of Figs. 31 a, b, c, d, f, h, j, or any combination thereof are possible for the slip part of the combined model. As we found in Sec. IV-B, the difference in the displacement fields of cases h and f is the undetermined combined mechanism of Fig. 30 at the bottom and the undetermined single mechanism at node o at the top. Other undetermined mechanisms are obtained if we subtract case b from case a, case c from case b, case d from case c, case f from case a, and finally, case j from case i where case i is the average of cases f and h. The six additional undetermined mechanisms at the end of stage 76 cause certain complications which can be handled by an extension of the method used at the end of stage 40 in the double-notched bar example in Chap. IV; they affect only the slip part of the solution. All mechanisms of this multiple collapse mode involve the same motion at the boundaries, hence in all cases Eqs. (5-31) and (5-33) become, for this size domain,

$$\dot{v}_{0s} = 6\,\dot{u}_{0s} \qquad \dot{T}_1 + \dot{T}_2 = 0 \tag{6-1}$$

As described in Sec. V-D, we enter a new phase of the solution, where we have one interacting force between the classical part and the slip part. As a

consequence the loading conditions of the classical part change. This change has a dramatic effect on the behavior of the triangular elements in that more than half of the elements which were yielding at the end of stage 76 (17 out of 29), now start to unload. In Fig. 43b, p. represents an element which was yielding at stage 76 and continues to do so until collapse, circles are elements which unload from yield at the start of stage 77, and numbers indicate the few elements which first become plastic in later stages.

Figure 41 shows that in this phase the load-deflection curve is no longer the same as the classical model due to the slip in the domain. Computation in this phase continues until the end of stage 91 when four simultaneously yielding edges cause limit load conditions.

The limit load is the same as we found for the Prandtl rough punch with the slip model. Moreover we have the same limit load mechanisms as illustrated in Fig. 13. During this loading a slight increase in the yield surface of some triangles was noted due to linearization of the constitutive equations and a maximum of 0.1% was allowed in any one stage. The resulting total increase in the yield surface was less than 1.0% at the end of the uncoupled range and less than 2.0% at the yield point load. In view of these small increases we feel justified in accepting these results without correction for the elastic/perfectly-plastic material behavior.

Also shown in Figure 41 is the continuation of the load deflection curve for the classical model up to stage 115 when the load was about 14% above the yield-point load for the combined model. Further computation up to stage 153 increased the load to about 30% above the combined yield-point load and caused plastic flow in more than half the triangles, as shown in Fig. 44, but still did not produce a yield-point mechanism. This phenomenon will be commented on in the concluding chapter.

Chapter VII More Combined Model Examples.

In this chapter we apply the combined and classical models to the examples discussed in Chap. IV for the slip model. Thus we consider here the Prandtl punch problem with a lubricated punch material contact, the deep double edge notched tensile specimen, and the single edge notched tensile specimen.

A. Smooth Punch

The difference between the smooth punch and the rough one is that in the tangent direction along DE (Fig. 9) the former prescribes zero traction force whereas the latter prescribes zero displacments. Since there is no traction force under the punch we have zero stress in edge qw (the notation is defined in Figs. 46, 47, and 48), which is hence deleted. Also u_q is no longer suppressed.

The slight modification of the boundary conditions has an imperceptible effect on the load-deflection curves in Fig. 41 and the fully elastic displacement field of Fig. 45 for the rough punch. However, the stages in the load-deflection curve are not identical, so that the numbers on the curve refer to the end of the stages of the rough punch only.

The sequence of yielding edges for the first ten stages is exactly the same for the rough and smooth punch, and Figs. 42 and 46 are very much alike in the

entire uncoupled phase. The important differences are that at the end of stage 53 (T_1 = - 5.48) we have an elastically undetermined unit mechanism at node s, and that at the point where the combined model separates from the classical model at the end of stage 73 (T_1 = - 5.67) the yielding of the edge connected with node b causes an additional elastically undetermined combined mechanism. These two mechanisms cause two more variations of the yielding mechanisms found for the rough punch at the separation point. They are the compressive analogue of Fig. 31 e and g.

In the second phase of the combined model solution, where we have one interacting force between the slip and classical part, Eq. (6-1) also holds. Figure 47 shows the continuation of the yielding sequence in the edges and triangles.

As with the rough punch, the limit load and possible mechanisms for the combined model are identical with those found earlier for the slip model, i.e. Figs. 13 and 22.

With the classical model the limit load had not been reached at a load 24% higher than the analytical limit load, and the computation was stopped at that point. The yielding sequence is shown in Fig. 48 in the same fashion as we showed Fig. 44 for the rough punch.

B. Double edge notched problem

The main difference between the punch problems and the double edge notched problem is that the condition of zero normal boundary displacement along AB in Fig. 9 is replaced by the condition of zero normal force (see Fig. 25). Therefore we no longer find an intermediate coupled range but we go directly from the uncoupled range to the limit load. As a consequence we have only one interacting force between the slip part and the classical part of the combined model and the solution of the combined model can be obtained by simply adding the displacements and equating the boundary force of the two parts.

The slip part of the combined model is indistinguishable from the slip model which is discussed in Sec. IV B. The difference is that presently the unknowable shear modulus in Eq. (2-12) is replaced by Eq. (2-13). Therefore the displacements due to the slip part are zero until limit load conditions are obtained, i.e. rigid perfectly plastic behavior. At limit load conditions the magnitude of v_{0s} is indeterminate.

The classical part of the combined model is the same as the classical model until the slip part causes a yielding mechanism at which the combined model reaches limit load conditions. The load-deflection curves are shown in Fig. 49 and the yielding sequence of the

triangles is shown in Fig. 50. The Poisson ratio was 0.3. Comparing the displacement field in the fully elastic range with the slip model (Fig. 26) and the classical model with Poisson ratios of respectively .49 (Fig. 27) and .3 (Fig. 51), we observe that the slip model results correspond better with the almost incompressible classical model. The results of the slip model in Fig. 49 are hence normalized in the fully elastic range with the almost incompressible classical model.

The difference between the slopes of the classical model solutions in the fully elastic range with Poisson ratios of respectively .49 and .30 is smaller than we obtained with the punch examples, Figs. 41 and 49. This can be understood because the material along side AB in Fig. 27 can move horizontally in this tensile specimen, which is prohibited in the punch of Fig. 16.

C. Single edge notched specimen

This problem differs from the double edge notched bar only in that CD is a traction-free boundary rather than a line of symmetry. For this reason we change one of the arbitrary kinematic constraints to $\theta_u = 0$ (corner node D) instead of $u_t = 0$ (corner node C). Also, we set $u_w = 0$ at D to specify the arbitrary horizontal rigid-body motion of the entire bar.

As with the double-notched bar, there is only

one coupling equation so that the combined-model solution can be obtained directly from the classical and slip models.

The load deflection curve and the yielding sequence of the triangles with the classical model are shown in Figs. 52 and 50 for a Poisson ratio of 0.3.

The displacement field in the fully elastic range of the slip model, Fig. 33, compares more favorably with the fully elastic range of the classical model with $\nu = .49$, Fig. 34, than it does with the fully elastic range of the classical mode with $\nu = .30$, Fig. 54. Therefore the unknowable shear modulus G' in the slip model is obtained by equating the fully elastic range of the slip model and classical mode ($\nu = .49$). The adjusted slip model load deflection curve is also shown in Fig. 52.

Poisson's ratio has less influence in the present problem than it has in previous problems. This can be explained because material can also move horizontally along boundary CD which is prohibited in all previous examples.

Chapter VIII Conclusions

In the present thesis three elastic/perfectly plastic plane strain finite element models are discussed. The classical model of Turner et al [3] has deformable triangles and a continuous velocity field, the slip model has rigid triangles and velocity discontinuities, and the combined model has deformable triangles and velocity discontinuities. As is shown in Chap. V the combined model can be separated into slip and classical parts, which are interrelated by boundary forces and are virtually the same as the corresponding models. Indeed, if there were no kinematic boundary conditions they would be exactly the same.

Different models may be compared by examining their methodology and their results. We shall first look at the various results obtained for the Prandtl rough punch problem treated in Chaps. III and VI. Comparisons will include elastic solutions, formation of plastic regions, load-displacement curves, and yield-point solutions.

We shall compare results of the three models with each other and with any other available information.

The elastic solutions for the combined and classical models are the same. The displacement pattern is shown in Fig. 16 for $\nu = 0.49$. It agrees well with

that of an analytic solution for a semi-infinite domain with $\nu = 0.50$ [14,15] shown in Fig. 15 except, of course, near the boundaries. Rather surprisingly, the relative displacements predicted by the slip model, Fig. 10, also show good agreement. However, the slip model does not depend on Poisson's ratio ν, and Fig. 45 for $\nu = 0.30$ shows that the classical model is highly sensitive to values of ν.

Figures 11, 42, 43, and 44 show the growth of the plastic regions for the various models. In Fig. 55 we have shown those elements which become plastic by the time the load reaches the continuum yield-point load value, $2 + \pi$, together with the continuum region of plastic flow associated with that load. The three models agree in predicting that the plastic domain extends well below the flow region, but it is difficult to make any other meaningful comparisons.

Load-displacement curves are shown in Fig. 41. Curve (d) is for the slip model with G' determined so as to give the same elastic slope as the other models for an incompressible material. Curve (a-c) is for the classical model with $\nu = 0.30$ and again shows the strong influence of Poisson's ratio. The combined model (a-b) also follows this curve in the elastic and uncoupled-plastic range, but then rapidly approaches curve (d) as the load increases to the yield-point load.

For the semi-infinite domain, Prandtl [9] obtained the dimensionless load $2 + \pi = 5.14$. Prager and Hodge [10] identified this value as an upper bound, and Shield and Drucker [16] later showed it was also a lower bound and hence the true yield-point load for the semi-infinite domain. Since the flow region of the Prandtl solution lies within the finite domain considered here, $2 + \pi$ is also an upper bound for the finite domain we are considering. Although no firm conclusion can be drawn since the box sides are smooth, it seems probable that the box is as constrained as the semi-infinite domain, so that $2 + \pi$ may tentatively be taken as the exact continuum yield-point load.

All three models are based on velocity fields which are kinematically admissible from the viewpoint of the continuum, so that their yield-point loads should be upper bounds on that of the continuum. For the slip and combined models the value 6.0 is obtained which certainly satisfies this condition. The computation for the classical model was stopped at a load of 7.2 which is greater still.

As mentioned in Chaps. III and VI the yield-point mechanisms for the slip and combined models are far from unique so that no real information is available here. Among the possibilities is the one in Fig. 13b which closely resembles the Prandtl continuum solution

in Fig. 17.

To compare the computational aspects of the various models we focus our attention on the number of unknowns of each model, the method by which stiffness matrix is assembled and "inverted", the way yielding is handled, the unloading in yielding triangles and edges, the singularities in the stiffness matrix, the memory requirements of the computer program, and the necessary computation time.

The slip model has on the average one degree of freedom per node. For the classical and combined models these numbers are respectively two and three. As is discussed in Chap. V, the combined model separates into a classical part and a slip part, which are similar to the corresponding models. The two parts are connected on a few spots on the boundary. Therefore, the computer program for the combined model uses large parts from the computer programs for the slip and classical models.

Most of the existing finite element programs use the direct stiffness method [12], i.e., the stiffness contribution of an element is computed and directly added to the stiffness matrix of the entire problem. In our models this computation method is used for both the edges and the triangles.

Once the stiffness matrix is computed, its

product with the vector of basic unknowns is set equal to the known force vector and solved. In an elastic-plastic problem, this solution must be obtained in each stage. This computation is frequently done with the decomposition method of Cholesky [12], i.e., the stiffness matrix is divided in an upper and lower triangular matrix. However, in our case the stiffness matrix at each stage differs from that of the preceding stage in only a few elements. The Woodbury and Sherman-Morrisson formulas [13] allow us to make these adjustments directly in the inverted matrix. Therefore, we decided to invert the fully elastic stiffness matrix rather than use the method of Cholesky.

This method is particularly advantageous when a new stage is caused by a yielding edge. Since there is only one generalized stress per edge, a yielding edge implies a one-time adjustment of the inverted stiffness matrix. A triangle, on the other hand, has three generalized stresses. The plastic strain rates depend on the stress state which may vary during loading. This requires re-adjustment of the inverted stiffness matrix in triangles already at yield. For this reason, the slip part or model is much more economical than the classical part or model.

Unloading is handled automatically for both triangles and edges. The program checks that the work

rate for each yielding element is positive. If it is negative for one element, the rate problem is solved with that element again assumed elastic. If more than one element has negative work rate, the element with the numerically largest work rate is set elastic, a new rate solution is found and checked, and the process is continued until all elements at yield are either plastic with non-negative work rate, or elastic with non-increasing yield function.

Singularities are handled automatically if they are due to an elementary mechanism such as in Figs. 2 and 3. However, if a linear combination of elementary mechanisms is causing the singularity, as in Fig. 30, the program will exit and store the necessary data. The mechanism needs to be found manually and the program restarted. Also, an a posteriori manual check is required on the sign of the work rate in the edges of the singular mechanism. These manual readjustments are obvious drawbacks to the present versions of the slip model and combined model, but one could presumably develop a more sophisticated program which would be fully automatic.

Because large parts of the central memory can be made free by using peripheral memory, the storage requirements do not form a proper base to evaluate the program.

Based upon very limited information, the slip model appears to be the most efficient in terms of CPU time. For the double notched specimen with 71 degrees of freedom, the total CPU time up to the yield-point load was 31 seconds, or a measure of 0.44 seconds per degree of freedom (s/dof). The figures for the combined model for the Prandtl punch are 130/211 = 0.62 s/dof and for the classical model punch they are 80/146 = 0.55 s/dof. It is interesting to note that whereas the slip part alone took only about 30 seconds, it added 50 seconds in its interaction with the classical to form the combined model. It would be worth studying where that extra 20 seconds went in order to make the combined program more efficient.

Although we were able to use the different models to obtain numerical results, we encountered various difficulties in both modeling and computation. These problems are now discussed for the classical, slip, and combined models respectively.

With the classical model we observe that during early loading conditions the results of this model coincide with the classical part of the combined model. For the punch problem this is up to the separation point and for both notched problems it is up to the limit load. The classical model results can be extracted in this range from the combined model results

by deleting the slip part. This is due to the fact that the kinematic variables associated with the slip part are effectively zero.

When we were considering the computational aspects the Woodbury formula was mentioned. Because the stress state of a yielding triangle is changing, the stiffness matrix may need to be adjusted frequently for every triangle at yield. The modification of the inverted stiffness matrix for every triangle at yield--especially when there are many triangles at yield--is most likely uneconomical compared with the adjustment of the non-inverted stiffness matrix and the decomposition method of Cholesky. Further research in this matter is desired.

Another problem we encountered with the classical model is in reaching the limit load. As mentioned on the introduction, the element arrangement we use should leave sufficient degrees of freedom to reach the limit load.

To clarify this problem we focus our attention at the results of the Prandtl punch problem of Chap. VI. Without any difficulty we reach, at the end of stage 153, a compressive load $-T_1$ of 7.23. Starting from stage 154 a stage was only determined by the yielding of another triangle and no verification was made on unloading. The answers are acceptable up to

and including stage 163 when $-T_1 = 7.25$. Up to this stage, the slope of the load-deflection curve never increased, and at this stage the slope is .01% of the fully elastic slope. However, after this stage the numerical scheme appears to become unstable. Large stress increments are observed, and the slope of the load deflection curve begins to increase. These indications of instability continued, and hence computation was halted at stage 163.

Since the elastic-plastic approach did not predict a limit-load, we used the upper bound theorem of plasticity to show that the true limit load for the model is $T_1 = -7.23$. Details are given in Appendix C. The slight overshoot of the classical model in stages 154-163 is presumably due to the linearization of the constitutive equations in the yielding triangles.

The instability is presumably related to the constraint of incompressibility of the plastic strains. Although we theoretically have 83 degrees of freedom left, the computation scheme may be inadequate to handle them. Using a classical model based on constant dilatation isoparametric elements, Nagtegaal et al [8] were able to obtain a satisfactory approach to the limit load for the double-edged notched bar.

The problems concerning the slip model are the edge expansion, the singularities in the stiffness

matrix and the way they are handled, the unloading in yielding edges, and the limit load values.

In Chap. II we stated that an equal expansion of every edge is assumed. Unequal expansion will influence the results. This can be understood when we observe that all kinematical and statical relations are independent of the edge expansion. The constitutive behavior, Eq. (2-12), (2-13), shows that the elastic stress rate is linear in the strain rate, but is inversely proportional to the dimensionless area of the expanded edge ($\ell_{PQ}\delta/\ell_o$).

A reason why the edge expansion should not be dependent on the edge length can be demonstrated with Fig. 2. The edges CO and OD are expanded an equal amount. Because of compatibility the strains are equal in both edges, and due to the constitutive equations the stresses in both edges are equal. The two edges can hence be considered as a single edge. The expansion of this single edge is the same as the two separate edges although this single edge is twice as long.

The singularities which occurred in the stiffness matrix were quite unexpected. This is a topic which deserves further research. Singularities are caused by an equilibrium equation that becomes a trivial identity.

A necessary requirement for the creation of a

singularity is that at least two edges yield simultaneously. This can be understood when we consider a homogeneous equilibrium equation with only two nonzero stress rates left. This equilibrium equation can only become a trivial identity when both stress rates vanish simultaneously. In the case where one stress rate vanishes, the other stress rate is automatically zero due to the equilibrium equation.

This consideration suggests a possible way to escape singularities from the computational viewpoint. In any case where two edges, say A and B, yield simultaneously the adjustment of the stiffness matrix due to edge A is easily carried out with Eq. (2-28).

Now, if A and B were not the last two elastic edges in some equilibrium equation, the adjustment of the stiffness matrix due to edge B can be carried out in a normal manner. However, if they were the last two, an attempt to adjust the stiffness matrix due to edge B will result in a zero denominator in Eq. (2-28b). In this case we keep the stiffness matrix such that edge B remains elastic. Due to the equilibrium equation the resulting solution will necessarily predict $\dot{\tau}_B = 0$. Since B is now assumed elastic $\dot{\omega}_B = 0$ also, and a unique velocity field will be obtained.

However, the resulting strain-rate field may or

may not be acceptable. For example, in the small problem considered in Sec. II-D, at the end of stage 5 edges 6-7 and 7-12 both yield. If we let only 6-7 be plastic, the unique solution will include $\dot{\omega}_{7-12} = \dot{\theta}_9 = 0$ which satisfies Eq. (2-35). However, if we had let only edge 7-12 be plastic, $\dot{\omega}_{6-7} = 0$ would lead to $\dot{\theta}_9 = -5\dot{d}/16$ which violates Eq. (2-35). Thus, this suggested procedure might lead to other problems. As we mentioned, this topic needs further research.

Another way to avoid singularities is to assume a slight work hardening. This has, however, the disadvantage that a terminal slope in the load deflection curve will occur and there will not be any limit load.

Unloading of edge is another problem. In Fig. 28 for the double edge notched tensile specimen, we note that quite a large number of edges started to unload after they reached yielding conditions. Most of these edges become plastic again during later loading conditions. This unloading was unexpected because the external load was monotonically increasing. It is by no means clear whether this phenomenon is a true feature of the continuum, if it is a pecularity of the slip model, or if it is a result of numerical imprecision. To see if this unloading influences our results significantly we ran the same problem again

with a relaxation of the constitutive equation such that an edge remains at yield once it becomes plastic. To the scale used in Fig. 29 the load deflection curve did not show any change. As far as the yielding sequence is concerned, four edges yielded out of sequence and we had one additional yielding edge. This indicates that unloading should be considered as an insignificant feature, at least in this example.

To conclude our discussion of the slip model we want to point out that by taking a different finite element arrangement the limit load can most likely be brought down. This is discussed in the last part of Chap. III with Figs. 18-20 as illustrative examples.

Although the combined model can be considered as the sum of the classical and the slip models, it does have its own characteristics, such as its behavior at the separation point. Other considered aspects are the global behavior of the slip part and an alternative approach to the computations.

We already mentioned that the classical model and combined model coincide during early loading conditions. The usefulness of the modified Woodbury formula as discussed earlier also applies here. The questions of the edge expansion, the singularities in the stiffness matrix and the way they are handled, the unloading in yielding edges, and the limit load

values are identical with the slip model.

To illustrate the features at the separation point with the classical model we will use the Prandtl rough punch of Chap. VI. At the separation point we get multiple slip patterns. These slip patterns are equivalent. At this point we have seven singularities which cause eight different slip patterns, which are all associated with the same boundary motion. As a consequence, the classical part changes from a displacement controlled problem into a force controlled problem, i.e., Eq. (6-1) must hold. This causes quite a change in the classical part. The unloading we observe in the classical part is significant. The stress state of the shaded area in Fig. 43b drops at least 10% from the yield value when limit load conditions are reached. Starting from the separation point edges start to yield in the same pattern as we observed in the slip model. At the limit load the same yielding mechanisms are found as with the slip model.

The function of the slip part can be seen as a supplementary yield surface for the entire domain with built-in yielding mechanisms. Up to the separation point this surface is not reached. At the separation point it is reached and we get a normality criterion as formulated by Eq. (6-1). Further loading then finally leads to the velocity fields already obtained

with the slip model.

When we were reviewing the computational aspects we noted that the combined model was the most computer time consuming model. An alternative solution procedure might improve the efficiency of this model. First we solve the Prandtl punch problem with the classical model, either partially or entirely, and save the boundary reaction forces. Secondly, the slip model is solved and the boundary reaction forces are now used as external loading conditions. In case we solved the classical model beyond the separation point, the slip model will form yielding mechanisms so that the separation point will be easily located. After the separation point we know there is only one interaction force between the slip part and the classical part. Hence the slip model computation can be continued up to the point where the limit load is found. Thirdly, the classical model is restarted at a stage before the separation point. The classical model continues to compute up to the separation point. At the separation point the slip mechanism is added to the classical model. Computation then continues until the collapse load already found with the slip model. If this method does not save computer time it will at least save memory space in comparison with the procedure used in this thesis.

To illustrate that the present research is a base for future research we would like to mention some possible extensions.

The slip model used here is a close analogy to the plate bending model developed by McMahon and Hodge [21]. In that model, bending occurs "between" triangles and the triangles themself remain rigid. It would be interesting to extend their method to a combined bending model in which the triangles are no longer rigid.

The bending model as well as our three models can be extended to arbitrarily shaped triangles. In Appendix A the kinematic relations are given for the combined model. It is also shown that the slip and classical models are subcases of the combined model. The derivation of stress-strain relations, constitutive equations, and equilibrium equations should be done in the same manner as derived in Chaps. II and V.

Another topic might be to study problems where there are several interaction forces between the slip part and classical part of the combined model. How should prescribed displacements tangent to the boundary be handled?

In all our models we assumed plane strain. Of course, plane stress can be investigated too. However, we should realize that the rigid slip model will behave

the same as in the plane strain situation. The compressible classical model (part) is, of course, sensitive for a change to plane stress but the incompressibility constraint near limit load conditions does not cause locking up degrees of freedom, which eases the conditions near the limit load.

If the constitutive equations for the slip model are interpreted in the same way as in the slip part of the combined model we create a rigid perfectly plastic material. Because small displacements are assumed in our derivation, the slip model will give the initial velocity field in this case. As applications we think about extrusion, drawing, and rolling.

Another aspect to be investigated is the usefulness of the newly presented models. How can we obtain the maximum information out of these models? One possible way is indicated at the end of Chap. III where it is shown that a different element arrangement can bring down the limit load. This indicates that we can solve a problem with the slip model for various element arrangements. With this cheap solution model we can take the element arrangement which gives the lowest limit load, and solve the combined model. We know that the limit load of the combined model will not exceed the one found with the classical model. This chosen element arrangement does not imply the best

arrangement for the fully elastic range. Because the slip part and classical part of the combined model are weakly connected we might take different element arrangements for the two parts in certain areas of the domain.

The application of the slip and combined models in three dimensions needs to be explored.

Based on the present information we are now able to evaluate the various models.

The classical model gives rather good results in early loading conditions. Due to the plastic incompressibility constraint we get a loss of degrees of freedom "near" limit load conditions. Unless special element arrangements are made we have no degrees of freedom left. With the special element arrangement we still get a numerical instability near limit load conditions.

The slip model has the disadvantage of having an undetermined shear modulus, which needs to be determined by other means. The results are applicable for incompressible materials. An advantage is that no loss of degrees of freedom occurs near the limit load. This model produces rather good limit load mechanisms, which can be non-unique.

The combined model behaves like the classical model in early loading stages and like the slip model

near the limit load. Hence it is combining the good features of both models. It is a compressible model in which velocity discontinuities can occur as is observed in perfectly plastic materials.

BIBLIOGRAPHY

[1] A. Hrennikoff, Solution of problems of elasticity by the framework method, J. Appl. Mech., 8, A169 - A175 (1941).

[2] D. McHenry, A lattice analogy for the solution of stress problems, J. Inst. Civil Engrs., 21, No. 2, 59-82 (1943-1944).

[3] M. J. Turner, R. W. Clough, H. C. Martin, and L. J. Topp, Stiffness and deflection analysis of complex structures, J. Aero. Sci., 23, 805-823 (1956).

[4] E. Reissner, On a variational theorem in elasticity, J. Math. Physics, 29, 90-95 (1950).

[5] P. G. Hodge Jr., "Continuum Mechanics", McGraw-Hill Book Co., New York, 1970.

[6] P. G. Hodge Jr., A consistent finite element model for the two-dimensional continuum, Ingenieur-Archiv, 39, 375-382 (1970).

[7] A. A. Gvozdev, The determination of the value of the collapse load for statically indeterminate systems undergoing plastic deformation, "Proceedings of the Conference on Plastic Deformations", Akademiia Nauk SSSR, Moscow-Leningrad, 19-33 (1938); translation into English by R. M. Haythornthwaite, Int. J. Mech. Sci., 1, 322-335 (1960).

D. C. Drucker, H. J. Greenberg, and W. Prager, The safety factor of an elastic-plastic body in plane strain, J. Appl. Mech., 18, 371-372 (1951).

D. C. Drucker, W. Prager, and H. J. Greenberg, Extended limit design theorems for continuous media, Q. Appl. Math, 9, 381-389 (1952).

R. Hill, On the state of stress in a plastic-rigid body at the yield point, Phil. Mag., 42 (7), 868-875 (1951).

R. Hill, A note on estimating the yield-point loads in a plastic-rigid body, Phil. Mag., 43 (7), 353-355 (1952).

[8] J. C. Nagtegaal, D. M. Parks, and J. R. Rice, On numerically accurate finite element solutions in the fully plastic range, Comp. Meth. Appl. Mech. & Engr., 4, 153-177 (1974).

[9] L. Prandtl, Ueber die Haerte plastischer Koerper, Goettinger Nachr, Math-Phys., KL1920, 74-85 (1920).

[10] W. Prager and P. G. Hodge Jr., "Theory of Perfectly Plastic Solids", Wiley, New York, 1951.

[11] W. Prager, The general theory of limit design, "Proc. 8th Intern. Congr. Appl. Mech.", Istanbul 1952, 2, 65-72 (1956).

[12] C. S. Desai and J. F. Abel, "Introduction to the Finite Element Method", van Nostrand, New York, 1972.

[13] G. Dahlquist and Å. Bjorck, "Numerical Methods", CWK Gleerup, Bokfoerlag, Lund, Sweden, 1969; translated into English by N. Anderson, Prentice-Hall, Englewood-Cliffs, 1974.

[14] L. M. Milne Thomson, "Plane Elastic Systems", Springer Verlag, Heidelberg, 1968.

[15] A. E. Green and W. Zerna, "Theoretical Elasticity" Clarendon Press, Oxford, 1954.

[16] R. T. Shield and D. C. Drucker, The application of limit analysis to punch identation problems, J. Appl. Mech., 20, 453-460 (1953).

[17] P. G. Hodge, Jr., Approximation solutions of problems of plane plastic flow, J. Appl. Mech. 17, 257-264 (1950).

[18] R. Hill, The plastic yielding of notched bars under tension, Q. J. Mech. Appl. Math., 2, 40-52 (1949).

[19] J. H. Argyris, S. Kelsey, and H. Kamel, Matrix methods of structural analysis, a precis of recent developments, "AGARD"; edited by B. M. Fraeijs de Veubeke, Pergamon Press, New York, 1964.

[20] S. P. Timoshenko and J. N. Goodier, "Theory of Elasticity", McGraw-Hill, New York, 1970.

[21] A. McMahon and P. G. Hodge, Jr., A simple finite element model for elastic-plastic plate bending, DOMIIT 1-46.

[22] R. Hill, On the state of stress in a plastic-rigid body at the yield point, Phil. Mag., 42 (7), 868-875 (1951).

R. Hill, A note on estimating the yield-point loads in a plastic-rigid body, Phil. Mag., 43 (7), 353-355 (1952).

[23] International Mathematical & Statistical Libraries, INC., Houston, Texas, USA 77036.

Appendix A Kinematics for arbitrary shaped elements

In this appendix, the slip, strain, and displacement relations for the slip model are given where the elements are arbitrary triangles. The relations are justified by showing that the normality conditions across an edge are satisfied, and that the equations in Chap. II are a subclass of this general case. The appendix ends by giving the kinematic relations for the vertex displacements of the arbitrary shaped triangles for the combined model and shows that the kinematic relations in Chap. V are reduced from these relations.

The strain in edge AB of Fig. 56 is given by

$$\omega_{AB} = [(\theta_C-\theta_B)\cot\alpha_1 + (\theta_C-\theta_A)\cot\beta_1 + (\theta_D-\theta_B)\cot\alpha_2 + (\theta_D-\theta_A)\cot\beta_4]/2 \qquad (A\text{-}1)$$

with similar relations for the remaining edges. The strain-slip relations are again given by Eq. (2-1).

To show that the normality conditions across an edge are satisfied, it is sufficient to consider the effects of one arbitrary nonzero displacement, say θ_A. Hence, we get for the edges AB, DB, and BC

$$\begin{aligned} \omega_{AB} &= -\theta_A(\cot\beta_1 + \cot\beta_4)/2 \\ \omega_{DB} &= \theta_A(\cot\beta_3 + \cot\beta_4)/2 \\ \omega_{BC} &= \theta_A(\cot\beta_1 + \cot\beta_2)/2 \end{aligned} \qquad (A\text{-}2)$$

Using the geometrical relations

$$\ell_{DB} = \ell_{AB} \sin\beta_4(\cot\ \beta_3 + \cot\ \beta_4)$$
$$\ell_{BC} = \ell_{AB} \sin\beta_2(\cot\ \beta_1 + \cot\ \beta_2) \qquad \text{(A-3)}$$

and Eq. (2-1), we obtain

$$d_{AB} = -\theta_A \ell_o^2(\cot\ \beta_1 + \cot\ \beta_4)/(2\ell_{AB})$$
$$d_{DB} = \theta_A \ell_o^2/(2\ell_{AB} \sin\beta_4) \qquad \text{(A-4)}$$
$$d_{BC} = \theta_A \ell_o^2/(2\ell_{AB} \sin\beta_1)$$

The domain outside the drawn triangles of Fig. 56 remains at rest. Because of the nonseparation requirement across edge DB and BC, the displacement of triangle ADB and ABC are respectively d_{DB} and d_{BC}. Therefore, the requirements across edge AB require

$$d_{DB} \sin\beta_4 = d_{BC} \sin\beta_1 \qquad \text{(A-5)}$$
$$d_{AB} = -d_{DB} \cos\beta_4 - d_{BC} \cos\beta_1$$

which are met with Eq. (A-4). Since θ_A was an arbitrary displacement and since the principle of superposition can be used, the above kinematics are a proper base for any displacement field. The constitutive equations are the same as Eqs. (2-12), and the equilibrium equations can be obtained as in Sec. IIC.

Substituting 45° in all angles of Eq. (A-1) we obtain directly Eq. (2-4a). Due to constant slip in a diagonal edge from large node to large node (Fig. 2), Eq. (2-1), and Eq. (2-4b), the strain in the edge from small node to large node is half the strain of Eq. (2-4b). Indeed, substituting $\alpha_1 = \alpha_2 = 90°$ and $\beta_1 = \beta_2 = 45°$ in Eq. (A-1) we obtain half the value of Eq. (2-4b).

For the combined model the vertex displacements at node A are given in a generalization of Eq. (5-18) by

$$\bar{u}_1 = \ell_o(u_A\cos\alpha_o + v_A\sin\alpha_o) + [(\theta_C-\theta_B)\cot\ \alpha_1 + (\theta_C-\theta_A)\cot\ \beta_1]\ell_o^2/(2\ell_{AB})$$
$$\bar{u}_2 = \ell_o[u_A\cos(\alpha_o+\alpha_1) + v_A\sin(\alpha_o+\alpha_1)] - [(\theta_B-\theta_C)\cot\ \alpha_1 + (\theta_B-\theta_A)\cot\ \beta_2]\ell_o^2/(2\ell_{AC})$$
$$\bar{u}_3 = \ell_o[u_A\cos(\alpha_o-\alpha_2) + v_A\sin(\alpha_o-\alpha_2)] + [(\theta_B-\theta_D)\cot\ \alpha_2 + (\theta_B-\theta_A)\cot\ \beta_3]\ell_o^2/(2\ell_{AD})$$
$$\bar{u}_4 = \ell_o(u_A\cos\alpha_o + v_A\sin\alpha_o) - [(\theta_D-\theta_B)\cot\ \alpha_2 + (\theta_D-\theta_A)\cot\ \beta_4]\ell_o^2/(2\ell_{AB}) \qquad \text{(A-6)}$$

with similar relations for the remaining vertices at node A. The slip obtained by Eqs. (2-1) and (A-1) is the same as $\bar{u}_1$-$\bar{u}_4$ of Eq. (A-6). If $\alpha_1 = \beta_2 = -\alpha_o = 45°$ and $\beta_1 = 90°$,

then $\bar{u}_1$-$\bar{u}_2$ of Eq. (A-6) are the same as $\bar{u}_1$ and $\bar{u}_2$ of the large node of Fig. 39 and Eq. (5-18). Similarly $\bar{u}_{17}$ and $\bar{u}_{18}$ of the small node in Fig. 40 and Eq. (5-19) correspond with $\bar{u}_1$ and $\bar{u}_2$ of Eq. (A-6) with $\beta_1 = \beta_2 = -\alpha_o = 45°$ and $\alpha_1 = 90°$.

Appendix B Computation

In this appendix we give a brief discussion of the programs we used in our numerical examples. Outline flowcharts are used to illustrate some of the salient features. The appendix is concluded with the program listing of all routines, which are written in MNF (Minnesota Fortran). The emphasis of the thesis is to explore the mechanical aspects in the finite element method and we are aware that programming can certainly be done more efficiently.

Each run was concerned with only one physical problem and with only one of the three models. For this reason, three distinct main programs were written, although each main program served as driver for essentially the same package of subroutines. These main programs were denoted by* MINDS, MINDC, and MINDR for, respectively the slip, combined, and classical (regular) models. Figure 57 outlines MINDC; flow charts for the other two main programs are quite similar.

The main purpose of the driver program is to declare the dimensions of the arrays, to obtain information previously computed, to store information for future computation, and above all to direct

*Programs are listed at the end of this appendix in the order they are mentioned the first time.

the program to the slip part or classical part for which the subroutines SLIP and REG are written. As explained in Chapter V the combined model separates into a slip part and a classical part and hence the routines SLIP and REG do most of the computation. For this reason we have included flowcharts of these two routines as Figs. 58 and 59.

Most of the matrix calculations are done with IMSL routines [23], i.e. subroutines LIN1PB, LINV1F for matrix inversion, VMULSF, VMULFF, VMULFS for matrix multiplication, and VCVTFS for matrix rearrangement. The subroutine VMULOO was written in case the product of two full matrices result in a symmetric matrix. Internal node condensation was applied in the classical part as is described in Desai and Abel [12]. This means that the two displacement components of every small node will be eliminated from the final stiffness matrix by using equilibrium equations, constitutive relations, and the strain displacement relations. This is done by the subroutine QUAD. The four elements around a small node are identified as a QUAD (= quadrilateral elements), see Fig. 59.

The subroutine CREATE, Fig. 60, will form the stiffness matrix $\underline{A}$ with the same division as in Eq. (2-26) for the slip and classical parts. When an edge yields, this subroutine can correct the $\underline{A}_{22}^{-1}$ matrix by using the Sherman-Morrison formula

Eq. (2-28). When an element yields in the classical part the adjustment in the stiffness matrix can be done directly in the inverted stiffness-matrix. In this case we make use of the Woodbury formula [13]:

$$(\underline{A} - \underline{U}\underline{V}^T)^{-1} = \underline{A}^{-1} + \underline{A}^{-1}\underline{U}(\underline{I} - \underline{V}^T\underline{A}^{-1}\underline{U})^{-1}\underline{V}^T\underline{A}^{-1} \qquad \text{(B-1)}$$

where $\underline{A}$ is an n x n matrix, $\underline{U}$ and $\underline{V}$ are n x r matrices, and $\underline{I}$ is the r x r identity matrix. In our particular case we chose:

$$\underline{V} = -\underline{U}\underline{C} \qquad \text{(B-2)}$$

with $\underline{C}$ an r x r symmetrix matrix, which contains the change of the stiffness matrix of a QUAD due to yielding of one or more triangles within this QUAD. Hence Eq. (B-1) becomes:

$$(\underline{A} + \underline{U}\underline{C}\underline{U}^T)^{-1} = \underline{A}^{-1} - \underline{A}^{-1}\underline{U}(\underline{I} + \underline{C}\underline{U}^T\underline{A}^{-1}\underline{U})^{-1}\underline{C}\underline{U}^T\underline{A}^{-1} \qquad \text{(B-3)}$$

The other main program is ADJUST, Fig. 61. When either the combined model or slip model is aborted due to a singularity in the stiffness matrix caused by the indeterminancy of a combined mechanism, we determine this mechanism manually. The program ADJUST enables us to incorporate the undetermined mechanism in the slip part after which the computation with either the combined or slip model resumes.

```
      PROGRAM MINDS(INPUT,TAPE5=INPUT,TAPE6,TAPE7,TAPE8,TAPE9,TAPE10,OUT
     1PUT=2000,TAPE20)
      DIMENSION U(77),D2(150),D4(300),A3(1050),DI(2850),ET(540),IET(540
     1),C0(135),W(135),TE(135),DE(135),ITU(85),AU(77),AE(1050)
      COMMON N1,N2,N3,N4,N5,N6,N7,M0,RL,ITEL,DR(2),FMR,FMS,SL/TW0/DI(3),
     1DS(3),SR(2),UT(2)
      READ(5,100) N1,N2,N3,N4,N8,FMAX,P,RL
      N6=2 $ IF(N1.NE.0) GO TO 200
      RE=IND 7
      RE=IND 8
      RE=IND 10
      READ (10) N1,N2,N3,N4,N5,N6,N8,FMAX,P,RL,ITEL,SL
      IF(N5.GT.8) GO TO 150
C *** TAPE8 CONTAINS ADJUSTED INFORMATION FROM ADJUST
      READ(8) SR,DI,D2,ET,IET,C0,TE,AU,AE,U,DI,UT
      M0=4 $ IF(N5.GE.0) GO TO 125 $ M0=3 $ N5=N5-10
  125 WRITE(6,175) $ GO TO 250
  150 WRITE(6,175)
      READ(7) D1,DS,D2,D4,DI,ET,IET,C0,TE,AU,AE,UT $ M0=2 $ GOTO 250
  200 M0=0 $ N7=N8 $ RL=1./RL
  250 WRITE(6,110) N1,N2,N3,N4,N6,N8,FMAX,P,RL
      RE=IND 9
      RE=IND 20
      IF(M0.GT.0) GO TO 300 $ N6=3
      CALL SLIP(D2,A3,D4,DI,ET,IET,C0,W,U,ITU,TE,DE,AU,AE)
      ITEL=1 $M0=1 $ N5=2
      RE=IND 7
C *** TAPE7 TO BE USED IN MINDC
      WRITE (7) D1,DS,D2,D4,DI,ET,IET,C0,TE,AU,AE,UT
      END FILE 7
  300 N7=N8
      CALL SLIP(D2,A3,D4,DI,ET,IET,C0,W,U,ITU,TE,DE,AU,AE)
      IF(N5.GT.195)  N5=N5-200
C *** TAPE9 TO BE USED IN ADJUST
      WRITE(9) SR,DI,D2,ET,IET,C0,TE,AE,U,DI,UT
      WRITE(20) N1,N2,N3,N4,N5,N6,N8,FMAX,P,RL,ITEL,SL
      END FILE 9
      END FILE 20
      IF(N5.LT.5) STOP 104 $ IF(N5.LT.10)  STOP 1014
  100 FORMAT(5I2,F5.2,2F5.4)
  110 FORMAT(" N1=",I2," N2=",I2," N3=",I2," N4=",I2," N6=",I2," N7=",I2
     1," FMAX=",F5.2," P=",F5.4," RL=",F5.4)
  175 FORMAT(//" CINTINUATION OF SLIP ONLY PHOBLEM")
  225 FORMAT(" DIMENSIONS IN MINDS ARE INCORRECT")
      STOP $ END
```



```
      PROGRAM MINDC(TAPE1,TAPE2,TAPE6,TAPE7,TAPE10,OUTPUT=2000,INPUT,
     1TAPE4,TAPE5,TAPE8,TAPE9,TAPE20)
      DIMENSION A2(174),A3(1479),A1(3828),A4(696),IR(288),IDV(98),
     1S(576),DS(576),V(89),DV(89),U(77),D2(150),D4(300),DI(2850),ET(540)
     1,IET(540),C0(135),W(135),TE(135),DE(135),AU(77),AE(1050)
      COMMON N1,N2,N3,N4,N5,N6,N7,M0,RL,ITEL,DR(2),FMR,FMS,SL/ONE/A1(3),
     1A5(4),RR(2),P,FMAX/TW0/DI(3),DS(3),SR(2),UT(2)
      READ(10)N1,N2,N3,N4,N5,N6,N8,FMAX,P,RL,ITEL,SL
      READ 10,N5
   10 FORMAT(I5)
      M=0
      FMS=-1.
   25 IF(N6.EQ.2.OR.N5.GT.10) GOTO 100
      READ (4) FMR,FMS,DR,RR,DS,S,DV,V,A1,A4,A5
      READ (8) SR,DI,D2,ET,IET,C0,TE,AU,AE,U,DI,UT
      M0=4
      IF(N5.GE.0) GOTO 50
      M0=3
      N5=N5-10
   50 IF(N5.LT.5) GOTO 200
      N5=N5-5
      M=5
      GOTO 200
  100 READ (7) D1,DS,D2,D4,DI,ET,IET,C0,TE,AU,AE,UT
      M0=2
      N6=0
      IF(N5.GT.10) N6=1
  200 K=0
      WRITE(6,110) N1,N2,N3,N4,K,N8,FMAX,P,RL
C ***
C ***
  300 CALL SLIP(D2,A3,D4,DI,ET,IET,C0,W,U,ITU,TE,DE,AU,AE)
      IF(M.GT.0) N5=N5+5
      M=0
      IF(N6.EQ.1) M0=2
      N6=0
      IF(N5.LT.5) GOTO 600
      IF(N5.LT.195) GOTO 400
      K=200
      N5=N5-200
      GOTO 600
  400 IF(N5.NE.7)K=-200
  600 CALL REG(IDV,IR,A2,A3,A4,S,DS,A1,V,DV,U)
      IF(K) 800,700,900
  700 IF(N5.LT.5) GOTO 300
      GOTO 900
  800 IF(N5.NE.2) GOTO 900
      K=0
      N6=1
  900 WRITE (5) FMR,FMS,DR,RR,DS,S,DV,V,A1,A4,A5
      WRITE (9) SR,DI,D2,ET,IET,C0,TE,AE,U,DI,UT
      WRITE (20) N1,N2,N3,N4,N5,N6,N8,FMAX,P,RL,ITEL,SL
      STOP
  110 FORMAT(//" N1=",I2," N2=",I2," N3=",I2," N4=",I2," N6=",I2," N7=",
     1I2," FMAX=",F5.2," P=",F5.2," RL=",F6.4)
      END
```

```
      PROGRAM MINOR(INPUT,TAPE5=INPUT,TAPE1,TAPE2,TAPE3,TAPE6,TAPE10,OUT
     1PUT=2008,TAPE4,TAPE20)
      DIMENSION A2(174),A3(1479),AI(3828),A4(696),IR(288),IDV(98),
     1S(576),DS(576),V(89),DV(89),U(2)
      COMMON N1,N2,N3,N4,N5,N6,N7,M0,RL,ITEL,DR(2),FMR,FMS,SL,IMAX/ONE/A
     1(3),A5(4),RR(2),P,FMAX
      READ(5,100) N1,N2,N3,N4,N7,FMAX,P,RL,IMAX
      IF(N1.NE.0) RL=1./RL
      M0=0 $ IF(N1.NE.0) GOTO 200
      READ(20) N1,N2,N3,N4,N5,N6,N7,FMAX,P,RL,ITEL,SL
      READ(4) FMR,DR,RR,DS,S,DV,V,A1,AS
      RE=IND 20
      RE=IND 4
      M0=4
  200 N6=1
      WRITE(6,110) N1,N2,N3,N4,N6,N7,FMAX,P,RL
  300 CALL REG(IDV,IR,A2,A3,A4,S,DS,AI,V,DV,U)
      RE=IND 10
      RE=IND 3
      WRITE(3) FMR,DR,RR,DS,S,DV,V,A1,AS $ END FILE 3
      WRITE(10) N1,N2,N3,N4,N5,N6,N7,FMAX,P,RL,ITEL,SL $ END FILE 10
      IF(N5.LT.5) STOP 104 $ IF(N5.LT.10) STOP 1014
  100 FORMAT(5I2,F5.2,2F5.4,I5)
  110 FORMAT(//" N1=",I2," N2=",I2," N3=",I2," N4=",I2," N6=",I2," N7="
     1,I2," FMAX=",F5.2," P=",F5.4," RL=",F5.4)
      END
```



```
      SUBROUTINE SLIP(D2,AA,D4,A1,ET,IET,C0,W,U,ITU,TE,DE,AU,AE)
      DIMENSION A1(4),D2(1),AA(9),D4(15),A1(1),ET(4,1),IET(4,1),C0
     1(1),W(1),U(3),ITU(2),TE(1),DE(1),AE(1),IT(4),AU(1)
      COMMON N1,N2,N3,N4,N5,N6,N7,M0,RL,ITEL,DR(2),FMR,FMS,SL/TWO/D1(3),
     1DS (3),SR(2),UT(2)
C *** M0=0 SETUP, M0=1 REGULAR CYCLES, M0=2 FIRST TIME IN MINOC
C *** M0=3 AFTER ADJUSTING SLIP PART, M0=4 DO NOT COMPUTE INVERSE
      IF(M0.EQ.1) GO TO 400
      M1=2*(N1-1)* N2-N1-N3 $ FDR=1.
      IF(N4.GE.2) M1=M1-N1+2
      IF(N4.LT.3) GO TO 2 $ M1=M1-N1+2
    2 M2=N1*(2*N2-1)-N2+1
      M3=4*N1*N2-5*(N1+N2)+6 $ M6=2*N1-1
      IF(N4.EQ.4) M3=M3+(N3-1)
C *** VALUES A1
      A1(1)=1. $ A1(2)=0. $ A1(3)=0. $ A1(4)=1.
C *** DI DISPL INCR
      DY=1. $ IF(N4.GT.2)DY=-1.
      IF(M0.EQ.3) GO TO 330 $ IF(M0.EQ.4) GO TO 400
      SR (1)=0. $ SR(2)=0. $ ITEL=0 $ N5=1 $IF(N4.GT.2) N5=3
      IF(N6.LT.2) N5=0 $ UT(1)=0. $ UT(2)=0.
      IF(M0.NE.2) GO TO 3 $ M0=0 $ GO TO 460
    3 DO 4 I=1,M3
    4 TE(I)=0.
C *** COMPUTATION AA AND ITU VECT UI ALONG DE U2 ALONG AB
      DO 5 I=1,M2
    5 AA(I)=1.
      J=M2
      DO 10 I=1,N3
      ITU(J)=1
      AA(J)=FLOAT (I-1)
   10 J=J-N1*2+1 $ ITU(2)=2 $ ITU(1)=1 $ AA(1)=0.
      IF(N4.LT.3) GOTO 30
      DO 20 I=3,N1
      ITU(I)=2
   20 AA(I)=FLOAT(I-1)
      J=3
      GOTO 50
   30 DO 40 I=3,N1
   40 ITU(I)=1
      J=N1+1
   50 N=2*N2-2 $ A=1. $ M=N1+1 $ K=N-2*N3+2 $ IF (N4.EQ.1) N=N+1
      DO 80 L=2,N $ A=-A $ IF(A.LT.0.) GOTO 60 $ ITU(M)=1 $ AA(M)=0.
      M=M+1
   60 DO 70 I=3,N1 $ ITU(M)=J $ J=J+1
   70 M=M+1 $ IF(A.GT.0..AND.L.GT.K) GO TO 80 $ ITU(M)=J $ J=J+1
   80 M=M+1
      IF(N4.EQ.1) GOTO 100
      DO 95 I=2,N1 $ ITU(M)=1 $ AA(M)=0.
   95 M=M+1
  100 C0(1)=.05/SQRT(2.) $ M=4*M3 $ N=1
      DO 102 K=1,M*4 $ ET(K)=2. $ ET(K+1)=-4. $ ET(K+2)=2. $ ET(K+3)=0.
      IET (K+3)=1 $ C0(N)=C0(1)
  102 M=M+1      $ K=1 $ M=N1 $ L=-4*N1+5 $ N=1-N1
      DO 115 I=2,N2 $ M=M-N1+1
      DO 105 J=2,N1 $ IET(K)=M $ IET(K+1)=M+N1 $ IET(K+2)=M+2*N1
      IET(K+4)=M+1 $ IET(K+5)=M+N1 $ IET(K+6)=M+2*N1-1 $ M=M+1
```

```
  105 K=K+12 $ L=(N1+1)*4+L $ N=N+N1+1
      DO 110 J=3,N1 $ IET(L)=N+N1-1 $ IET(L+1)=N $IET(L+2)=N+N1
      IET(L+3)=N+2*N1-1 $ ET(L+1)=-2. $ ET(L+3)=-2. $ C0((L+3)/4)=.05
      N=N+1
  110 L=L+12 $ IF(I.EQ.N2) GOTO 120 $ K=K-4 $ M=M+N1
      DO 115 J=2,N1 $ IET(K)=M-N1+1 $ IET(K+1)=M $IET(K+2)=M+N1
      IET(K+3)=M+1 $ ET(K+1)=-2. $ ET(K+3)=-2. $ C0((K+3)/4)=.05$M=M+1
  115 K=K+4
  120 IF(N-LE.3) GOTO 170
C *** SLIP UNDER PRANDTL ROUGH
      N4=M3 $ I=N-4*N1+5 $ L=M2
      DO 160 M=1,N4 $ IET(M)=L-N1 $ IET(M+1)=L $ IET(M+2)=L-2*N1+1
      ET(M+1)=-1. $ ET(M+2)=-1. $C0((M+3)/4)=.05
  160 L=L-2*N1+1
  170 M=N+M3
      DO 220 I=1,M,4 $ N=I+3
      DO 190 J=I,N $ K=IET(J) $ IET(J)=ITU(K)
  180 ET(J)=ET(J)*AA(K) $ N=N-1
      DO 190 J=1,N
      DO 190 L=J,N $ IF(IET(J).NE.IET(L+1).OR.ET(L+1).EQ.0) GOTO 190
      ET(J)=ET(J)+ET(L+1) $ ET(L+1)=0.
  190 CONTINUE
      DO 210 J=I,N $ IF(IET(J).NE.0.) GO TO 210
      DO 200 L=J,N $ IF(ET(L+1).EQ.0.) GO TO 200 $ ET(J)=ET(L+1)
      ET(L+1)=0. $ IET(J)=IET(L+1) $ GO TO 210
  200 CONTINUE
  210 CONTINUE $ N=N+1
      DO 220 J=I,N $ IF(ET(J).GT.-.5.AND.ET(J).LT..5) IET(J)=0
  220 CONTINUE
      WRITE(6,260)
      DO 265 I=1,M3 $ L=4*I $ N=L-3
  265 WRITE(6,270) (I,C0(I),(IET(K),K=N,L),(ET(K),K=N,L))
      M=M+2
      DO 280 I=1,M
  280 AU(I)=0.
C *** COMPUTE AA IN SYM BAND STORAGE MODE AND COMPUTE AI
      M=2*M1
      DO 305 K=1,M
  305 D2(K)=0.
      D1(1)=0. $ D1(2)=0. $ D1(3)=0. $ N=M1*(M6+1)
      DO 310 I=1,N
  310 AE(I)=0.
      DO 320 I=1,M3
      IF(C0(I).LT.0.) GO TO 320 $ AA(I)=C0(I)
      L=-1 $ K=4*I $ M=K-3
      DO 315 J=M,K $ L=L+1 $ IF(IET(J).EQ.0) GO TO 317 $ AA(L*2)=ET(J)
  315 CONTINUE $ L=4
  317 CALL CREATE(D1,D2,AA,D4,AE,D6,IET(M),2,M1,M6,L,-1)
  320 CONTINUE
  330 N=(M6+1)*M1
      DO 335 I=1,N
  335 AA(I)=AE(I)
C$    WRITE(6,316) D1 $ N=M6+1    $ M=2*M1
C$    WRITE(6,345) (D2(I),I=1,M)
C$    WRITE(6,341)
C$    WRITE(6,345)((AA(I+J*M1-M1),J=1,N),I=1,M1)
      CALL LINIPP(AA,M1,M6,M1,A1,I,AA1,A,J) $ AA1=AA1*2.**A
```



```
C$    WRITE(6,360)AA1,J
C$    DO 346 N=1,M1 $ L=M*(N-1)/2+1 $ M=N+L-1
C$346 WRITE(6,345)(AI(I),I=L,M)
C *** DEBUGGING
      IF(J.EQ.0.AND.AA1.GT..001) GOTO 400
      WRITE(6,375) AA1,J
      IF(J.GT.127) STOP
C *** COMPUTATION D4
  400 CALL VMULSF(A1,M1,D2,2,M1,D4,M1) $ M=2*M1
      DO 410 I=1,M
  410 D4(I)=-D4(I) $ D5(1)=D1(1) $ D5(2)=D1(2) $ D5(3)=D1(3)
      CALL VMUL00(D2,D4,M1,2,D5,1)
C$    WRITE(6,321) D5
C$    WRITE(6,345) (D4(I),I=1,M)
      D5(1)=D5(1)*2.*RL $ D5(2)=D5(2)*2.*RL $ D5(3)=D5(3)*2.*RL
  460 AA1=1. $ IF(NS.EQ.3) GO TO 590
C *** COMPUTATION MATRIX A1(2,2)
      IF(NS.EQ.1) GOTO 470
      A1(1)=D5(1) $ A1(3)=D5(2)
      IF(NS.EQ.2) GOTO 490
  470 A1(2)=D5(2) $ A1(4)=D5(3)
  490 AA1=A1(1)*A1(4)-A1(2)*A1(3)
      IF(ABS(AA1).GT.1.E-9) GO TO 540
      WRITE(6,500) $ IF(NS.GT.0) GOTO 540
      IF(N4.GT.2.AND.ABS(A1(3)).GT.1.E-4) GOTO 520
      A1(1)=1. $ A1(3)=0. $ DR(2)=0. $ DR(1)=SIGN(10.,U(1))
      NS=NS+6 $ AA1=A1(4) $ GO TO 610
  520 A1(4)=1. $ A1(2)=0. $ DR(1)=-A1(3)/A1(1) $ DR(2)=SIGN(10.,U(2))
      WRITE(6,530)DR(1) $ DR(1)=0. $ NS=NS+7 $ AA1=A1(1) $ GO TO 610
  540 A1(1)=1. $ A1(2)=0. $ A1(3)=0. $ A1(4)=1. $ AA1=1.
      DR(1)=DY $ DR(2)=0. $ NS=A $ GO TO 610
  590 IF(NA.NE.2)RETURN $ ITEL=ITEL+1
C *** INCREMENT IN U(1) AND U(2)
  600 IF(NS.EQ.1.OR.NS.EQ.3) DR(1)=DY
      IF(NS.GE.2.OR.N6.EQ.2) DR(2)=0.
  610 U(1)=(A1(4)*DR(1)-A1(3)*DR(2))/AA1*.1
      U(2)=(A1(1)*DR(2)-A1(2)*DR(1))/AA1*.1 $ K=0
      CALL VMULFF(D4,U,M1,2,1,M1,2,U(3),M1,J)
C$    WRITE(6,731)
C$    M=M1+2
C$    WRITE(6,345)(U(I),I=1,M)
C *** SLIPDISPLACEMENT,SLIPSTRESS, POS WORK, FMS
      FMS=0. $ K=0
      DO 760 I=1,M3
      W(I)=0.
      N=4*I $ L=N-3
      DO 750 M=L,N $ J=IET(M) $ IF(J) 743,755,745
  743 J=-J
  745 W(I)=W(I)+ET(M)*U(J)
  750 CONTINUE
  755 DE(I)=C0(I)*W(I)*10.
      IF(C0(I).GT.0.) GO TO 760 $ DE(I)=0.
      IF(TE(I)*W(I).GE.FMS) GO TO 760
C *** EXCLUDED EDGES
      IF(I.EQ.48.OR.I.EQ.93.OR.I.EQ.96.OR.I.EQ.97.OR.I.EQ.98.OR.I.EQ.116
     1.OR.I.EQ.117.OR.I.EQ.119) GO TO 760
      M=4*I
```

```
      IF(IET(M-3).LT.0.OR.IET(M-2).LT.0.OR.IET(M-1).LT.0.OR.IET(M).LT.0)
     1 GO TO 760
      FMS=TE(I)*W(I) $ IT(I)=I
  760 CONTINUE $ IF(NS.GT.5.AND.NS.LT.9) GO TO 767
      IF(FMS.LT.0.) GO TO 875
C$    WRITE(6,761)
C$    WRITE(6,345)(W(I),I=1,M3)
C$    WRITE(6,762) NS,N6
C$    WRITE(6,345)(CO(I),I=1,M3)
      IF(NS.LT.5) GO TO 775 $ WRITE(6,765)
  767 DR(1)=0. $ DR(2)=0. $ L=0
      DO 768 I=1,2
  768 U(I)=FLOAT(INT(1.E4*U(I)+SIGN(.2,U(I))))/1.E4
      DO 770 I=1,M3 $ IF(ABS(W(I)).LT.1.E-4) W(I)=0. $ DE(I)=0.
      IF(CO(I).LT.0.) GO TO 769
      IF(W(I).EQ.0.) GO TO 770 $ L=200
      WRITE(6,756)I $ DE(I)=W(I)*CO(I)*10. $ GO TO 770
  769 IF(TE(I)*W(I).GE.0.) GO TO 770
      L=200 $ WRITE(6,757)I
  770 CONTINUE
      IF(L.NE.0) WRITE(6,763) $ IF(L.GT.100.AND.NS.GT.4) K=0
C$    DO 931 N=1,M1 $ L=N*(N-1)/2+1 $ M=N+L-1
C$931 WRITE(6,345)(AI(I),I=L,M)
C$    WRITE(6,771)
C$    WRITE(6,345)(U(I),I=1,M)
      GO TO 860
  775 FMS=1.1E10
      DO 830 I=1,M3
      IF(DE(I)) 790,830,780
  780 A=(1.-TE(I))/DE(I)
      GOTO 800
  790 A=(-1.-TE(I))/DE(I)
  800 IF(FMS.GT.A) FMS=A
  830 CONTINUE
      IF(FMS.LT.1.E4) GOTO 835 $ NS=NS+200 $ K=0
      WRITE(6,831)
      GOTO 767
  835 A=FMS
      IF(N6.NE.2.AND.FMR.LT.FMS) A=FMR
      DO 850 I=1,M3
      W(I)=W(I)*A*PL*PL
      DE(I)=A*DE(I)
  850 TE(I)=TE(I)+DE(I) $ U(1)=A*U(1) $ U(2)=A*U(2)
      DR(1)=(DS(1)*U(1)+DS(2)*U(2))*10.*(N2-1)/(N3-1) $SR(1)=SR(1)+DR(1)
      DR(2)=(DS(2)*U(1)+DS(3)*U(2))*10.*(N2-1)/(N3-1) $ K=0
      IF(ABS(DR(2)).LT.1.E-10)   DR(2)=0. $ SR(2)=SR(2)+DR(2)
      U(1)=U(1)+PL**2 $ U(2)=U(2)*PL**2
      UT(1)=UT(1)+U(1) $ UT(2)=UT(2)+U(2)
      IF(N4.NE.2.AND.N7.EQ.-1) GOTO 865
      IF(ITEL.EQ.1.AND.N6.EQ.2) SL=.001*DR(1)/U(1)
      IF(DR(1)/U(1).GT.SL.OR.N6.NE.2) GOTO 854 $ K=200 $ GOTO 860
  854 FOR=FOR+ABS(DR(1)*U(1)) $ IF(N7.EQ.-1.AND.FOR.LT..2) GOTO 865
      FOR=0.
C ***
C ***
      GO TO 860
      IF(N7.EQ.1.OR.ITEL.EQ.1) GOTO 860
```



```
      WRITE(6,855) ITEL,DR,SR,U(1),U(2),UT
      IF(N7.LE.-1) GOTO 865 $ WRITE(6,858)
      WRITE(6,856)(TE(I),I=1,M3)
      WRITE(6,857)
      WRITE(6,856)(W(I),I=1,M3) $ GOTO 865
  860 WRITE(6,855) ITEL,DR,SR,U(1),U(2),UT $ WRITE(6,852)
      IF(ITEL.NE.1) N7=1
      WRITE(6,318)(I,DE(I),TE(I),W(I),CO(I),I=1,M3)
      IF(K.EQ.200) GOTO 925
  865 IF(A.NE.FMS.OR.NS.GT.5) RETURN
  875 AA1=1.-1.E-4 $ K=-2 $ B=0.
      DO 920 I=1,M3
      IF(FMS.GT.0.) GOTO 880 $ IF(I.NE.IT(I))GOTO 920 $ WRITE(6,890) I,
     1ITEL
      GOTO 885
  880 IF(TE(I).GT.-AA1.AND.TE(I).LT.AA1.OR.CO(I).LT.0.) GOTO 920
      WRITE(6,870) I,ITEL
  885 L=0 $ M=4*I $ N=M-3 $ CO(I)=-CO(I) $ AA(1)=CO(I)
      DO 905 J=N,M $ IF(IET(J)) 905,910,900
  900 L=L+1 $ AA(L+1)=ET(J) $ IT(L)=IET(J)
  905 CONTINUE
  910 CALL CREATE(D1,D2,AA,D4,AE,AI,IT,2,M1,M6,L,K)
      IF(FMS.LT.0.) GOTO 920
      IF(K.GE.-2) GOTO 920 $ N=4*M3 $ A=0.
      DO 915 J=1,L
      DO 914 M=1,N $ IF(IET(M).NE.IT(J)) GOTO 914
      IF(ABS(TE((M+3)/4)).GT.AA1) GOTO 914 $ IT(J)=-IT(J) $ GOTO 915
  914 CONTINUE $ B=1. $ A=1.
  915 CONTINUE $ IF(A.GT.0.) GOTO 910 $ K=-1
  920 CONTINUE $ IF(B.EQ.0.AND.K.EQ.-2) GOTO 400 $ IF(B.EQ.0.) GOTO 925
      M=M4*M1 $ N=M3*4
      N12=M+1 $ N13=M+M1
      DO 924 I=N12,N13 $ IF(AE(I).GT.1.E-10) GOTO 924
      AE(I)=1. $ D2(I-M)=0. $ D2(I-M+M1)=0.
      WRITE(6,926) I-M+2
      DO 923 J=1,N $ IF(IET(J).EQ.I-M+2) IET(J)=-IET(J)
  923 CONTINUE
  924 CONTINUE $ IF(K.EQ.-2) GOTO 400
  925 WRITE(6,921)
      M=(M6+1)*M1
      DO 930 I=1,M1
  930 WRITE(6,345)(AE(I+J-M1),J=M1,M,M1) $ NS=NS+200
      WRITE(9)M1,M3,M6
      WRITE(6,260)
      DO 966 I=1,M3 $ L=4*I $ N=L-3
  966 WRITE(6,270) (I,CO(I),(IET(K),K=N,L),(ET(K),K=N,L))
      RETURN
  240 FORMAT("0VALUES CO,IET AND ET"/" I",13X,"CO",13X,"IET",22X,"ET")
  270 FORMAT(1X,I3,6F10.4,5X,4(I3,2X),5X,4(F4.1,1X))
  318 FORMAT(1X,I7,8X,E11.4,2X,E12.6,21X,E11.4,21X,E11.5)
  345 FORMAT(4X,10E12.3)
  375 FORMAT("0***WARNING******WARNING******WARNING******DET AT INVERSE"
     1,E12.5,"AND ERROR MODE",I5)
  500 FORMAT(" SLIPLINE IS POSSIBLE")
  530 FORMAT(1H0,T22,"U(1)=",E10.4,"  U(2)=")
  757 FORMAT(//" NEGATIVE WORK IN PLASTIC EDGE NO",I4,"NOT CAUSED BY PL
     1ASTIC MECHANISM VARIABLE")
```

```
758 FORMAT(" MECHANISM INFLUENCES ELASTIC EDGE",I3)
763 FORMAT(" NO PROPER MECHANISM IS FOUND BUT COMPUTATION CONTINUES")
765 FORMAT(//" NONZERO SLIPDISPLACEMENT CAN OCCUR")
831 FORMAT(//" DISPLACEMENTCONTROLLED SLIPMODEL REACHED LIMITLOAD")
852 FORMAT(//" EDGE NO STRESSINCREMENT TOTAL STRESS SLIP*EDGELENGTH*
   1G/K/RL/RL/DELTA CO(PLASTIC,LT.0.,LT.ELASTIC)")
855 FORMAT(////" SUBROUTINE SLIP ********************* CYCLE NUMBER",I3/
   1X,"LOAD INCREMENTS AT RESPECTIVELY DE AND AB ",2E12.4," /K/RL"/
   2X," TOTAL LOAD AT RESPECTIVELY DE AND AB ",2E12.4," /K/RL"/
   3"MECHANISM INCREMENTS AT RESPECTIVELY DE AND AB ",2E12.4,"G/K/RL/
   4RL/DELTA"/
   5" TOTAL MECHANISMS AT RESPECTIVELY DE AND AB ",2E12.4,"G/K/RL/
   6RL/DELTA")
856 FORMAT(10E12.5)
857 FORMAT(/" STRAININCREMENTS*EDGELENGTH*G/K/RL")
858 FORMAT(//" TOTAL STRESS/K IN THE EDGES")
870 FORMAT(" EDGE",I3," BECOMES PLASTIC IN CYCLE",I3)
960 FORMAT(" EDGE",I3," BECOMES ELASTIC IN CYCLE",I3)
921 FORMAT(/" BAND SYMMETRIC MATRIX WHICH IS SINGULAR IN SLIP")
926 FORMAT(/" MECHANISM",I4," IS UNDETERMINED")
955 FORMAT(//" SLIPMECHANISM VARIABLE",I3," IS UNDETERMINED")
    END
```



```
    SUBROUTINE REG(IDV,IR,A2,A3,A4,S,DS,AI,V,DV,U)
    DIMENSION IDV(2),R(80),IR(1),A2(1),A3(128),A4(80),S(1),DS(1),AI(1)
   1,V(3),DV(3),U(2),CCE(36),CTE(40)
    COMMON N1,N2,N3,N4,N5,N6,N7,M0,RL,ITEL,DR(2),FMR,FMS,SL,IMAX/ONE/A
   11(3),AS(4),RR(2),P,FMAX
    DATA R/.5,3*0.,.5,6*0.,.2*.5,3*0.,.-.5,4*0.,.-.5,3*0.,.,5,3*0.,.,5,4*0.
   1,-.5,3*0.,.-.5,2*0.,.-.5,4*0.,.-.5,3*0.,.,5,4*0.,.,5,3*0.,.-.5,3*0.,.-.5,
   24*0.,.-.5,2*.5,.-.5,4*0.,.2*-.5,2*.5/
    IF(M0.EQ.1) GOTO 250
    M1=2*N1*N2-N2-N3-2 $ IF(N4.EQ.1) GOTO 1
    M1=M1-N1+1 $ IF(N4.EQ.2) GOTO 1
    M1=M1-N1+1
    IF(N4.EQ.4) M1=M1-N3+1
  1 M2=(M1+1)*M1/2 $ M3=M1+2 $ M4=2*N1 $ M5=16*(N1-1)*(N2-1)
    M7=2*M1 $ M8=M5/2 $ IF(N6.EQ.1) N5=0 $ FDW=1. $ IC=0 $ SL1=0.
    IF(N6.NE.1) IMAX=0
    D1=1. $ IF(N4.GT.2) D1=-1. $ IF(N7.LT.0) N7=-2 $ YM=1.000
    IF(M3.LT.3) GOTO 3 $ M0=1 $ REWIND 1
    L1=M4*N2
    READ(1) $ READ(1) CCE,CTE,(IR(I),I=1,M8),(IDV(I),I=1,L1)
    IF(N5.GT.4) GOTO 155 $ IF(N6.EQ.1) GOTO 250 $ RETURN
  3 ITEL=0 $ RR(1)=0. $ RR(2)=0.
    AS(1)=1. $ AS(2)=0. $ AS(3)=0. $ AS(4)=1.
    DO 2 I=1,M3
  2 V(I)=0.
    DO 100 I=1,M5
100 S(I)=0. $ IF(M0.NE.2) GOTO 5 $ M0=1 $ REWIND 1
    READ(1)(AI(I),I=1,M2),A1,(A2(I),I=1,M7)
    L1=M4*N2
    READ(1)CCE,CTE,(IR(I),I=1,M4),(IDV(I),I=1,L1) $ GOTO 150
  5 M0=1 $ P=P/(1.-2.*P) $ M6=M4+2
    IDV(1)=2 $ IDV(2)=0 $ IF(N4.GT.2) GOTO 15
    DO 10 J=3,M4
 10 IDV(J)=J $ J=M4
    GOTO 25
 15 J=2
    DO 20 I=4,M4,2
    IDV(I-1)=2 $ J=J+1
 20 IDV(I)=J
 25 M=N2-N3-1 $ I=M4
    IF(M.EQ.0) GOTO 35
    DO 30 L=1,M
    I=I+2 $ J=J+1 $ IDV(I-1)=J $ IDV(I)=0
    DO 30 K=3,M4
    I=I+1 $ J=J+1
 30 IDV(I)=J
 35 M=N3-1 $ IF(N4.EQ.1) M=N3
    DO 50 L=1,M
    I=I+2 $ J=J+1 $ IDV(I-1)=J $ IDV(I)=0 $ IF(N4.LE.4) GOTO 45
    DO 40 K=5,M4
    I=I+1 $ J=J+1
 40 IDV(I)=J
 45 I=I+2 $ J=J+1 $ IDV(I-1)=J $ IF(N4.LT.4) GOTO 50 $ IDV(I-1)=0
    J=J-1
 50 IDV(I)=1 $ IF(N4.EQ.1) GOTO 65
    I=I+2 $ IDV(I-1)=0 $ IDV(I)=0
    DO 60 L=4,M4,2
```

```
      I=I+2 $ IDV(I-1)=0 $ J=J+1
   60 IDV(I)=J $ IDV(I)=1
   65 IDV(I-1)=0
      I=1 $ J=1
      DO 80 N=2,N2
      DO 75 K=2,N1
      IR(J)=IDV(I+2+M4) $ IR(J+1)=IDV(I+3+M4) $ IR(J+2)=IDV(I+2)
      IR(J+3)=IDV(I+3) $ IR(J+4)=IDV(I) $ IR(J+5)=IDV(I+1)
      IR(J+6)=IDV(I+M4) $ IR(J+7)=IDV(I+1+M4) $ I=I+2
   75 J=J+8
   80 I=I+2 $ R=P
      CALL QUADIS(CTE,A3,A4,B,R)
      DO 81 I=1,36
   81 CGE(I)=A4(I)
      IF(P.EQ.R) GO TO  82 $ I=100 $ WRITE(6,390) I $ NS=100 $ RETURN
   82 N=I*(M5+1)
      DO 85 I=1,N
   85 A3(I)=0.
      DO 90 I=1,M7
   90 A2(I)=0.
      A1(1)=0. $ A1(2)=0. $ A1(3)=0. $ K=1
      DO 105 I=1,M8,8
  105 CALL CREATE(A1,A2,A3,A4,A5,A6,IR(I),2*M1,M6,8,K)
      CALL LINIPR(A3,M1,M6,M1,A1,I,A,B,J)
      A=A**2,**6
      IF(A.GT.1.E-10.AND.J.EQ.0) GOTO 110
      WRITE(6,107) A,J
      IF(J.LT.128) GOTO 110 $ NS=100 $ RETURN
  110 REWIND 1
      WRITE (1)(A1(I),I=1,M2),A1,(A2(I),I=1,M7)
      L1=M4*N2
      WRITE(1) CGE,CTE,(IR(I),I=1,M8),(IDV(I),I=1,L1)
      END FILE 1
  150 CALL VMULSF(A1,M1,A2,2,M1,A4,M1)
      DO 152 I=1,M7
  152 A4(I)=-A4(I)
      CALL VMULSF(A2,A4,M1,2,A1,1)
      A1(1)=A1(1)*RL $ A1(2)=A1(2)*RL $ A1(3)=A1(3)*RL
      IF(N4.GT.2.AND.NS.EQ.2) GOTO 160
      IF(N4.GT.2) GOTO 165
      A5(2)=A1(2) $ A5(4)=A1(3) $ GOTO 165
  155 IF(NS.EQ.7) GOTO 156 $ FMR=0. $ GOTO 250
  156 A5(3)=-V(1)/U(2) $ NS=NS-5
  160 A5(2)=A1(2)-A5(3)*A1(1) $ A5(4)=A1(3)-A5(3)*A1(2)
  165 DV(2)=D1/(A5(1)*A5(4)-A5(2)*A5(3))
      DV(1)=A5(4)*DV(2) $ DV(2)=-A5(2)*DV(2)
      CALL VMULFF(A4,DV,M1,2,1,M1,2,DV(3),M1,J)
      RE=1.0 2
      FMR=1.1E10 $ A=1.-1.E-4 $ N=0
      DO 200 I=1,M8,8
      K=I+7 $ M=1
      DO 170 J=I,K
      A3(M)=0. $ IF(IR(J).EQ.0) GOTO 170 $ L=IR(J) $ A3(M)=DV(L)
  170 M=M+1
      M=2*I+2
      IF(S(M).GE.A.OR.S(M+4).GE.A.OR.S(M+8).GE.A.OR.S(M+12).GE.A)
     1GOTO 185
```



```
      DO 175 J=1,40
  175 A3(J+20)=CTE(J)
      GOTO 190
  185 READ(2)  (A3(J),J=21,60)
  190 CALL VMULFF(A3(N5),A3,2,8,1,2,8,A3(9),2,J)
      CALL VMULFF(R,A3,8,10,1,8,10,A3(13),8,J)
      A3(1)=A3(13) $ A3(4)=A3(14) $ A3(7)=A3(15) $ A3(10)=A3(16)
      A3(2)=A3(17) $ A3(5)=A3(19) $ A3(8)=A3(18) $ A3(11)=A3(17)
      A3(3)=A3(18) $ A3(6)=A3(18) $ A3(9)=A3(20) $ A3(12)=A3(20)
      M=M-3
      DO 195 J=1,10,3
      CALL VMULSF(A3(2*J+19),3,A3(J),1,3,DS(M),3)
C ***
C ***
C ***
C ***
      IF(S(M+3).GE.A) GOTO 193
      A3(3)=4.*(1.-S(M+3)) $ IF(S(M+3).LT.-.5) A3(3)=0. $ GOTO 194
  193 DS(M+3)=S(M)*(2.*A3(J)-A3(J+1)-A3(J+2))+(S(M+1)-S(M+2))*(A3(J+1)-A
     13(J+2))
      IF(DS(M+3).GT.-1.E-8) GOTO 192 $ IF(DS(M+3).GT.FMR) GOTO 195
      FMR=DS(M+3) $ N=M+3 $ GOTO 195
  192 A3(3)=4.E-3
  194 A3(1)=DS(M)**2+(DS(M+1)-DS(M+2))**2
      A3(2)=(DS(M)*S(M)+(DS(M+1)-DS(M+2))*(S(M+1)-S(M+2)))/A3(1)
      DS(M+3)=-A3(2)+SQRT(A3(2)**2-A3(3)/A3(1))
      IF(DS(M+3).LT.FMR) FMR=DS(M+3)
  195 M=M+4
  200 CONTINUE $ IF(FMR.LT.1.E4.AND.FMR.GT.0.) GOTO 210
      IF(FMR.GT.1..OR.N.EQ.0) GOTO 204 $ S(N)=-S(N) $ K=(N+12)/16
      WRITE(6,191) K,N/4+(1-K)*4,ITEL $ IC=IC+1 $ IF(IC.EQ.50) STOP
      GOTO 200
  204 FMR=1. $ NS=5 $ N6=1 $ N7=1 $ WRITE(6,205)
  210 CALL VMULSF(A1,2,DV,1,2,DR,2)
      ITEL=ITEL+1 $ IC=0
      IF(N6.NE.1) RETURN
  250 A=FMR
      IF(N6.NE.1.AND.FMS.LT.FMR) A=FMS $ B=A*RL
      IF(A.LE.0..AND.NS.LT.5) GOTO 279
      DO 255 I=1,M3
  255 V(I)=V(I)+DV(I)*B
      DO 265 I=1,M5,4
      M=I+2
      A3(1)=0. $ IF(S(I+3).GE.1.-1.E-4) A3(1)=1.1
      DO 260  J=I,M
  260 S(J)=S(J)+DS(J)*A
      S(I+3)=(S(I)**2+(S(I+1)-S(I+2))**2)/4.
      IF(S(I+3).GT.YM) YM=S(I+3)
      IF(A3(1).GT..5.OR.S(I+3).LT.1.-1.E-4) GOTO 265 $ J=(I+15)/16
      WRITE(6,264) J,(I+19)/4-J*4,ITEL
  265 CONTINUE
      CALL VMULSF(A1,2,DV,1,2,DR,2)
      DR(1)=DR(1)*A*(N2-1)/(N3-1) $ DR(2)=DR(2)*A*(N2-1)/(N3-1)
      IF(ABS(DR(2)).LT.1.E-10) DR(2)=0.
      RR(1)=RR(1)+DR(1) $ RR(2)=RR(2)+DR(2)
      B=B*(DV(1)+A5(3)*DV(2)) $ FMS=V(1)+A5(3)*V(2)
      IF(ITEL.EQ.1) SL=DR(1)/8
```

```
      IF(NS.GE.5) GOTO 274
      IF(ITEL.LT.IMAX) GOTO 266
      IF(DR(1)/B.LT..05*SL.AND.SL1-.0005.GT.DR(1)/B) NS=100 $SL1=DR(1)/B
      IF(SL1.LT.(YM-1.)*SL.OR.ABS(RR(1)).GE.FMAX.OR.SL1.LT..005*SL)
     1NS=100
      IF(NS.GE.5) GOTO 274
  266 CONTINUE
C ***
C ***
      GO TO 274
      IF(N7.EQ.1.OR.ITEL.EQ.1) GOTO 274
      IF(N7.EQ.-1) GOTO 281
      A3(1)=0. $ IF(IDV(1).NE.0) A3(1)=DV(IDV(1))*B
      WRITE(6,458) ITEL,DR(1),RR(1),B,FMS,DR(2),RR(2),A3(1),V(2)
      IF(N7.EQ.-2) GOTO 281 $ WRITE(6,455)
      K=0 $ J=(M8+4)/8 $ M=8*J $ L=J/2
      DO 273 I=16,M8,16 $ K=K+1 $ L=L+1
  273 WRITE(6,460) K,S(I-12),S(I-8),S(I-4),S(I),L,S(I-12+M),S(I-8+M),S(I
     1-4+M),S(I+M)
      K=K+1 $ IF(M8.NE.M) WRITE(6,460) K,S(M8-4),S(M8),S(M-4),S(M)
      GOTO 279
  274 N=4*N1*N2 $ B=A*RL
      DO 275 I=2,N,2 $ L=IDV(I/2) $ IF(L.EQ.0) GOTO 270
      A3(I-1)=DV(L)*B $ A3(I)=V(L) $ GOTO 275
  270 A3(I-1)=0. $ A3(I)=0.
  275 CONTINUE $ B=B*(DV(1)+A5(3)*DV(2))
      WRITE(6,400) ITEL,DR,RR,B,FMS $ N=M+N2 $ J=(N+2)/4 $ M=4*J $ K=0
      DO 276 I=4,N,4 $ K=K+1 $ L=K+J
  276 WRITE(6,410) K,A3(I-3),A3(I-1),A3(I-2),A3(I),L,A3(I-3+M),A3(I-1+M)
     1,A3(I-2+M),A3(I+M)
      K=K+1 $ IF(N.NE.M) WRITE(6,410) K,A3(N-1),A3(M-1),A3(N),A3(M)
      WRITE(6,420)
      J=1 $ L=1
      DO 277 I=1,M5,4 $ A3(1)=DS(I)*A $ A3(2)=DS(I+1)*A $ A3(3)=DS(I+2)
     1*A
      WRITE(6,430) L,J,A3(1),A3(2),A3(3),S(I),S(I+1),S(I+2),S(I+3)
      J=J+1 $ IF(J.LT.5) GOTO 277 $ J=1 $ L=L+1
  277 CONTINUE $ GOTO 279
  281 N7=-1 $ FDR=FDR+ABS(DR(1)*B) $ IF(FDR.LT..2) GOTO 279
      FDR=0. $ N7=-2
  279 IF(NS.EQ.7) GOTO 155
      IF(NS.LT.5) GOTO 278
      NS=100 $ FMR=0.
      RETURN
  278 IF(FMR.EQ.A) GOTO 280
      CALL VMULSF(A1,2,DV,1,2,DR,2) $ FMR=FMR-A $ ITEL=ITEL+1
      RETURN
  280 REWIND 1
      REWIND 2
      READ(1) (A2(I),I=1,M2),A1,(A2(I),I=1,M7) $ K=2 $ A=1.-1.E-4
      DO 290 I=1,M5,16 $ L=8
      IF(S(I+3).LT.A.AND.S(I+7).LT.A.AND.S(I+11).LT.A.AND.S(I+15).LT.A)
     1GOTO 290
      B=P
      CALL QUAD(S(I),A3(56),A4,A3,B,R)
      IF(P.EQ.B) GOTO 282 $ J=280 $ WRITE(6,390)J $ NS=100 $ RETURN
  282 DO 285 J=1,36
```



```
  285 A3(J)=A3(J)-CQE(J) $ WRITE(2) (A3(J),J=56,95)
      CALL CREATE(A1,A2,A4,A3,A3,A1,IR((I+1)/2),2,M1,0,L,K)
      IF(K.EQ.2) GOTO 290 $ J=(I+15)/16 $ NS=100 $ WRITE(6,291)J
      RETURN
  290 CONTINUE
      END FILE 2
      IF(NS.GT.10) RETURN $ GOTO 150
  107 FORMAT(1X," LINPB AT 105 IN REG DETERMINANT IS",E11.4," J IS",I4,"
     1***WARNING*** ***WARNING*** *** WARNING***")
  191 FORMAT(" QUAD",I3," ELEMENT",I2," BECOMES ELASTIC IN CYCLE",I3)
  205 FORMAT(" LIMITLOAD REACHED IN SUBROUTINE REG")
  264 FORMAT(" QUAD",I3," ELEMENT",I2," BECOMES PLASTIC IN CYCLE",I3)
  291 FORMAT(1H0,146" CALLED BY REG. QUAD ELEMENT NO",I3)
  390 FORMAT(" DETERMINANT IN LINIPB IS NEGATIVE CALLED BY QUAD CALLED
     1BY REG NEAR STATEMENT NO",I3)
  400 FORMAT(///" SUBROUTINE REGULAR ********** CYCLE NUMBER",I3/
     1"  LOAD INCREMENTS AT RESPECTIVELY DE AND AB ",2E12.4," /K/RL"/
     2"        TOTAL LOAD AT RESPECTIVELY DE AND AB ",2E12.4," /K/RL"/
     2" INCREMENT AND TOTAL PRESCRIBED DISPLACEMENT",2E12.4," /K/RL"/
     2" DISPLACEMENT TIMES G/K/RL "/
     3" NODE    DISPLACEMENT .     TOTAL DISPLACEMENT  NODE
     4  DISPLACEMENT INCREMENT .     TOTAL DISPLACEMENT"/
     5"   NO  X DIRECTION  Y DIRECTION  X DIRECTION  Y DIRECTION  NO
     6X DIRECTION  Y DIRECTION  X DIRECTION  Y DIRECTION")
  410 FORMAT(2X,2(I3,4(3X,E10.4),3X))
  420 FORMAT(/" STRESSES OF ALL TRIANGULAR ELEMENTS"/
     1" QUAD ELEM STRESS INCREMENT STRESS INCREMENT TOTAL STRESS
     2      TOTAL STRESS      YIELD"/
     3"  NO   NO        Q(1)          Q(2)          Q(3)        Q(1)
     4     Q(2)          Q(3)        VALUE")
  430 FORMAT(1X,I4,I6,1X,7(2X,E10.4))
  450 FORMAT(///" SUBROUTINE REGULAR********** CYCLE NUMBER ",I3/
     1" AT DE",10X," LOADINCREMENT=",E10.4," /K/RL",10X,
     2" TOTAL LOAD=",E10.4," /K/RL"/
     29X," DISPLACEMENTINCREMENT=",E10.4," G/K/RL TOTAL DISPLACEMENT=",
     3E10.4," G/K/RL, I.E. PRESCRIBED DISPLACEMENT="/
     1" AT AB",10X," LOADINCREMENT=",E10.4," /K/RL",10X,
     2" TOTAL LOAD=",E10.4," /K/RL"/
     29X," DISPLACEMENTINCREMENT=",E10.4," G/K/RL TOTAL DISPLACEMENT=",
     3E10.4," G/K/RL, I.E. DISPLACEMENT U*(1)")
  455 FORMAT(//" YIELD VALUES/K OF THE 4 ELEMENTS IN EACH QUAD"/
     62(" QUAD",6X,"ELEMENT 1",6X,"ELEMENT 2",6X,"ELEMENT 3",6X,
     7"ELEMENT 4",2X))
  460 FORMAT(2(2X,I3,4E15.6,2X))
      END
```

```
      SUBROUTINE VMUL00(B,C,I2,I1,A,I3)
      DIMENSION A(1),B(1),C(1)
      IF(I3.NE.0) GOTO 110 $ N=(I1+1)*I1/2
      DO 100 I=1,N
  100 A(I)=0.
  110 N=0 $ M=-I2
      DO 120 I=1,I1 $ M=M+I2 $ L=-I2
      DO 120 J=1,I $ L=L+I2 $ N=N+1
      DO 120 K=1,I2
  120 A(N)=A(N)+B(M+K)*C(L+K) $ RETURN $ END
```



```
      SUBROUTINE QUAD(S,C,AA,D,P,R)
      DIMENSION S(1),C(40),AA(80),D(55),IR(12),R(60)
      DATA IR/1,5,6,2,7,6,3,7,8,4,5,8/
      C(1)=2. $ C(2)=-1. $ C(3)=1.5*P $ C(4)=-1. $ C(5)=.5*P $ C(6)=1.5*
     1P
      DO 70 I=1,18
   70 C(I+6)=C(I)
      N=4
      DO 110 I=1,19,6
      IF(S(N).LE.1.-1.E-10) GOTO 110
      A=S(N-3)/4./S(N) $ B=(S(N-2)-S(N-1))*A
      A=S(N-3)*A $ C(I)=C(I)-2.*A $ C(I+2)=C(I+2)-.5*B
      C(I+1)=C(I+1)+A-B
      C(I+3)=C(I+3)+A+B $ C(I+4)=C(I+4)+.5*A $ C(I+5)=C(I+5)-.5*B
  110 N=N+4
      DO 130 I=1,36
  130 D(I)=0.
      DO 140 I=1,10,3
  140 CALL CREATE(D,D,D,C(2*I-1),D,D,IR(I),8,6,1,3,1)
      CALL VMULSF(D,.8,R,10,8,AA,8)
      CALL VMUL00(R,AA,8,10,D,0)
      AA(17)=0. $ AA(18)=D(54) $ AA(19)=D(45) $ AA(20)=D(55) $ N=37
      DO 150 I=1,15,2 $ AA(I)=D(N) $ AA(I+1)=D(N+9)
  150 N=N+1
      CALL LINIPR(AA(17),2,1,2,AA(21),N,A,B,I)
      IF(A*2.**8.GT.1.E-10.AND.I.EQ.0) GOTO 160 $ P=P*100. $ RETURN
  160 DO 170 I=21,23
  170 AA(I)=-AA(I)
      CALL VMULSF(AA(21),2,AA,8,2,C(25),2)
      CALL VMUL00(AA,C(25),2,R,D,1) $ RETURN $ END
```

```
      PROGRAM ADJUST(INPUT,TAPE5=INPUT,TAPE6=TAPE8,TAPE8,TAPE9,TAPE10,OUTPUT=2
     100)
      DIMENSION N(15),SR(2),D1(3),D2(150),ET(540),IET(540),C0(135),
     1TE(135),AU(77),AE(1050),U(77),V(77),DI(2850),UT(2)
      RE=IND 8
      RE=IND 9
      RE=IND 10
      READ(10) N1,N2,N3,N4,N5,N6,N7,FMAX,P,RL,ITEL,SL
      RE=IND 10
      WRITE(6,75) N1,N2,N3,N4,N6,N7,FMAX,P,RL
   40 READ(5,100)N $ IF(N(1).LT.0) GOTO 350
      READ(9)M1,M3,M6 $ M=4*M3 $ K=M1*M6
      READ(9)SR,D1,D2,ET,IET,C0,TE,AE,V,DI,UT $ GOTO 60
   50 READ(5,100) N
   60 WRITE(6,110) N
      DO 250 I=1,15 $ K1=M1 $ K6=M6 $ IF(N(I)) 130,350,150
  130 N(I)=N(I) $ GOTO 350
  150 DO 200 J=1,M $ IF(IET(J).EQ.N(I)) IET(J)=-IET(J)
  200 CONTINUE $ L=N(I)-2 $ D2(L)=0. $D2(L+M1)=0. $ AE(L+K)=1.
      DO 250 J=L,K,M1 $ IF(J+K6.LE.K1) AE(J+K6)=0. $ K1=K1+M1 $ K6=K6-1
  250 AE(J)=0. $ GOTO 50
  350 READ(5,100) N5
      WRITE(6,120) N5 $ IF(N(1).LT.0) GOTO 675
      READ(5,400) AU $ K=M1+2 $ U(1)=SIGN(1.,V(1))
      WRITE(6,175)
      WRITE(6,125)(IET(J),J=1,M)
      WRITE(6,415)
      WRITE(6,425) AU
      DO 450 J=2,K
  450 U(J)=AU(J)*U(1) $ B=0. $ U(1)=U(1)*AU(1)
      WRITE(6,852) ITEL,B,B,SP,U(1),U(2)
      DO 550 J=1,M,4 $ L=J+3 $ A=0.
      DO 500 K=J,L $ IF(IET(K)) 465,525,475
  465 I=-IET(K) $ GOTO 500
  475 I=IET(K)
  500 A=A+ET(K)*U(I)
  525 I=L/4
      WRITE(6,318) I,B,TE(I),A,C0(I) $ IF(C0(I)) 550,550,600
  550 IF(TE(I)*A.LT.-1.E-10) WRITE(6,700) I $ GOTO 650
  600 IF(ABS(A).GT.1.E-10) WRITE(6,750) I
  650 CONTINUE
      WRITE(8) SP,D1,D2,ET,IET,C0,TE,AU,AE,V,DI,UT $ END FILE 8
  675 WRITE(6,910) $ STOP
   75 FORMAT(//" N1=",I2," N2=",I2," N3=",I2," N4=",I2," N6=",I2," N7="
     1I2," FMAX="F5.3," P="F5.4," RL="F5.4)
  100 FORMAT(15I5)
  110 FORMAT(" VALUES OF N"15I5)
  120 FORMAT(/" N5="I3)
  125 FORMAT(4I5)
  175 FORMAT(/" MATRIX IET")
  318 FORMAT(1X,I7,4X,E11.4,2X,E12.6,21X,E11.4,21X,E11.5)
  400 FORMAT(8F10.4)
  415 FORMAT(/" VECTOR AU")
  425 FORMAT(1X,8F10.4)
  700 FORMAT(" NEGATIVE WORK IN PLASTIC EDGE NO"I4)
  750 FORMAT(" PLASTIC MECHANISM DOES INFLUENCE ELASTIC EDGE NO"I4)
  852 FORMAT (///" SUBROUTINE SLIP  **************** CYCLE NUMBER="I3/
```



```
     1" LOAD INCREMENTS AT RESPECTIVELY DE AND AB ",2E12.4,"/K/RL"/
     2"       TOTAL LOAD AT RESPECTIVELY DE AND AB ",2E12.4,"/K/RL"/
     2"       MECHANISMS AT RESPECTIVELY DE AND AB ",2E12.4//
     3" EDGE NO"4X,"STRESSINCREMENT",2X,"TOTAL STRESS",4X,"(STRAIN INCR)
     4"EDGELENGTH*G/K",4X,"C0(PLASTIC,LT.0.,LT.ELASTIC)")
  900 FORMAT(" DIMENSION IN ADJUST ARE TOO SMALL")
  910 FORMAT(" PROGRAM ADJUST COMPLETED")
      END
```


123 - 124 blank

Appendix C Direct computation of yield-point load

Since the elastic-plastic analysis using the classical model appeared to encounter a numerical instability without reaching a limit load, it seemed advisable to compute directly the yield-point for the model. We did this by noting that the limit load is independent of Young's modulus so that we can use a rigid plastic material. We then used the upper bound theorem of limit analysis [7] to approach the yield point load from above. This appendix summarizes the analysis used, and concludes with a listing of the computer program.

We deal at yield point load with an incompressible material. As is known in a QUAD element consisting of four triangular elements, Fig. 62, only three triangles need to have an incompressibility constraint in order to have all four triangles incompressible. With two of these constraints we are able to eliminate the displacements u_9 and v_{10}. Hence we have one constraint left for each QUAD. The QUAD is a handy unit to use. Therefore rather than enforce the constraint directly an additional strain is introduced which should be zero in order to satisfy the incompressibility constraint, but we allow it to become a small value, many orders lower than the maximum of the other strains. This technique is equivalent to taking a Poisson ratio of .49999 instead of .5.

The internal dissipation of the QUAD element of Fig. 62 is

$$\dot{W}_{int} = \sum_{k=1}^{4} (\sigma_{ij}{}^{k}\, \dot{\varepsilon}_{ij}{}^{k})$$

$$= \left(\frac{\sigma^1_{xx}+\sigma^1_{yy}}{2}\right)(\dot{\varepsilon}^1_{xx}+\dot{\varepsilon}^1_{yy}) + \left(\frac{\sigma^2_{xx}+\sigma^2_{yy}}{2}\right)(\dot{\varepsilon}^2_{xx}+\dot{\varepsilon}^2_{yy}) +$$

$$\left(\frac{\sigma^3_{xx}+\sigma^3_{yy}}{2}\right)(\dot{\varepsilon}^3_{xx}+\dot{\varepsilon}^3_{yy}) + \left(\frac{\sigma^4_{xx}+\sigma^4_{yy}}{2}\right)(\dot{\varepsilon}^4_{xx}+\dot{\varepsilon}^4_{yy}) +$$

$$\sum_{k=1}^{4} \left(\frac{\sigma^k_{xx}-\sigma^k_{yy}}{2}\right)(\dot{\varepsilon}^k_{xx}-\dot{\varepsilon}^k_{yy}) + \tau^k_{xy}\,\dot{\gamma}^k_{xy} \qquad \text{(C-1)}$$

where superscripts are the element numbers.

We write the strains in terms of the nodal displacements and enforce the incompressibility requirement $\dot{\varepsilon}_{xx} + \dot{\varepsilon}_{yy} = 0$ on the elements 2 and 3 to obtain

$$\dot{u}_9 = (\dot{u}_3 - \dot{v}_4 + \dot{u}_5 + \dot{v}_6)/2$$
$$\dot{v}_{10} = (\dot{u}_5 + \dot{v}_6 - \dot{u}_7 + \dot{v}_8)/2 \qquad \text{(C-2)}$$

Then, if $\dot{\varepsilon}_7$ is defined by

$$\dot{\varepsilon}_7 = (\dot{u}_1 + \dot{v}_2 - \dot{u}_3 + \dot{v}_4 - \dot{u}_5 - \dot{v}_6 + \dot{u}_7 - \dot{v}_8)/4 \qquad \text{(C-3)}$$

it follows from (C-2) that

$$\dot{\varepsilon}^1_{xx} + \dot{\varepsilon}^1_{yy} = \dot{\varepsilon}^4_{xx} + \dot{\varepsilon}^4_{yy} = 2\,\dot{\varepsilon}_7 \qquad \text{(C-4)}$$

so that strict satisfaction of incompressibility would require $\dot{\varepsilon}_7 = 0$. Therefore the internal dissipation can be written

$$\dot{W}_{int} = (\sigma^1_{xx}+\sigma^1_{yy}+\sigma^4_{xx}+\sigma^4_{yy})\dot{\varepsilon}_7 + \sum_{k=1}^{4} \left(\frac{\sigma^k_{xx}-\sigma^k_{yy}}{2}\right)(\dot{\varepsilon}^k_{xx}-\dot{\varepsilon}^k_{yy}) + \tau^k_{xy}\,\dot{\gamma}^k_{xy} \qquad \text{(C-5)}$$

The strain rate nodal velocity relations for this QUAD element are derived in a similar way to the derivation in Chap. V. By means of (C-2) these relations are written

$$\dot{\varepsilon}^1_{xx}-\dot{\varepsilon}^1_{yy} = (\dot{u}_1-\dot{v}_2-\dot{u}_3-\dot{v}_4+\dot{u}_5+\dot{v}_6-\dot{u}_7+\dot{v}_8)/2$$

$$\dot{\varepsilon}^2_{xx}-\dot{\varepsilon}^2_{yy} = -\dot{v}_4+\dot{v}_6$$

$$\dot{\varepsilon}^4_{xx}-\dot{\varepsilon}^4_{yy} = (\dot{u}_1-\dot{v}_2-\dot{u}_3+\dot{v}_4-\dot{u}_5-\dot{v}_6+\dot{u}_7+\dot{v}_8)/2$$

$$\dot{\varepsilon}^3_{xx}-\dot{\varepsilon}^3_{yy} = -\dot{u}_5+\dot{u}_7$$

$$\dot{\gamma}^1_{xy}=\dot{\gamma}^4_{xy} = (\dot{u}_1+\dot{v}_2-\dot{u}_5-\dot{v}_6)/2$$

$$\dot{\gamma}^2_{xy}=\dot{\gamma}^3_{xy} = (\dot{u}_3-\dot{v}_4-\dot{u}_7+\dot{v}_8)/2 \qquad \text{(C-6)}$$

In the constitutive equation every element is assumed to be at yield which implies that the stress state satisfies

$$\left(\frac{\sigma_{xx}-\sigma_{yy}}{2}\right)^2 + \tau_{xy}^2 = 1 \qquad \text{(C-7)}$$

where we dropped the superscripts as element identification. The two generalized stresses can be

represented by

$$(\sigma_{xx}-\sigma_{yy})/2 = \cos\phi \qquad \tau_{xy} = \sin\phi \qquad \text{(C-8)}$$

and hence satisfies (C-7). From the normality condition on the yield surface the plastic strain rates must satisfy

$$\dot{\varepsilon}_{xx} - \dot{\varepsilon}_{yy} = \dot{c}\cos\phi \qquad \dot{\gamma}_{xy} = \dot{\varepsilon}\sin\phi \qquad \text{(C-9)}$$

Combining (C-8) and (C-9) we obtain

$$\frac{\sigma_{xx}-\sigma_{yy}}{2} = \frac{1}{\dot{\varepsilon}}(\dot{\varepsilon}_{xx}-\dot{\varepsilon}_{yy}) \qquad \tau_{xy} = \frac{1}{\dot{\varepsilon}}\dot{\gamma}_{xy} \qquad \text{(C-10a)}$$

$$\dot{\varepsilon} = \sqrt{(\dot{\varepsilon}_{xx}-\dot{\varepsilon}_{yy})^2 + \dot{\gamma}^2_{xy}} \qquad \text{(C-10b)}$$

The second constitutive relation should be $\dot{\varepsilon}_7 = 0$. However, it is useful to relate the additional generalized strain rate $\dot{\varepsilon}_7$ with the stress we introduced for every QUAD by setting

$$(\sigma^1_{xx}+\sigma^1_{yy}+\sigma^4_{xx}+\sigma^4_{yy}) = \alpha\dot{\varepsilon}_7 \qquad \text{(C-11)}$$

By taking α sufficiently large, say $\alpha = 10^{10}$, we can guarantee an insignificantly small value of $\dot{\varepsilon}_7$.

The computation method we followed is based on the principle of virtual work and the direct stiffness method already discussed with the classical model. However here we used an iterative procedure. During

a new iteration cycle $\dot{\varepsilon}$ of Eq. (C-10b) is computed from the results of the previous cycle, and is then incorporated in the stiffness matrix. As convergence occurs $\dot{\varepsilon}$ should become a constant value in each QUAD. The flow chart is shown in Fig. 63 and the computer program is listed at the end of this appendix.

Solving the Prandtl rough punch problem discussed in Chapt. VI by this method we obtain a yield point load of 7.232. We need to evaluate the accuracy of this answer. One way is to multiply the velocity vector, containing terms in the order of 10^{-2} and lower, with the stiffness matrix, containing terms in the order of 10^{10}, to obtain the force vector. Of course, not all of the supposedly homogeneous equations are exactly zero in the force vector. Considering the largest "error" in this force vector as the inaccuracy of the reaction force under the punch, we find the answer is reliable within 0.6%. Considering the error due to the homogeneous equation near the punch the reaction force deviates 0.002%. The other way to evaluate our answer is from a kinematical viewpoint. The largest $\dot{\varepsilon}_7$ in any QUAD is 5 orders lower in magnitude then the largest strain rate $\dot{\varepsilon}$.

The conclusion is that the yield-point load of 7.232 is reliable for the Prandtl rough punch with the element arrangement of Fig. 9.


```
      PROGRAM RPFLOW(INPUT,TAPE5=INPUT,TAPE6=OUTPUT=2008,TAPE1,TAPE2)
C ***
C *** BEGIN RPFLOW
C ***
      COMMON A(1)/ONE/N1,N2,N3,N4,IDV(98),IR(288),M6,ERR,IMAX
C *** DIMENSION IDV(2*N1*N2)  INTERNAL VERSUS EATERNAL NODE NUMBERS
C *** DIMENSION IR(8*(N1-1)*(N2-1)) QUAD VESUS INTERNAL NODE NUMBERS
      READ(5,100) N1,N2,N3,N4,ERR,IMAX
      A(1)=0. $ IF(N1.GT.0) GOTO 10 $ A(1)=1. $ N1=-N1
   10 M3=2*N1*N2-N2-N3 $ IF(N4.EQ.1) GOTO 20 $ M3=M3-N1+1
      IF(N4.EQ.2) GOTO 20 $ M3=M3-N1+1 $ IF(N4.EQ.4) M3=M3-N3+1
C *** MJ DEGREES OF FREEDOM
   20 WRITE(6,110) N1,N2,N3,N4,ERR,IMAX
  110 FORMAT("1*** VERTICAL ",I1," NODES"/" * HORIZONTAL ",I1," NODES"/
     1" UNDER PUNCH ",I1," NODES"/" **** PROBLEM ",I1/" ****** ERROR "
     2E10.4/" ******* IMAX ",I3)
  100 FORMAT(4I5,F10.6,I5)
      M4=M3+93 $ IF(M3.GE.16) M4=(M3-1)*M3/2+2 $ M6=2*N1+2
      M=M4-1+(M3-2)*(M6+3)*2
      N=LOCF(A(1)) $ M=M+N
      CALL MEMJOB(M)
      IF(N.GT.M) GO TO 30
      WRITE(6,120) M-N
  120 FORMAT("1",/////" ********** FIELDLENGTH IS ",I10," DECIMAL 100 S
     1ORT")
      STOP
   30 N=0
      CALL MEMREQ(N) $ M=M-N
      CALL MEMREQ(M)
      CALL RPREQ(M),A,A(P3+1),A(M4),A(M4+(M6+1)*(M3-2)))
      STOP
C ***
C *** END RPFLOW
C ***
      END
```

```
      SUBROUTINE RPREG(M3,U,A6,A3,A2)
C ***
C *** BEGIN SUBROUTINE RPREG
C ***
C *** A6 MAX OF 92 OR (M3-1)*(M3-2)/2
C *** A3 (M3-2)*(M6+1)
C *** A2 2*(M3-2)
      DIMENSION U(M3),A6(A6),A3(1),A2(1),S(18),A1(3)
      COMMON /CNE/N1,N2,N3,N4,IDV(98),IR(288),M6,ERR,IMAX
      M1=M3-2 $ M4=2*N1 $ M5=10*(N1-1)*(N2-1) $ M7=2*M1 $ M8=M5/2
      M9=(M6+1)*M1 $ M10=M7+1 $ PM1=16/FLOAT(M5) $ M2=N2*M4
      RL=FLOAT(2*(N1-1)) $ RL2=FLOAT(2*(N2-1))
      IF(U(1).GT..5) GOTO 90 $ ITEL=0
C *** IDV RELATES EXTERNAL AND INTERNAL NUMBERING OF NODES
      IDV(1)=2 $ IDV(2)=0 $ IF(N4.GT.2) GOTO 15
      DO 10 J=3,M4
   10 IDV(J)=J $ J=M4
      GOTO 25
   15 J=2
      DO 20 I=6,M4,2
      I2=(I-1)*2 $ J=J+1
   20 IDV(I)=J
   25 M=N2-N3-1 $ I=M4
      IF(M.EQ.0) GOTO 35
      DO 30 L=1,M
      I=I+2 $ J=J+1 $ IDV(I-1)=J $ IDV(I)=0
      DO 30 K=1,M4
      I=I+1 $ J=J+1
   30 IDV(I)=J
   35 M=N3-1 $ IF(N4.EQ.1) M=N3
      DO 50 L=1,M
      I=I+2 $ J=J+1 $ IDV(I-1)=J $ IDV(I)=0 $ IF(M4.LE.4) GOTO 45
      DO 40 K=5,M4
      I=I+1 $ J=J+1
   40 IDV(I)=J
   45 I=I+2 $ J=J+1 $ IDV(I-1)=J $ IF(N4.LT.4) GOTO 50 $ IDV(I-1)=0
      J=J-1
   50 IDV(I)=1 $ IF(M4.EQ.1) GOTO 65
      I=I+2 $ IDV(I-1)=0 $ IDV(I)=0
      DO 60 L=4,M4,2
      I=I+2 $ IDV(I-1)=0 $ J=J+1
   60 IDV(I)=J $ IDV(I)=1
   65 IDV(I-1)=0
C *** IN RELATES QUADS WITH INTERNAL GRIDS
      I=1 $ J=1
      DO 80 K=2,N2
      DO 75 K=2,N1
      IR(J)=IDV(I+2*M4) $ IR(J+1)=IDV(I+3*M4) $ IR(J+2)=IDV(I+2)
      IR(J+3)=IDV(I+3) $ IR(J+4)=IDV(I) $ IR(J+5)=IDV(I+1)
      IR(J+6)=IDV(I+M4) $ IR(J+7)=IDV(I+1+M4) $ I=I+2
   75 J=J+8
   80 I=I+2
C *** SET INITIAL DISPLACEMENTS ZERO
      U(1)=.001 $ IF(N4.GT.2) U(1)=-U(1)
      DO 81 I=2,M3
   81 U(I)=0.
      GOTO 100

                                - 133 -
```

```
   90 READ(1) IR,U,ITEL,IDV
C *** BEGIN OF CYCLE
C *** WRITE DISPLACEMENT FIELD
  100 ITEL=ITEL+1
      WRITE(6,101) ITEL
  101 FORMAT("1 **** ITERATION NUMBER ",I4," ****//// DISPLACEMENT FIEL
     1D////)
C *** PRINT DISPLACEMENTFIELD
      DO 105 I=11,M2,10
      DO 104 K=1,10 $ A6(K)=0. $ J=IDV(1+K-11)
      IF(J.NE.0) A6(K)=U(J)
  104 CONTINUE
  105 WRITE(6,106) (I-9)/2,(A6(J),J=1,10)
  106 FORMAT(1X,I5,5(E14.4,E12.4))
      J=(M2/10)*10+1
      DO 107 I=J,M2 $ A6(I+1-J)=0. $ K=IDV(I)
      IF(K.NE.0) A6(I+1-J)=U(K)
  107 CONTINUE $ I=M2-J+1
      WRITE(6,106) (J-1)/2,(A6(K),K=1,I)
      WRITE (6,108)
  108 FORMAT(////" DATA OF EACH QUAD ELEMENT")
C *** SET COEFFICIENTS OF STIFFNESS MATRICES ZERO
      DO 110 I=1,M7 $ A3(I)=0.
  110 A2(I)=0.
      DO 120 I=M10,M9
  120 A3(I)=0. $ A1(1)=0. $ A1(2)=0. $ A1(3)=0.
      SM1=0. $ SM2=0.
      DO 200 I=1,MM,8
C *** COMPUTE STIFFNESS CONTRIBUTION OF EACH ELEMENT
      CALL QUAD(U,IR(I),S(1),A6,S,A6(37))
      WRITE(6,400)(I+7)/8,S
      S1=SM1+S(17) $ SM2=SM2+ABS(S(18))
  200 CALL CREATE(A1,A2,A3,A6,IR(I),2,M1,M6,8)
      WRITE(6,401) SM1*PM1,SM2*PM1
C *** DETERMINE LOADS AND THE ERROR IN THE HOMOGENEOUS EQUATIONS
      CALL VMULSF(A1,2,U,1,2,A4,2)
      CALL VMULFF(A2,U,M1,2,1,M1,2,A4(3),1,J)
      CALL VMULOF(A3,M1,M6,M1,U(3),1,M1,A4(M1+5),M1)
      CALL VMULFM(A2,U(3),M1,2,1,M1,M1,A4(M1+3),2,J)
      SM3=0.
      DO 210 I=1,M3 $ A6(I)=A6(I)+A4(I+M3)
  210 SM3=SM3+ABS(A4(I))
      IF(SM3.EQ.0..OR.SM1.EQ.0.) GO TO 900
      SM3=(SM3-ABS(A6(1))-ABS(A6(2)))/FLOAT(M1)
      WRITE(6,402) A6(1)/RL,A6(2)/RL2,SM3/RL,SM3/RL2
      IF(SM2/SM1.LT.ERR.AND.SM3.LT.ERR) GO TO 900
      WRITE(6,403)
      DO 215 I=1,M3,10 $ J=I+9 $ IF(J.GT.M3) J=M3
  215 WRITE(6,404) (A6(K),K=I,J)
      IF(IMAA.LT.ITEL) GO TO  900
C *** INVERT STIFFNESS MATRIX
  220 CALL LINPH(A3,M1,M6,M1,A4,1,SM1,SM2,J)
      U(1)=.001 $ U(2)=0. $ IF(N4.LE.2) U(1)=-U(1)
  400 FORMAT(//" ***** QUAD ELEMENT ",I2," DISPLACEMENT NODES ",E12.4,/
     1"          STRESSES ",E12.4,"     STRAIN MEASURE ",E12.4)
  401 FORMAT(//" ** AVERAGED STRAIN ",E12.4," *** AVERAGED ERROR ",E12.4
     1)

                                - 134 -
```

```
  402 FORMAT(//" ********** LOADS ",2E12.4/" *** AVERAGED ERROR ",2E12
     1.4)
  403 FORMAT(////" FORCE VECTOR"///)
  404 FORMAT(1X,10E12.4)
C *** COMPUTE DISPLACEMENT VECTOR
      CALL VMULFF(A2,U,M1,2,1,M1,2,A3,M1,J)
      CALL VMULSF(A4,M1,A3,1,M1,U(3),M1) $ U(1)=-U(1)
      GOTO 100
  900 WRITE(2) IR,U,ITEL,IDV
      RETURN
C ***
C *** END SUBROUTINE MPREG
C ***
      END
```



```
      SUBROUTINE QUAD(U,IR,S,SK,D,W)
C ***
C *** BEGIN SUBROUTINE QUAD
C ***
      DIMENSION U(1),IR(8),S(10),SK(36),W(56),R(56),D(8)
      DATA R/.5,2*0.,.5,0.,.25,-.5,2*0.,-.5,.5,0.,.25,-.5,2*0.,-.5,0.,
     1.5,-.25,-.5,-1.,0.,.5,0.,-.5,.25,.5,0.,-1.,2*0.,.5,0.,-.25,.5,1.,0.,
     22*-.5,0.,-.25,-.5,0.,1.,.5,0.,-.5,.25,.5,2*0.,.5,0.,.5,-.25/
C *** U UNKNOWNS INTERNAL REPRESENTATION
C *** IR RELATES LOCAL QUAD REPRESENTATION AND INTERNAL REPRESENTAION
C *** S(1) THRU S(8) STRESSES IN ELEMENT
C *** S(9),S(10) INTERFORMATION OF STRAINS
C *** SK STIFFNESS MATRIX OF QUAD
C *** W WORKAREA
C *** D DISPLACEMENT
C *** NOTE: A STRESS OUTPUT OF 1000. INDICATES PLASTIC STRAIN OF
C ***       MAGNITUDE LESS THAN 1.E-8
C ***
C *** COMPUTE THE DISPLACEMENTS IN LOCAL COORDINATE SYSTEM
      DO 10 I=1,8 $ D(I)=0. $ J=IR(I) $ IF(J.EQ.0) GOTO 10 $ D(I)=U(J)
   10 CONTINUE
C *** COMPUTE THE 7 STRAINS W(1) THRU W(7)
      CALL VMULFF(R,D,7,,8,,1,7,8,W(11),7,J) $ S(10)=W(17)
C *** COMPUTE STIFFNESS COEFFICIENTS W(1) THRU W(7)
      W(10)=W(15)**2. $ W(6)=W(16)**2. $ S(9)=0.
      W(21)=SQRT(W(11)**2.+W(10))  $ W(22)=SQRT(W(12)**2.+W(9))
      W(24)=SQRT(W(14)**2.+W(10))  $ W(23)=SQRT(W(13)**2.+W(9))
      DO 20 I=1,4 $ W(I)=1.E10 $ IF(W(I+20).GT.1.E-10) W(I)=1./W(I+20)
   20 S(9)=S(9)+W(20+I)/4. $ W(5)=W(1)+W(4) $ W(6)=W(2)+W(3) $ W(7)=1.E10
C *** COMPUTATION OF THE STRESSES
      DO 30 I=1,8
   30 S(I)=1000.
      IF(W(1).GT.1.E10) GOTO 40 $ S(1)=W(11)*W(1) $ S(2)=W(15)*W(1)
   40 IF(W(2).GT.1.E10) GOTO 50 $ S(3)=W(12)*W(2) $ S(4)=W(16)*W(2)
   50 IF(W(3).GT.1.E10) GOTO 60 $ S(5)=W(13)*W(3) $ S(6)=W(15)*W(3)
   60 IF(W(4).GT.1.E10) GOTO 70 $ S(7)=W(14)*W(4) $ S(8)=W(15)*W(4)
C *** COMPUTATION OF STIFFNESS MATRIX
   70 DO 80 I=1,7 $ W(56)=W(I)
      DO 80 J=I,56,7
   80 W(J)=W(56)*R(J)
      CALL VMUL00(R,W,7,8,SK,0) $ RETURN
C ***
C *** END SUBROUTINE QUAD
C ***
      END
```

```
      SUBROUTINE VMULOD(A,B,C,I2,I1,A,I3)
C ***
C *** BEGIN SUBROUTINE VMULOD
C ***
      DIMENSION A(1),B(1),C(1)
      IF(I1.NE.0) GOTO 110 $ N=(I1+1)*I1/2
      DO 100 I=1,N
  100 A(I)=0.
  110 IA=0 $ M=-I2
      DO 120 I=1,I1 $ M=M+I2 $ L=-I2
      DO 120 J=1,I $ L=L+I2 $ N=N+1
      DO 120 K=1,I2
  120 A(N)=A(N)+B(IA+K)*C(L+K) $ RETURN
C ***
C *** END SUBROUTINE VMULOD
C ***
      END
```



```
      SUBROUTINE CREATE(D1,D2,D6,D5,IP,I1,I2,I3,NR)
C ***
C *** BEGIN SUBROUTINE CREATE
C ***
      DIMENSION D1(1),D2(1),D5(1),D6(1),IP(1),JP(16),KR(16)
C *** D1((I1+1)*I1/2),D2(I2,I1),D5((NR+1)*NR/2),D6(I2,I3+1),IR(NP)
C *** IP RELATES ELEMENT COORDINATES WITH GLOBAL COORDINATES
      L=0 $ M=0
      DO 120 I=1,NR $ IF(IR(I).EQ.0) GOTO 120 $ IF(IR(I)-I1) 100,100,110
  100 L=L+2 $ KR(L-1)=I $ KR(L)=IR(I) $ GOTO 120
  110 M=M+2 $ JR(M-1)=I $ JR(M)=IR(I)-I1
  120 CONTINUE
      IF(L.EQ.0) GOTO 170
      DO 150 I=2,L,2
      DO 150 J=2,I,2 $ I5=(KR(I-1)-1)*KR(I-1)/2+KR(J-1)
      I4=(KR(J)-1)*KR(J)/2+KR(I)
      IF(KR(I).GT.KR(J)) I4=(KR(I)-1)*KR(I)/2+KR(J)
      IF(I.NE.J.AND.KR(I).EQ.KR(J)) D1(I4)=D1(I4)+D5(I5)
  150 D1(I4)=D1(I4)+D5(I5)
      IF(M.EQ.0) RETURN
      DO 160 I=2,L,2
      DO 160 J=2,4,2 $ I5=(KR(I-1)-1)*KR(I-1)/2+JR(J-1)
      IF(JP(J-1).GT.KR(I-1)) I5=(JP(J-1)-1)*JR(J-1)/2+KR(I-1)
      I4=(KR(I)-1)*I2+JR(J)
  160 D2(I4)=D2(I4)+D5(I5)
  170 IF(M.EQ.0) RETURN
      DO 190 I=2,4,2
      DO 190 J=2,I,2 $ I5=(JR(I-1)-1)*JP(I-1)/2+JR(J-1)
      I4=(I3-IABS(JP(I)-JP(J)))*I2+JR(I)
      IF(JP(I).LT.JR(J)) I4=I4-JR(I)+JR(J)
  190 D6(I4)=D6(I4)+D5(I5) $ RETURN
C ***
C *** END SUBROUTINE CREATE
C ***
      END
```

LIST OF FIGURES

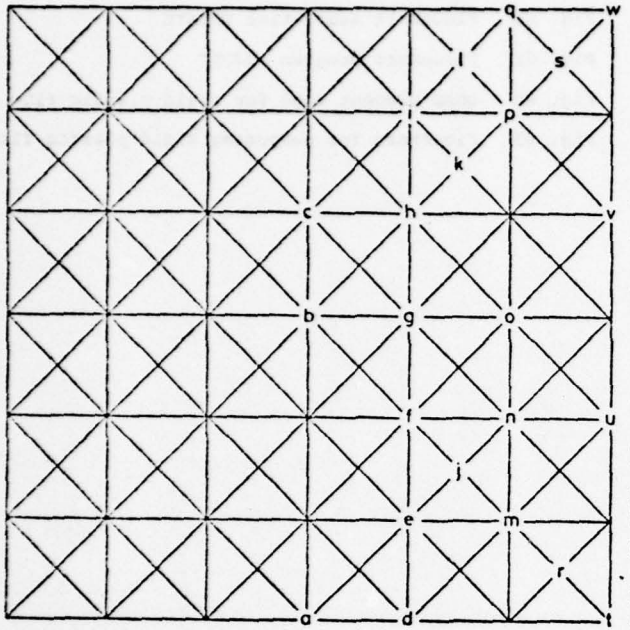

Fig. 1

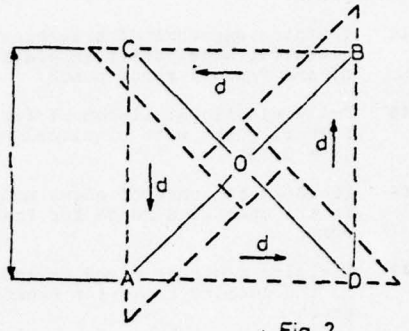

Fig. 2

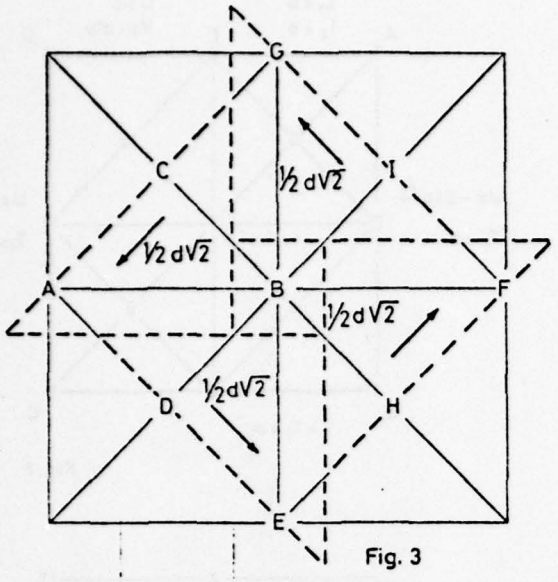

Fig. 3

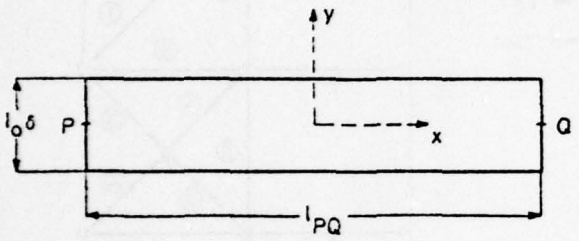

Fig. 4

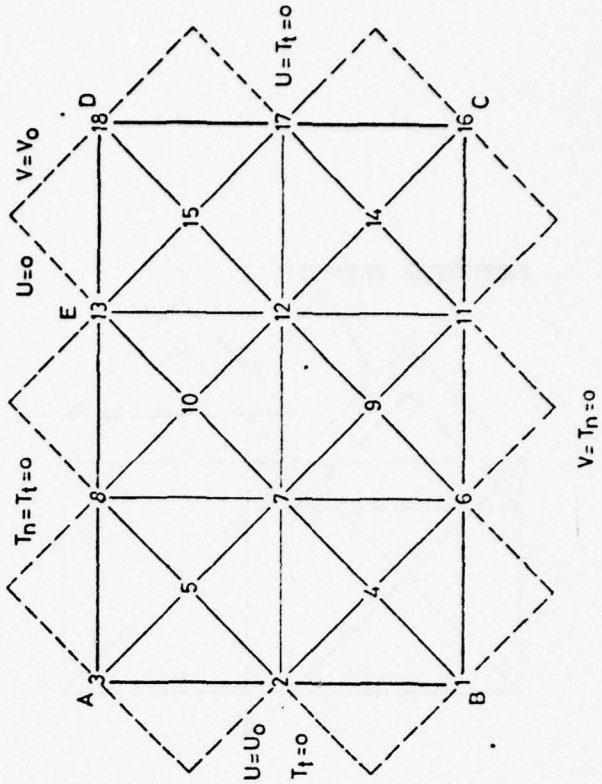

Fig. 5

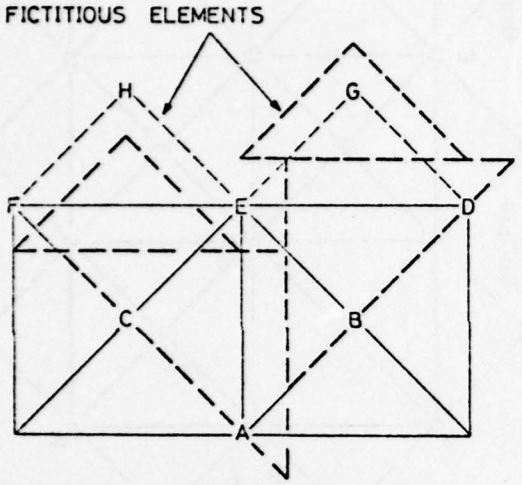

Fig. 6

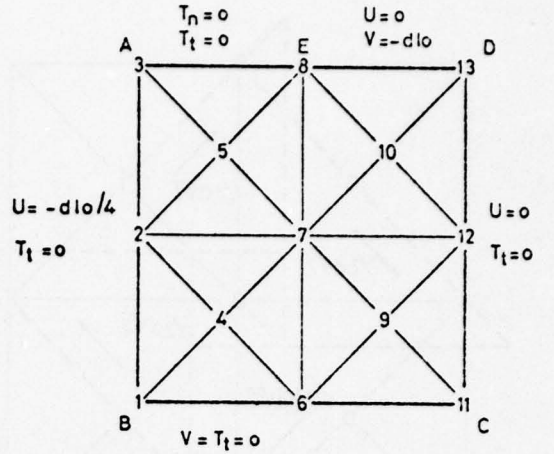

Fig. 7

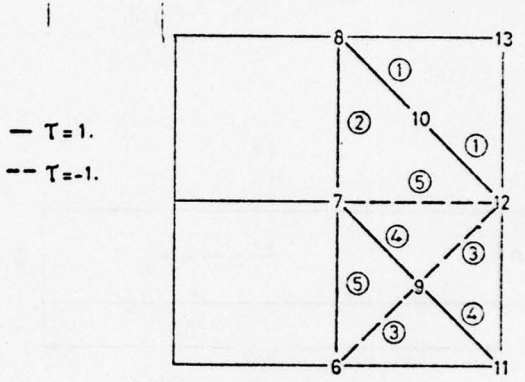

Fig. 8

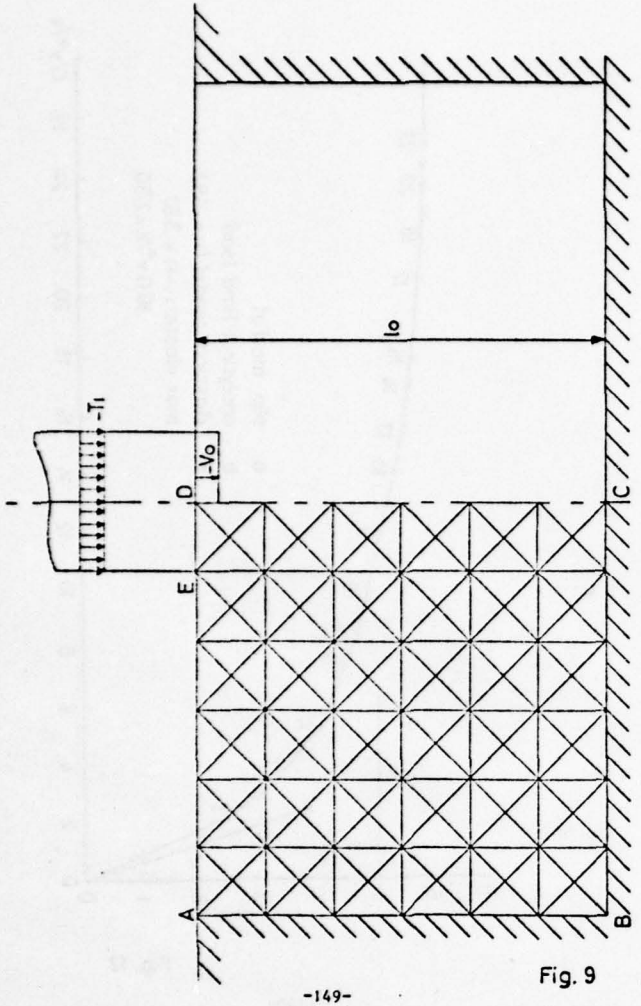

Fig. 9

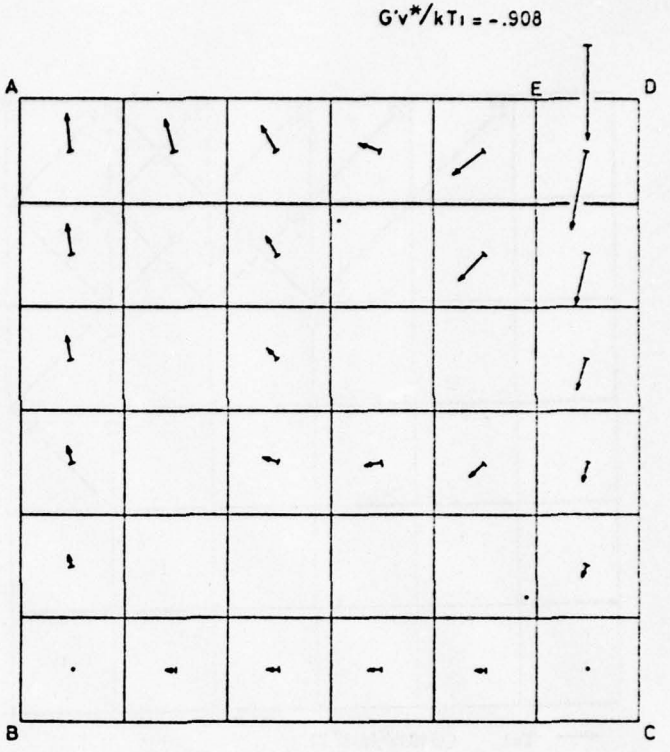

Fig. 10

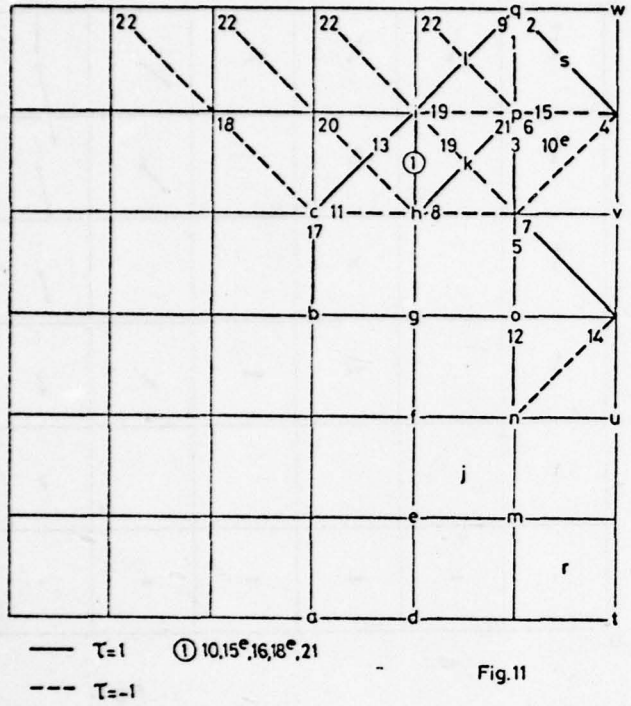
22
22
22
22
g
q
w
2
s
1
18
20
19
p
15
21
6
4
13
19
k
3
10e
c
11
h
8
v
17
7
5
b
g
o
12
14
f
n
u
j
e
m
r
a
d
t
τ=1
① 10,15e,16,18e,21
τ=-1

Fig.11

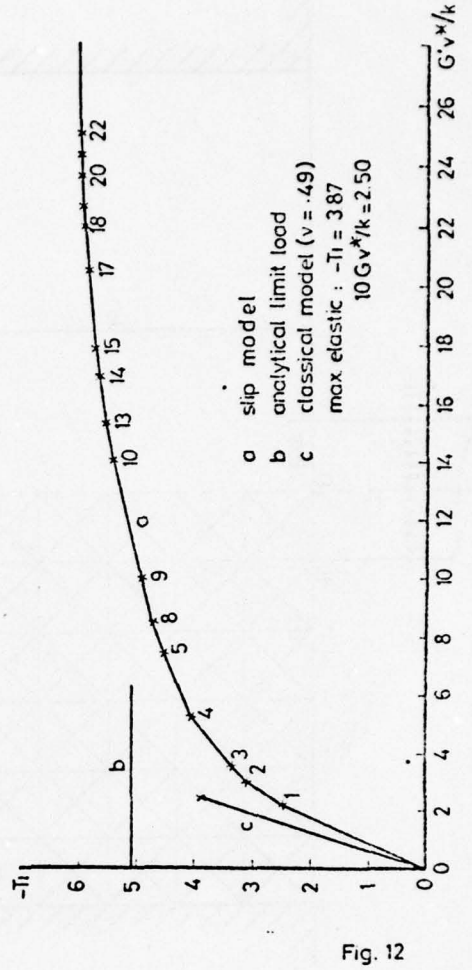
a slip model
b analytical limit load
c classical model (ν = .49)
max elastic : -Ti = 3.87
10 Gv*/k = 2.50
-Ti
G'v*/k
b
c
a

Fig. 12

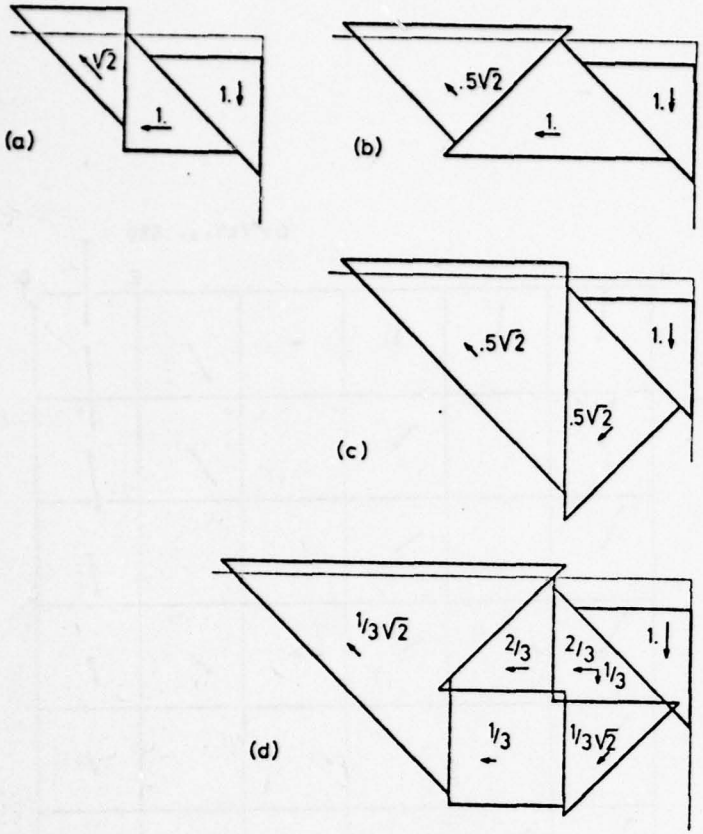
(a)
√2
1.
1.
(b)
.5√2
1.
1.
(c)
.5√2
1.
.5√2
(d)
1/3√2
2/3
2/3
1/3
1.
1/3
1/3√2

Fig. 13

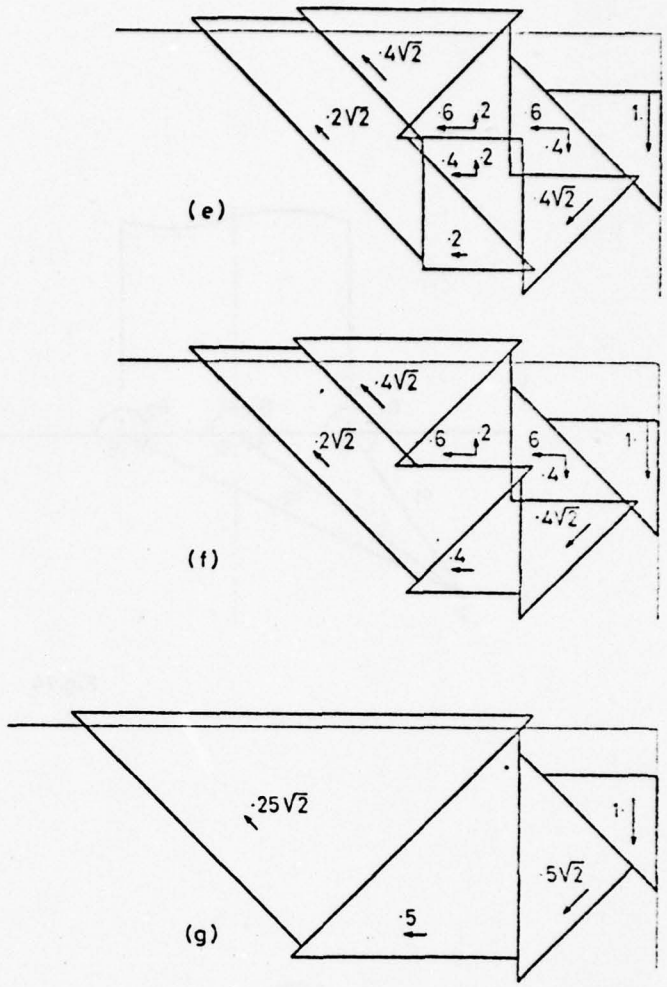
(e)
·4√2
·2√2
·6
2
6
1.
·4
·4
2
4√2
·2
(f)
·4√2
·2√2
·6
2
6
1·
·4
·4√2
·4
(g)
·25√2
·5
1·
·5√2

Fig. 13

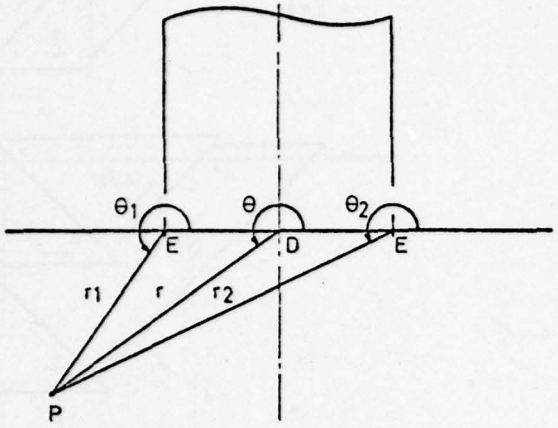

Fig. 14

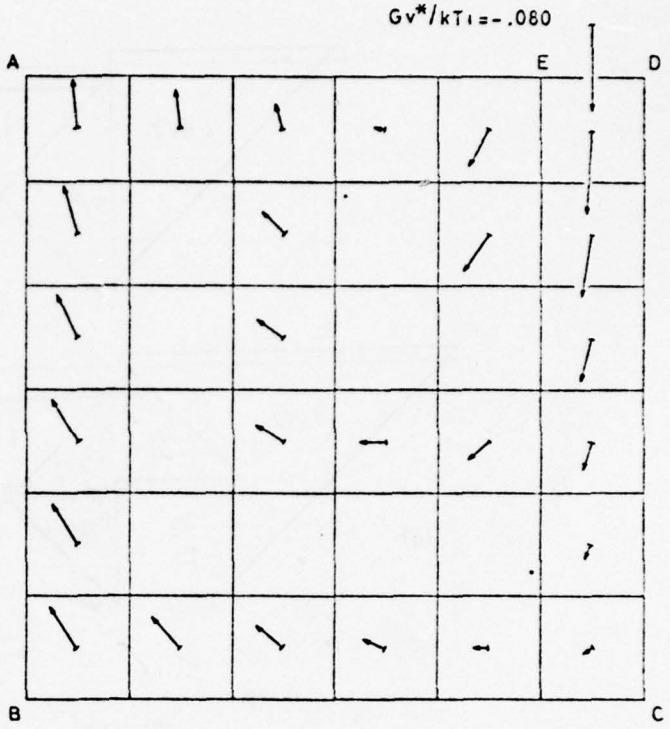

Fig. 15

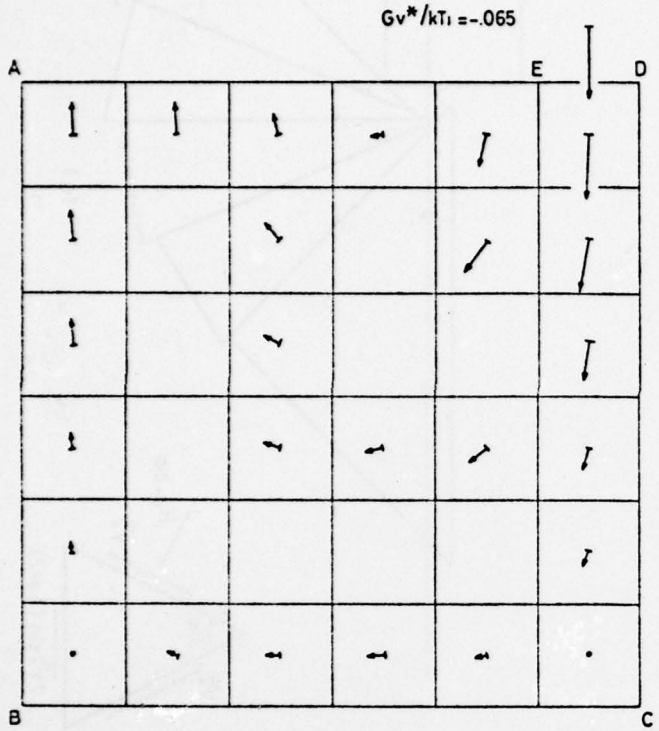

Fig. 16

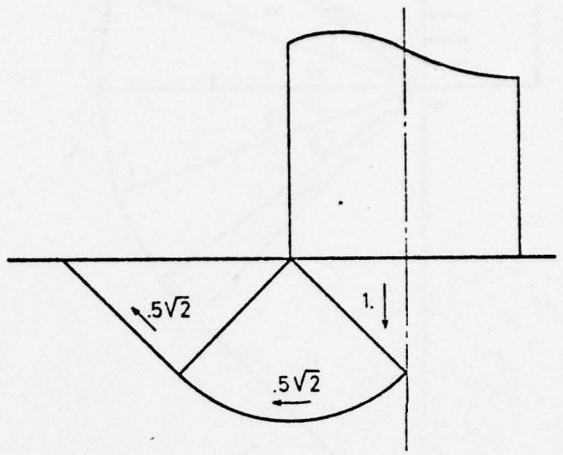

Fig. 17

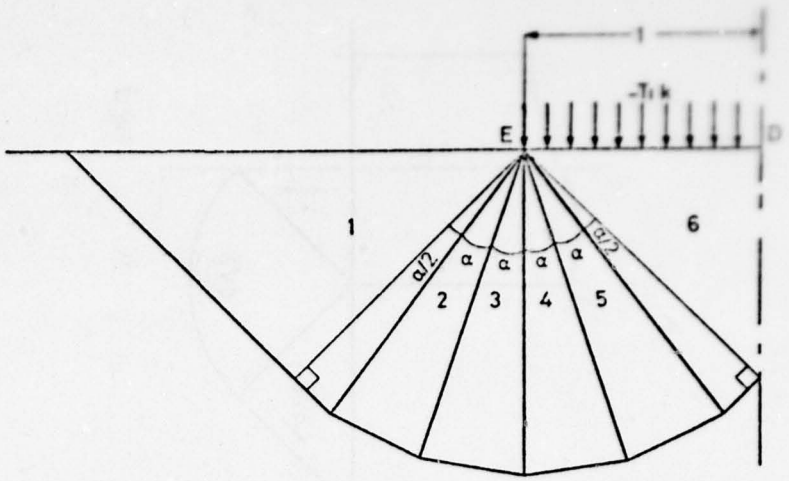

Fig. 18

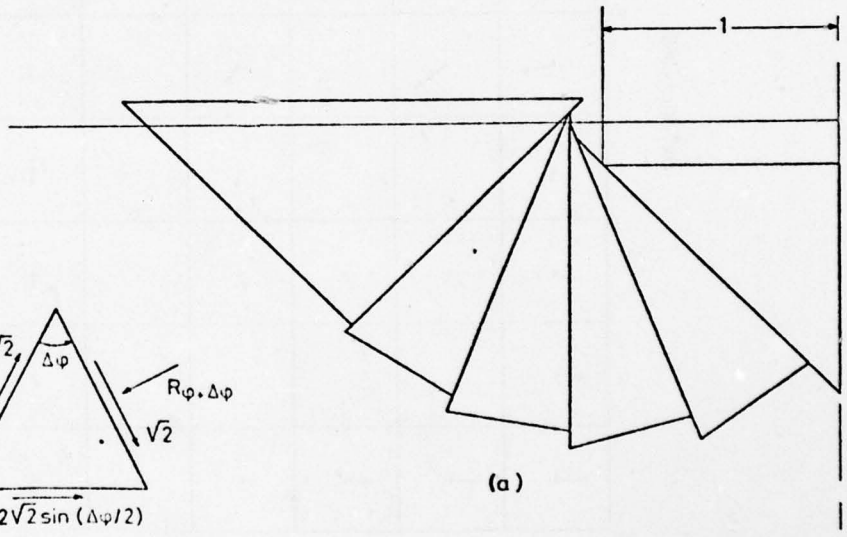

Fig. 19

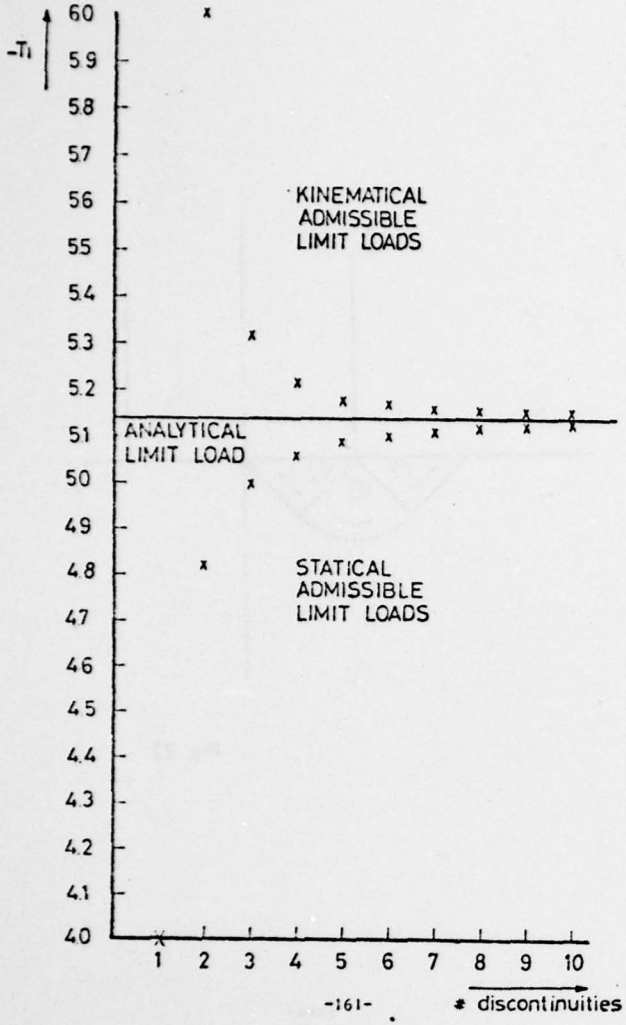
-T1
60
59
58
57
56
55
54
53
52
51
50
49
48
47
46
45
44
43
42
41
40
KINEMATICAL
ADMISSIBLE
LIMIT LOADS
ANALYTICAL
LIMIT LOAD
STATICAL
ADMISSIBLE
LIMIT LOADS
1 2 3 4 5 6 7 8 9 10
discontinuities

Fig. 20

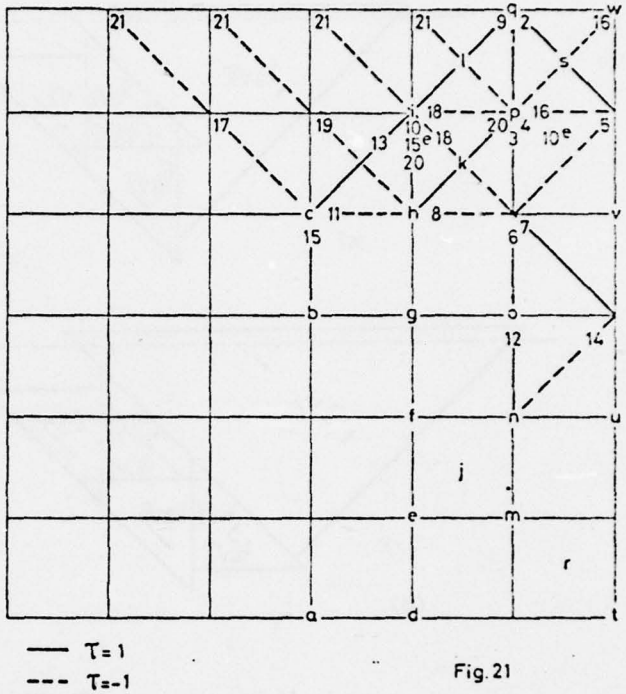
T = 1
T = -1

Fig. 21

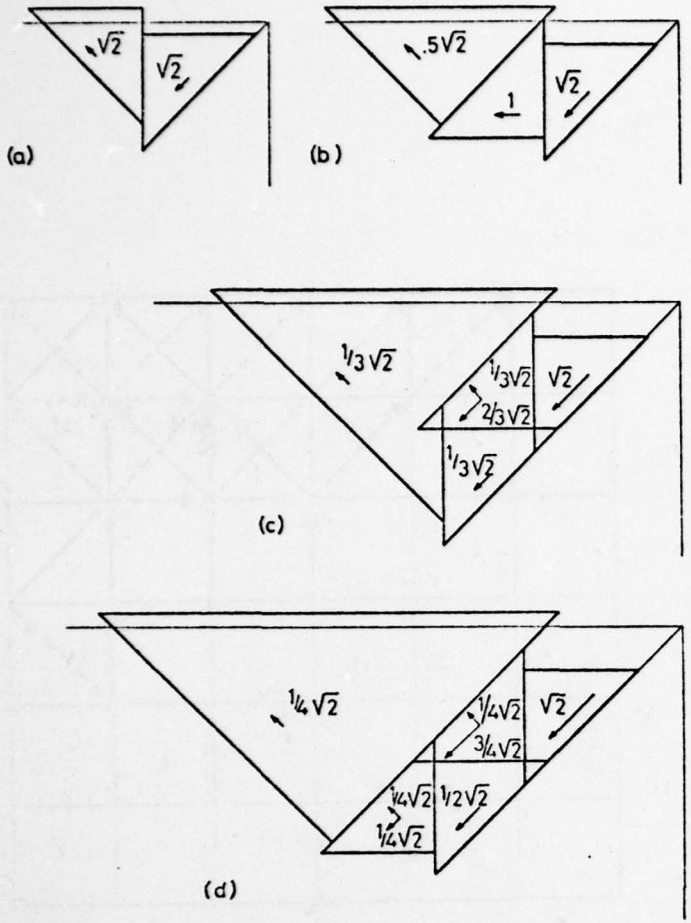

Fig. 22

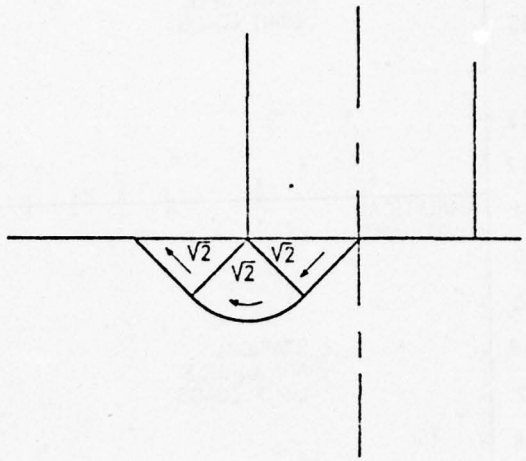

Fig. 23

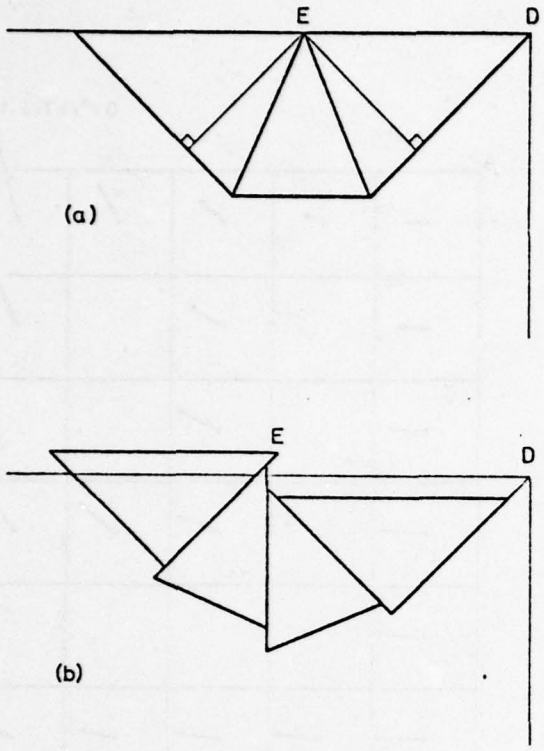

Fig. 24

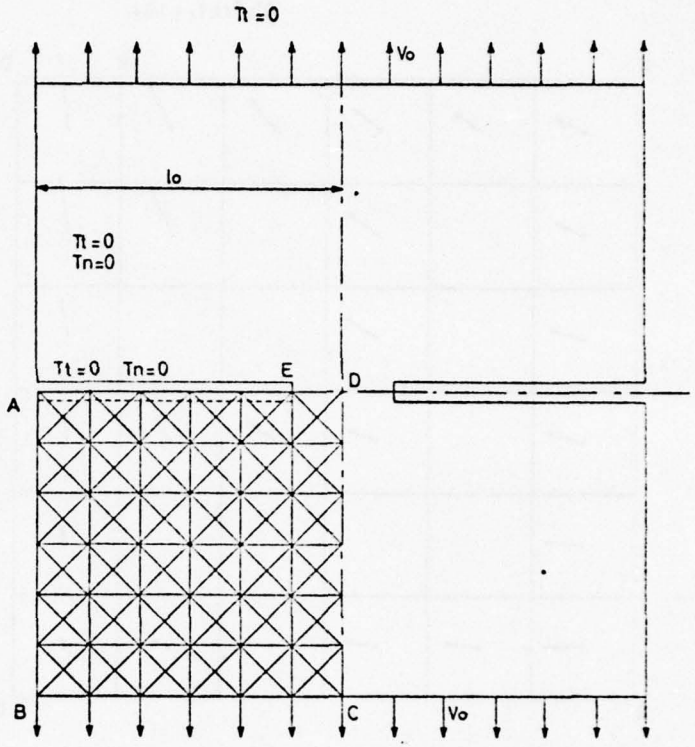

Fig. 25

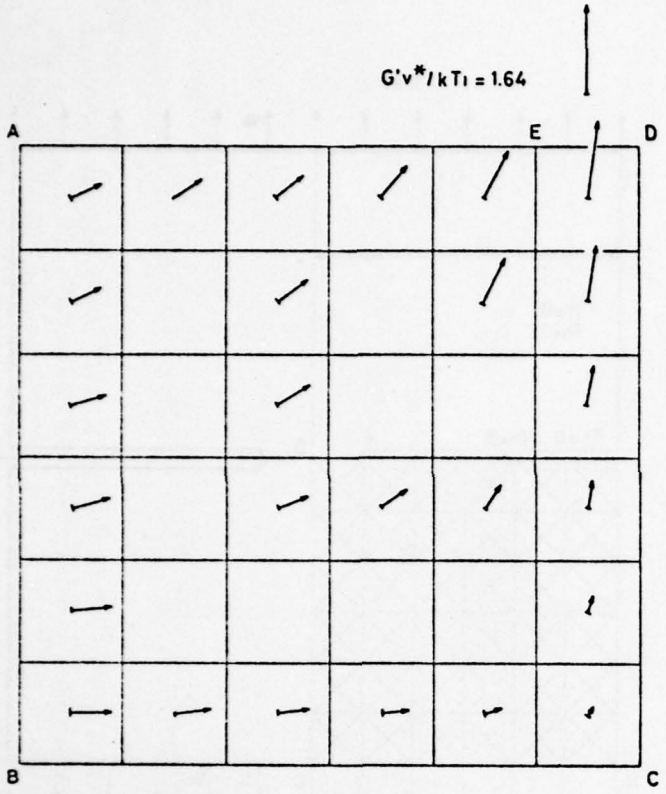

Fig.26

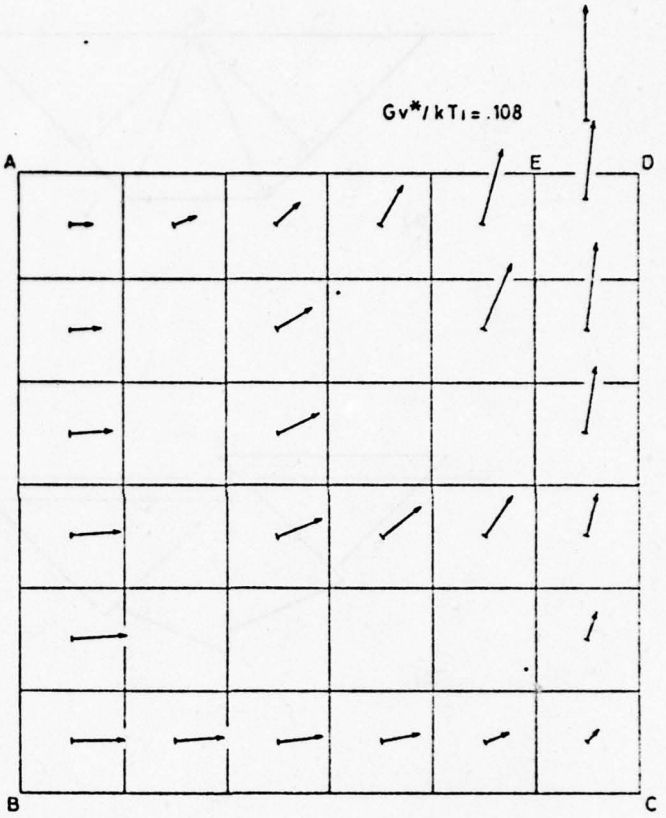

Fig.27

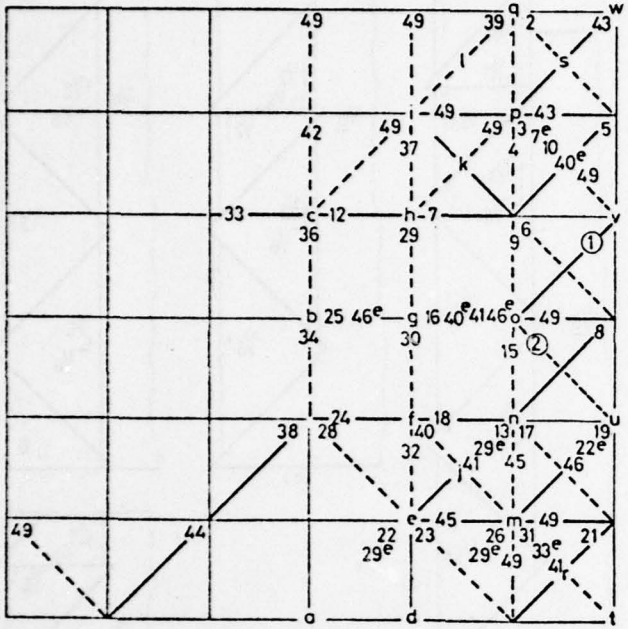
q
w
49
49
39
2
43
s
49
p
43
42
49
49
3
5
37
4
7e
10
40e
49
33
c
12
h
7
36
29
9
6
1
b
25
46e
g
16
40e
41
46e
o
49
34
30
15
2
8
24
f
18
n
u
38
28
40
13
17
19
29e
22e
32
41
45
46
e
45
m
49
49
44
22
23
26
31
21
29e
29e
49
33e
41
a
d
t
τ=1
τ=-1
① 11, 25e, 27, 40e, 48
② 14, 18e, 20, 22e, 35, 42e, 47

Fig. 28

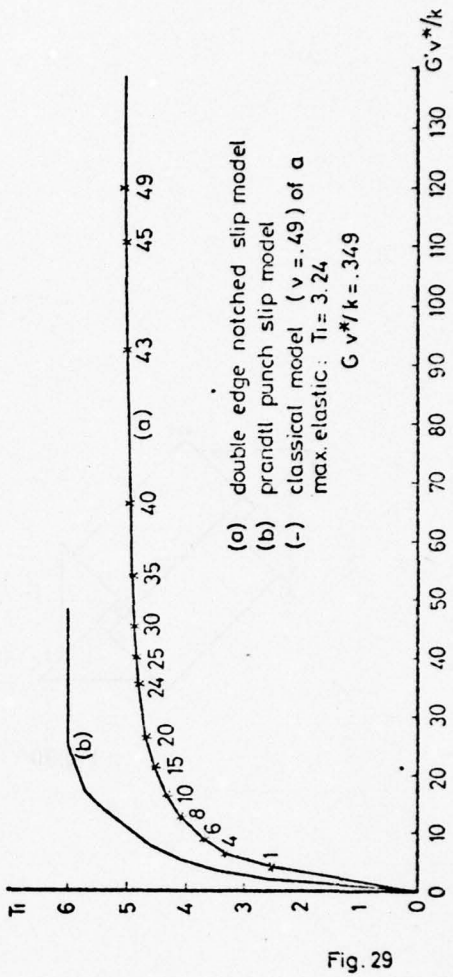
Ti
G v*/k
(b)
(a)
(o) double edge notched slip model
(b) prandtl punch slip model
(-) classical model (ν = .49) of a
max. elastic: Ti = 3.24
G v*/k = .349

Fig. 29

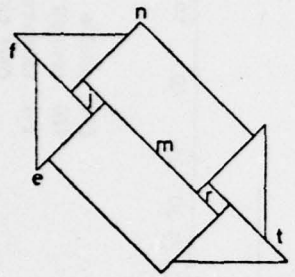
n
f
j
m
e
r
t

Fig. 30

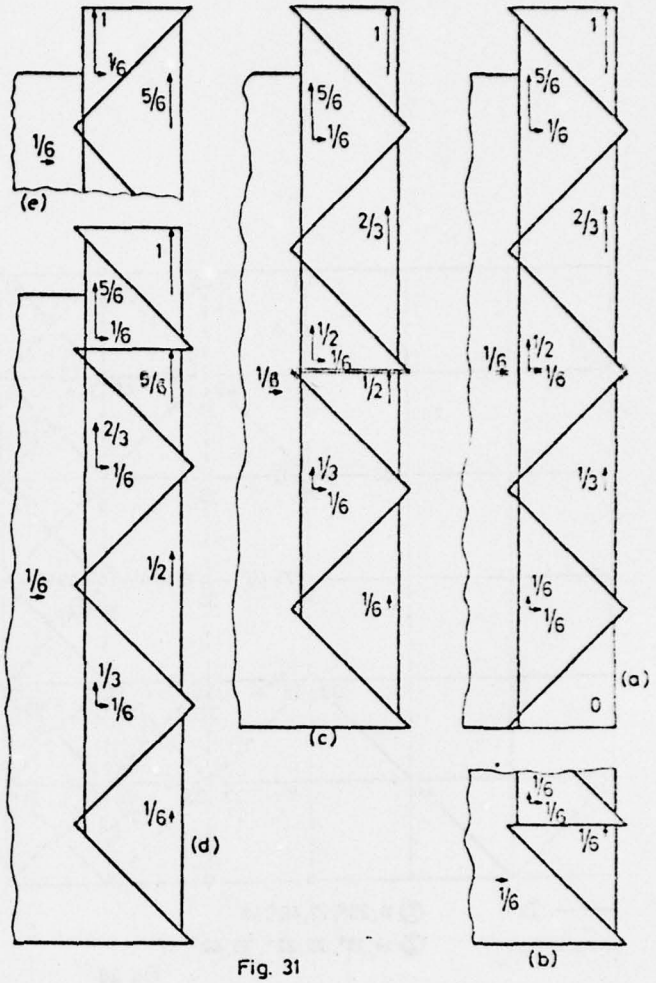
1
1/6
5/6
1/6
(e)
1
5/6
1/6
5/6
2/3
1/6
1/2
1/6
1/6
1/3
1/6
1/6
(d)
1
5/6
1/6
2/3
1/2
1/6
1/6
1/2
1/3
1/6
1/6
(c)
1
5/6
1/6
2/3
1/6
1/2
1/6
1/3
1/6
1/6
0
(a)
1/6
1/6
1/6
1/6
(b)

Fig. 31

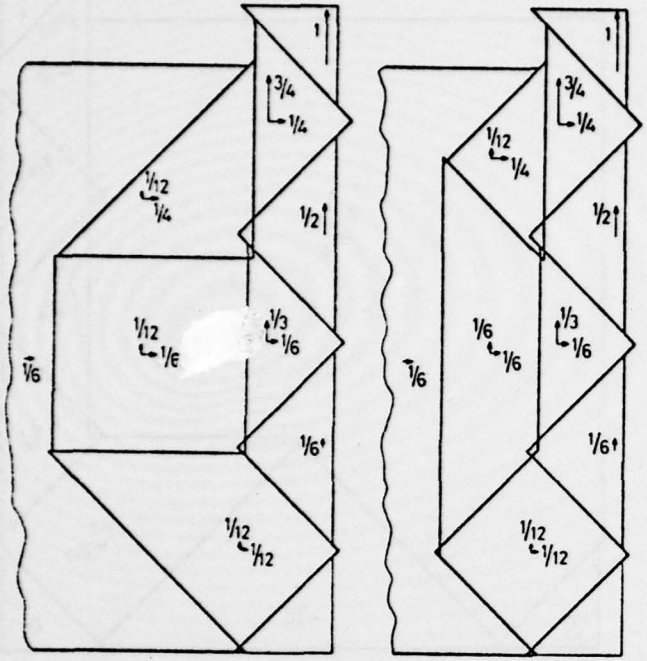
1
3/4
1/4
1/12
1/4
1/2
1/12
1/6
1/3
1/6
1/6
1/6
1/12
1/12
(g)
1
3/4
1/4
1/12
1/4
1/2
1/6
1/6
1/3
1/6
1/6
1/12
1/12
(f)

Fig. 31

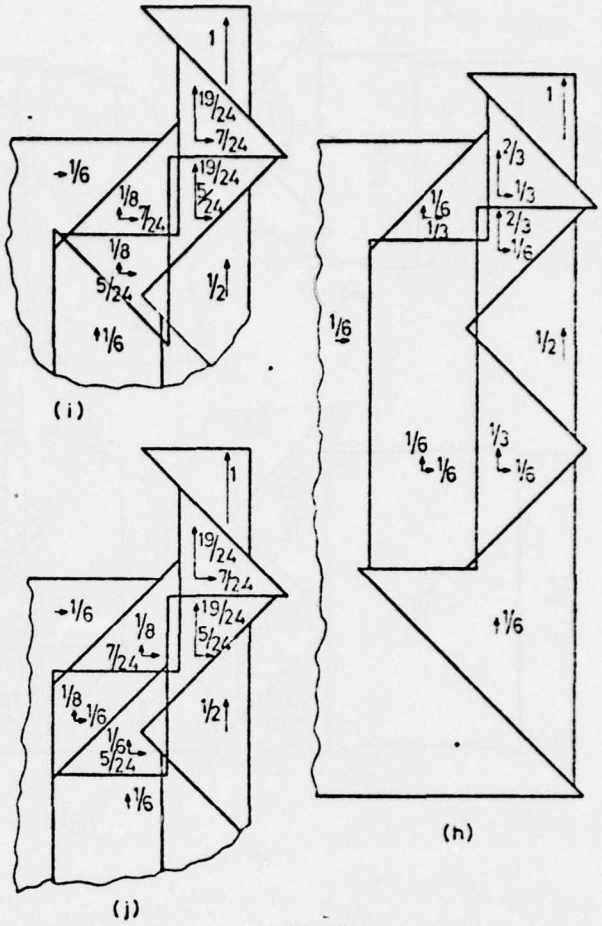
1
19/24
7/24
1/6
1/8
7/24
19/24
5/24
1/8
5/24
1/2
1/6
(i)
1
19/24
7/24
1/6
1/8
7/24
19/24
5/24
1/8
1/6
1/6
5/24
1/2
1/6
(j)
1
2/3
1/3
1/6
1/3
2/3
1/6
1/6
1/2
1/6
1/6
1/3
1/6
(h)

Fig. 31

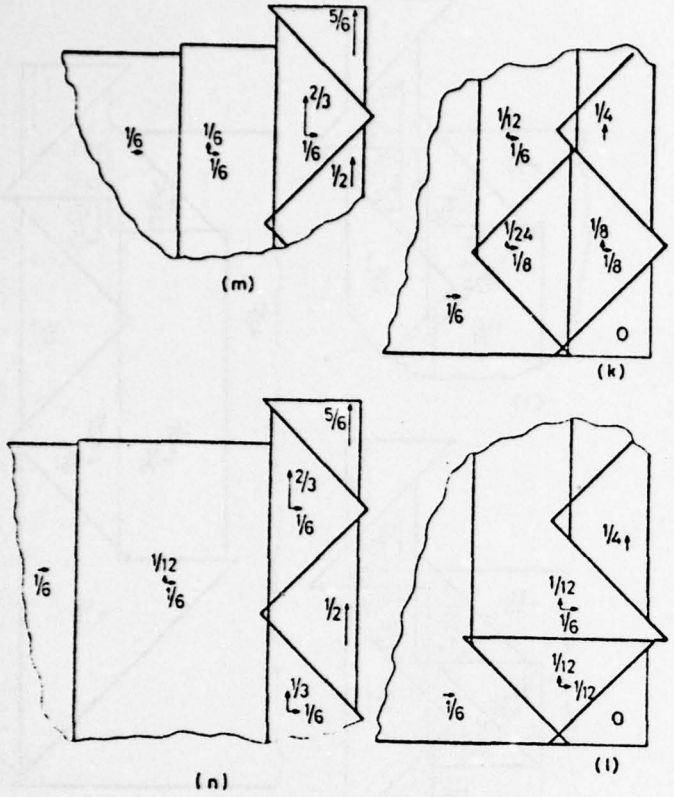
5/6
2/3
1/6
1/2
1/6
1/6
1/6
(m)
1/2
1/6
1/4
1/24
1/8
1/8
1/8
1/6
0
(k)
5/6
2/3
1/6
1/12
1/6
1/2
1/3
1/6
1/6
(n)
1/4
1/12
1/6
1/12
1/12
1/6
0
(l)

Fig. 31

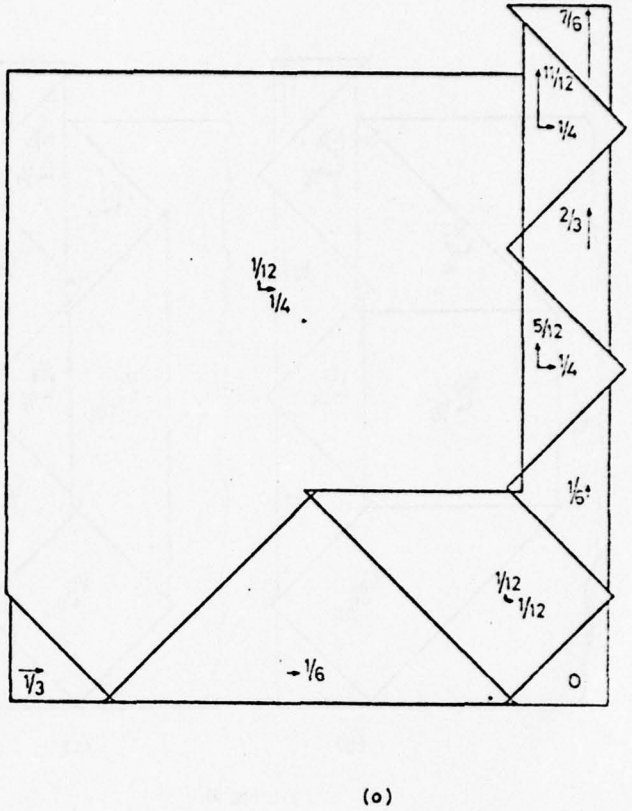
7/6
11/12
1/4
2/3
1/12
1/4
5/12
1/4
1/6
1/12
1/12
1/3
1/6
0
(o)

Fig. 31

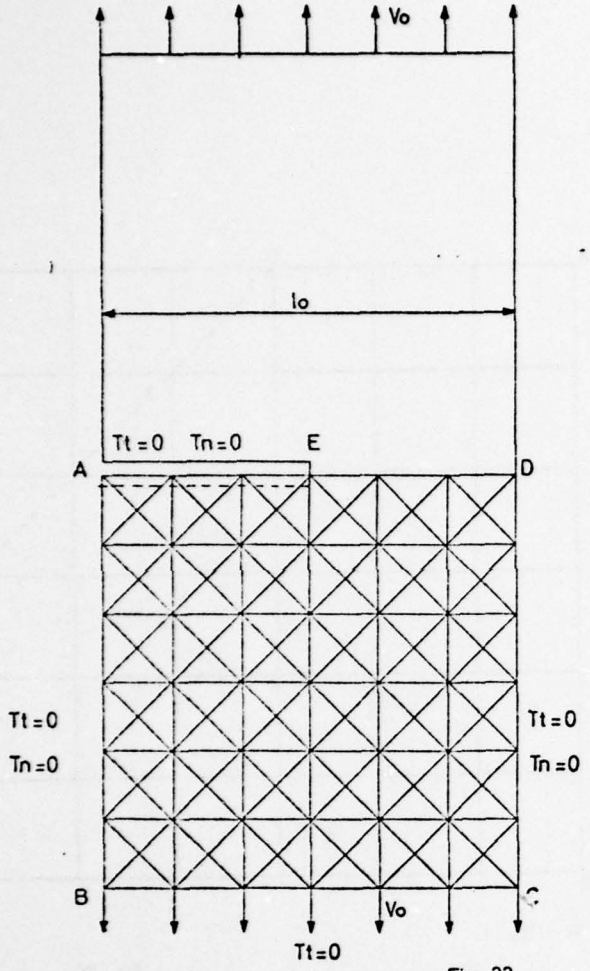

Fig. 32

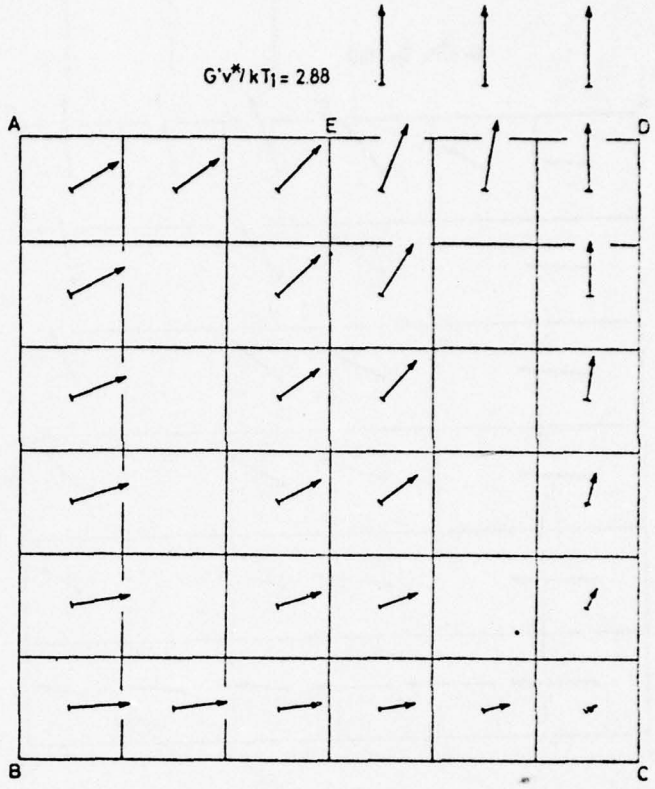

Fig. 33

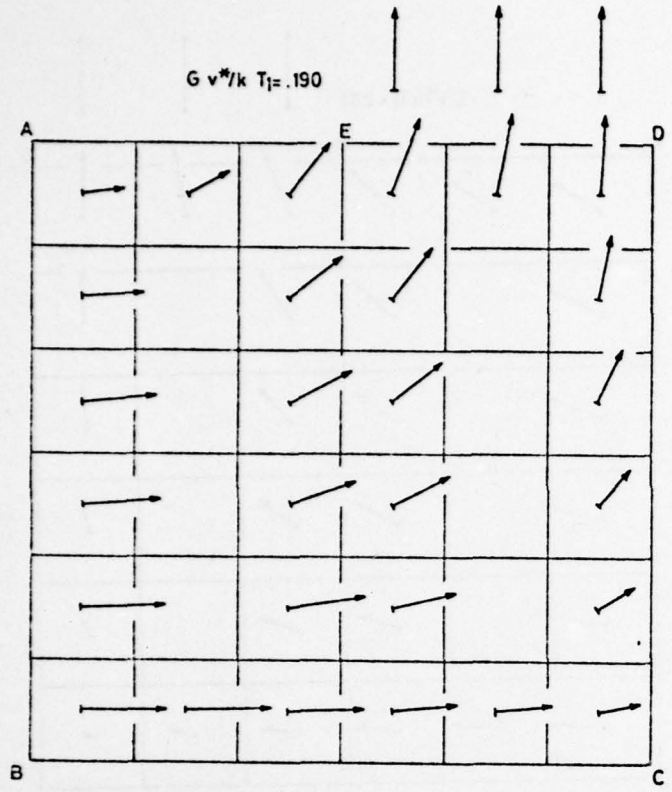

Fig. 34

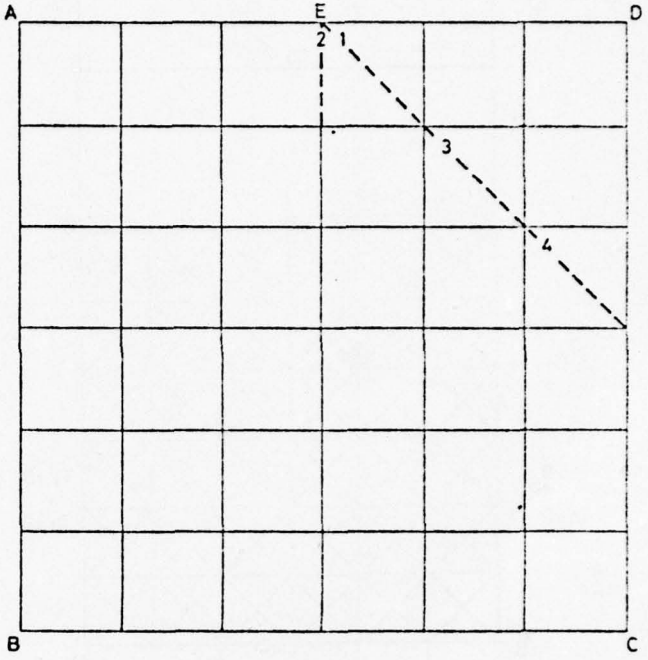

-- $\tau = -1$

Fig. 35

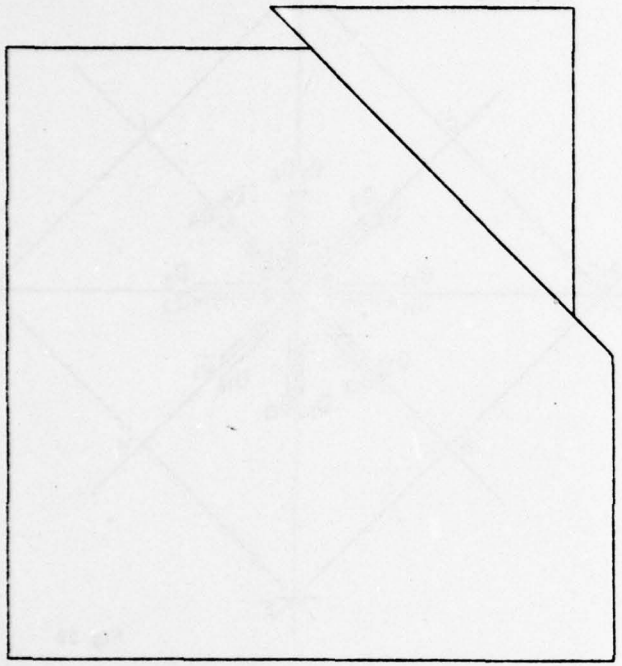

Fig. 37

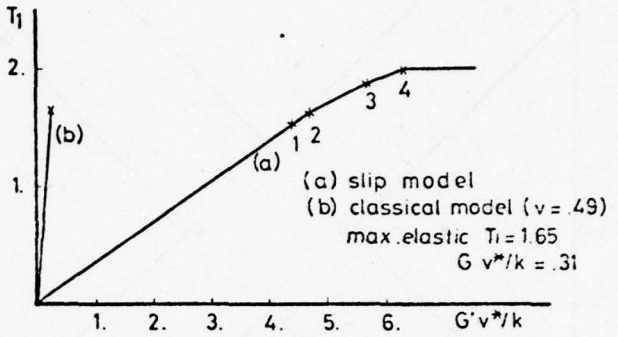
T1
2.
1.
(b)
(a)
1
2
3
4
(a) slip model
(b) classical model (v = .49)
max. elastic T1 = 1.65
G v*/k = .31
1. 2. 3. 4. 5. 6. G'v*/k

Fig. 36

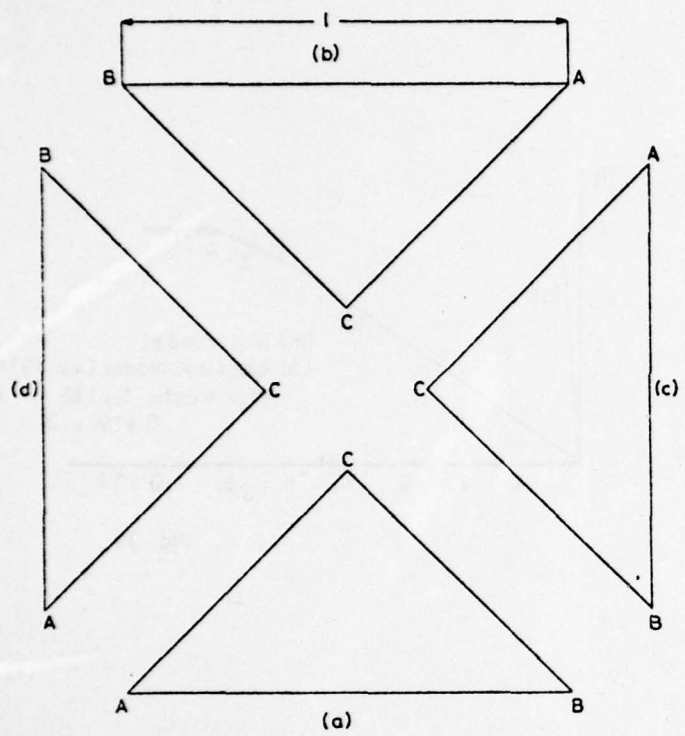
l
(b)
B
A
C
B
A
(d)
C
C
(c)
A
B
C
A
B
(a)

Fig. 38

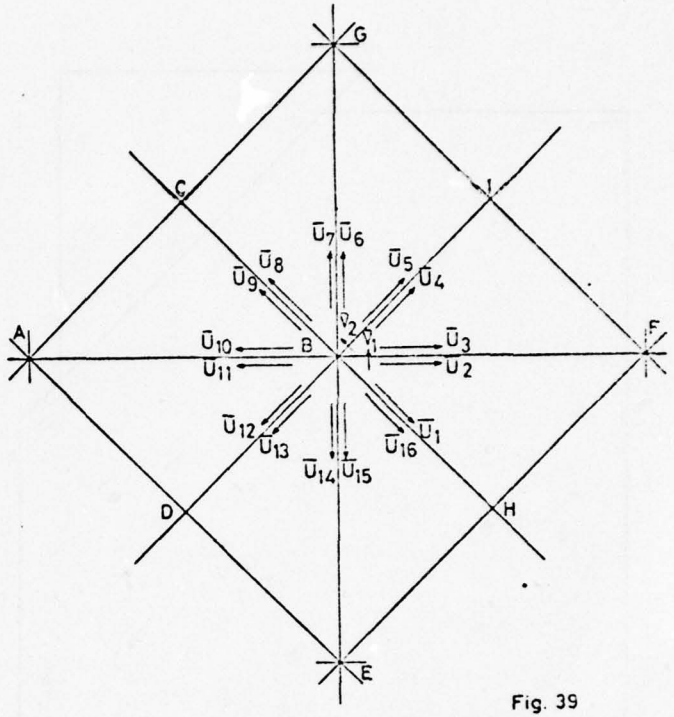
G
C
I
$\bar{U}_7$ $\bar{U}_6$
$\bar{U}_8$
$\bar{U}_9$
$\bar{U}_5$
$\bar{U}_4$
A
$\bar{U}_{10}$
B
$\bar{U}_{11}$
$\bar{U}_3$
$\bar{U}_2$
F
$\bar{U}_{12}$
$\bar{U}_{13}$
$\bar{U}_{14}$ $\bar{U}_{15}$
$\bar{U}_{16}$
$\bar{U}_1$
D
H
E

Fig. 39

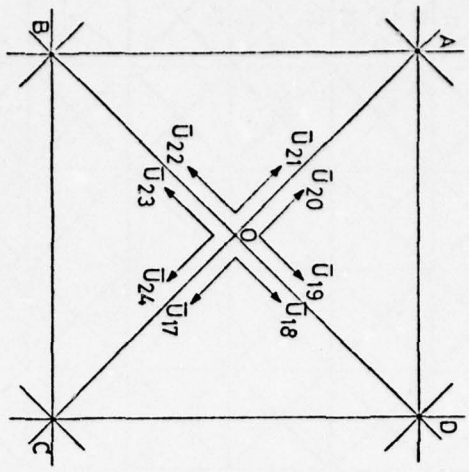
A
B
C
D
O
$\bar{U}_{17}$
$\bar{U}_{18}$
$\bar{U}_{19}$
$\bar{U}_{20}$
$\bar{U}_{21}$
$\bar{U}_{22}$
$\bar{U}_{23}$
$\bar{U}_{24}$

Fig. 40

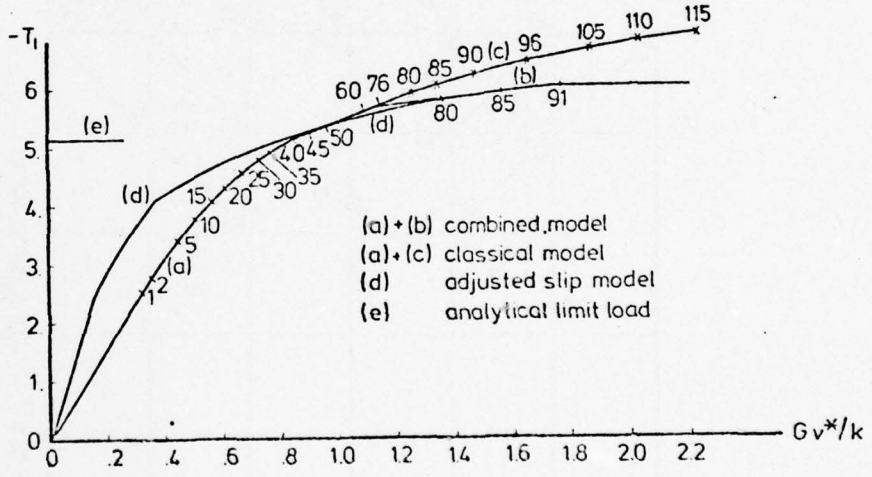
$-T_1$
Gv^*/k
(a) + (b) combined model
(a) + (c) classical model
(d) adjusted slip model
(e) analytical limit load

Fig. 41

AD-A058 086 MINNESOTA UNIV MINNEAPOLIS DEPT OF AEROSPACE ENGINE--ETC F/G 20/11
STRUCTURAL INELASTICITY XXI. FINITE ELEMENT MODELS WITH VELOCIT--ETC(U)
MAY 78 H M RIJ, P G HODGE N00014-75-C-0177
UNCLASSIFIED AEM-H1-21 NL

2 OF 2
ADA
058086

END
DATE FILMED
10 -78
DDC

END
DATE FILMED
10 -78
DDC

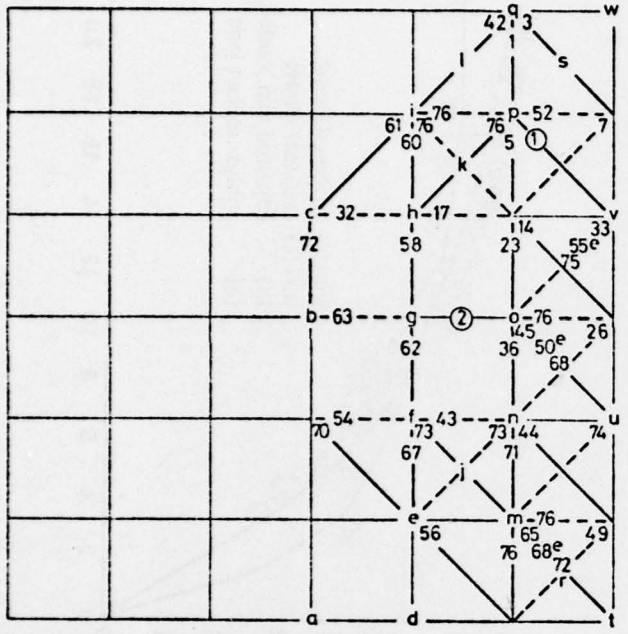

—— $\tau = 1$ ① 6, 15e, 20, 44e, 76

---- $\tau = -1$ ② 46, 63e, 66, 69e

Fig. 42a

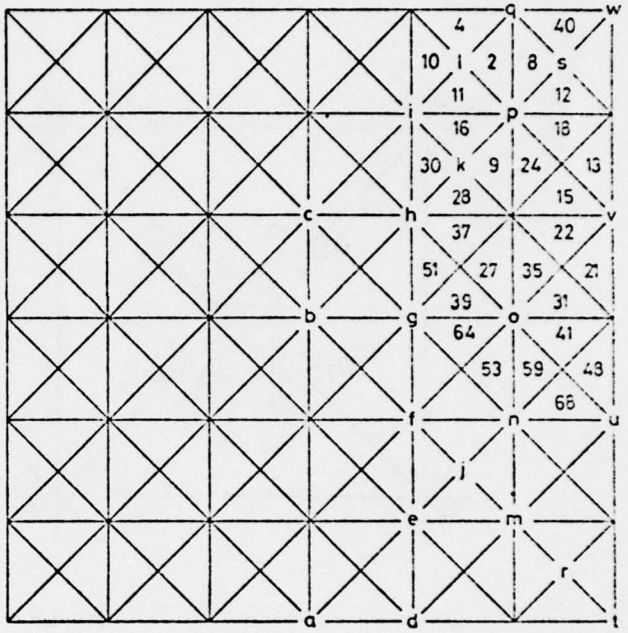

Fig. 42b

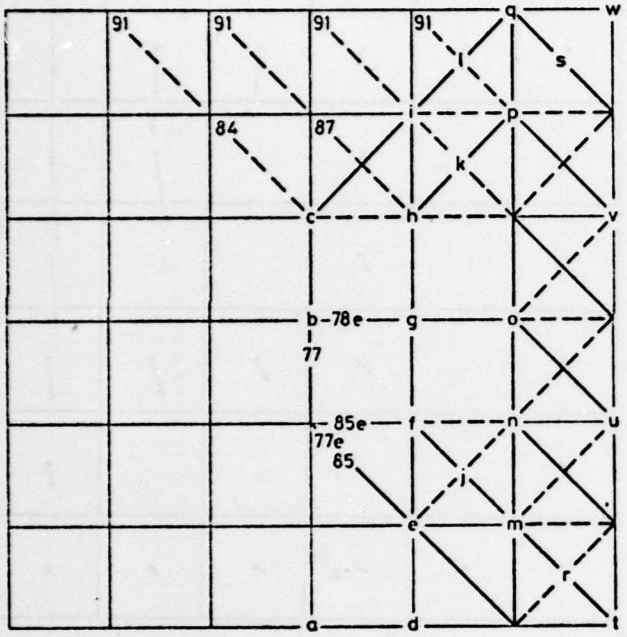

—— $\tau = 1$

---- $\tau = -1$

Fig. 43 a

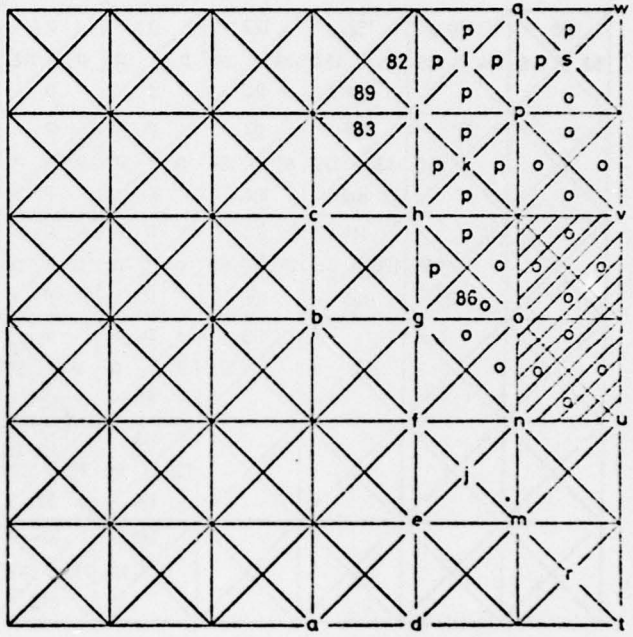

o elastic in 77

Fig. 43 b

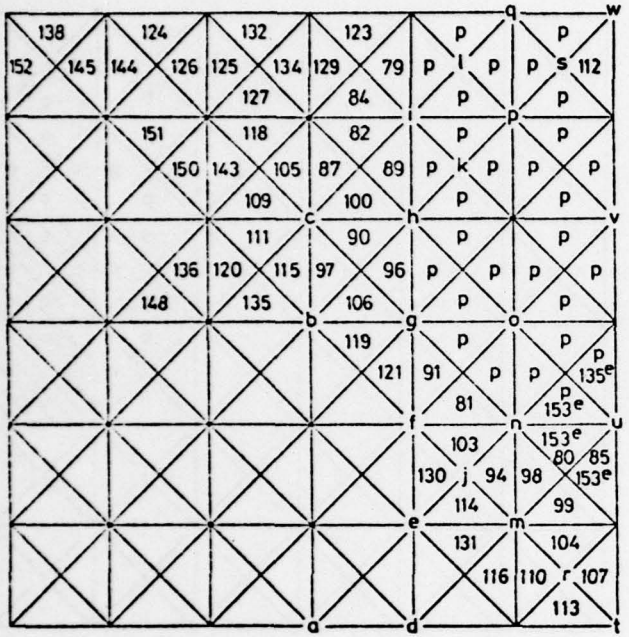
q
w
138
124
132
123
p
p
152
145
144
126
125
134
129
79
p
l
p
p
s
112
127
84
p
p
p
151
118
82
p
p
150
143
105
87
89
p
k
p
p
p
109
100
p
p
c
h
v
111
90
p
p
136
120
115
97
96
p
p
p
p
148
135
106
p
p
b
g
o
119
p
p
p
121
91
p
p
135e
p
81
153e
f
n
u
153e
103
80
85
130
j
94
98
153e
114
99
e
m
131
104
116
110
r
107
113
a
d
t

Fig. 44

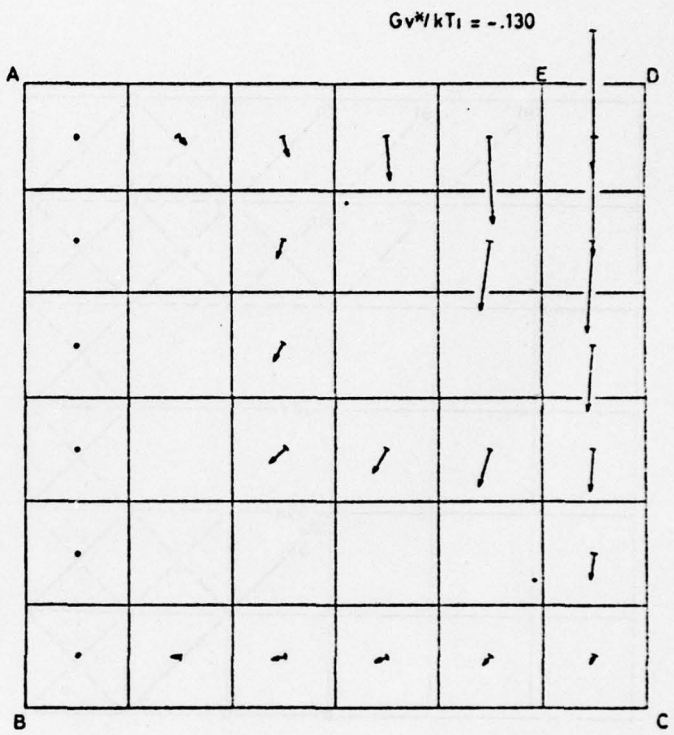
Gv*/kT1 = -.130
A
E
D
B
C

Fig. 45

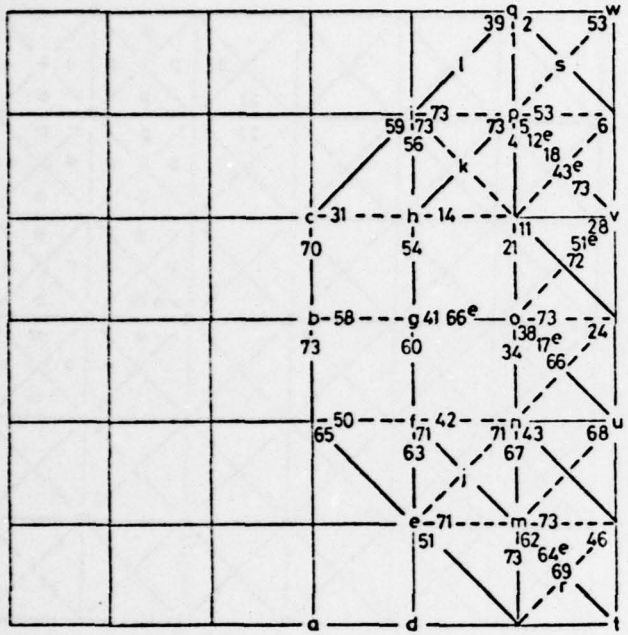

—— $\tau = 1$

---- $\tau = -1$

Fig. 46 a

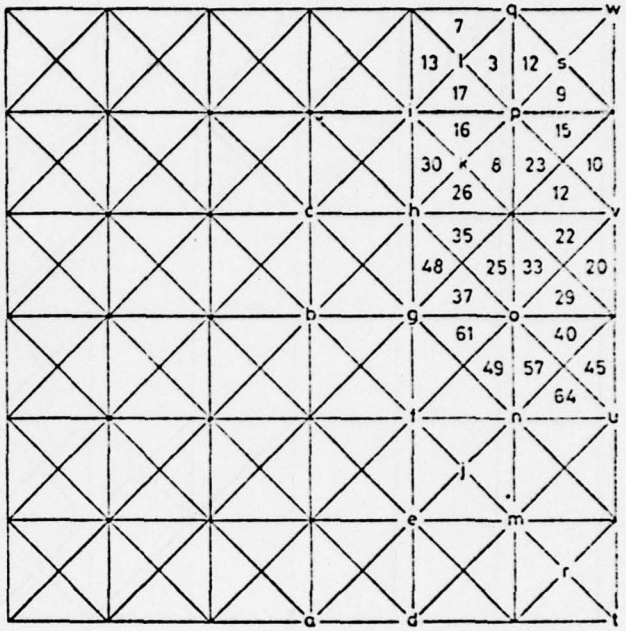

Fig. 46 b

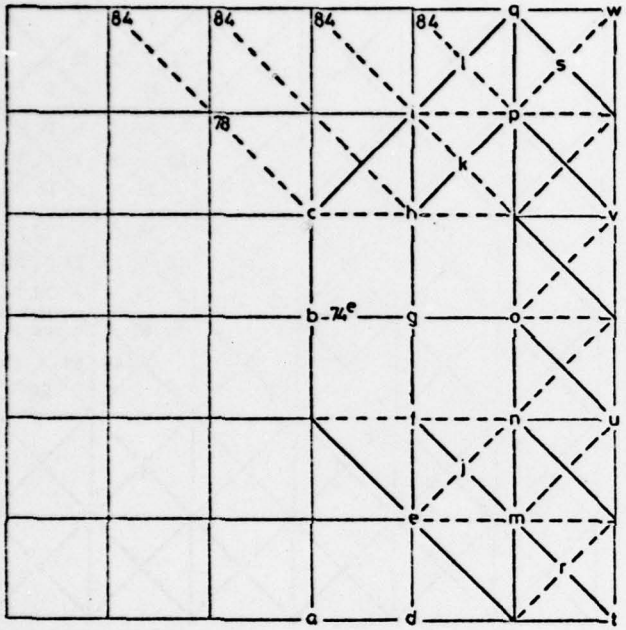

—— $\tau=1$

- - - - $\tau=-1$

Fig. 47a

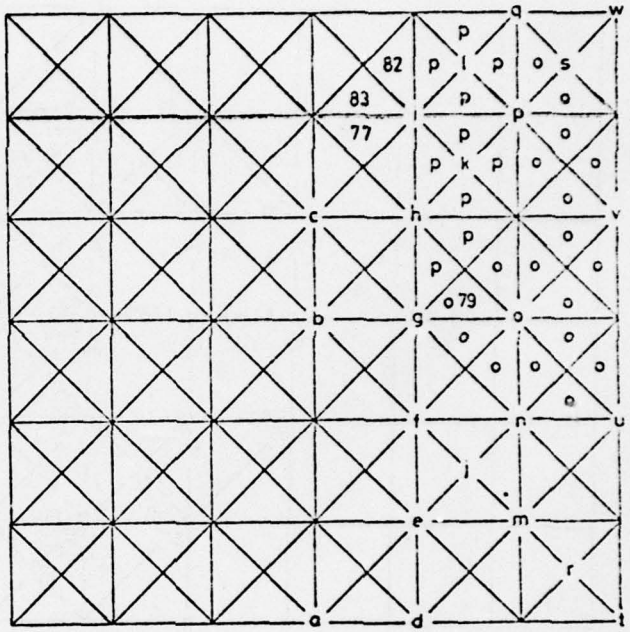

o elastic in 74

Fig. 47 b

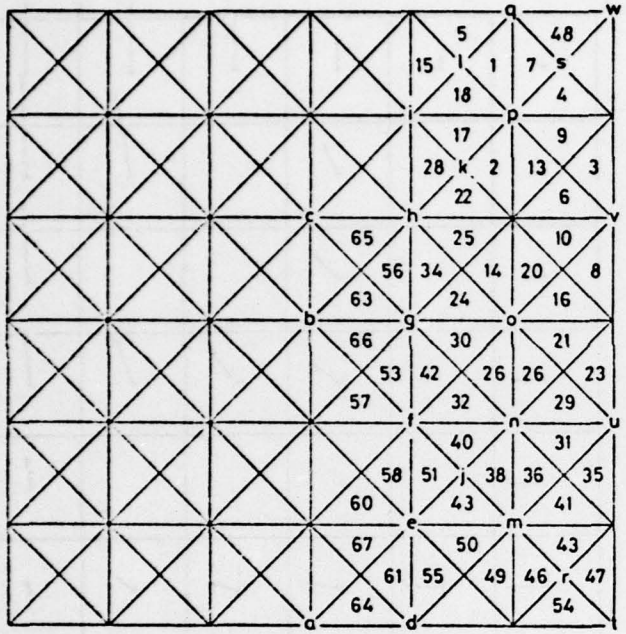
q
w
5
48
15
l
1
7
s
18
4
i
p
17
9
28
k
2
13
3
22
6
c
h
v
65
25
10
56
34
14
20
8
63
24
16
b
g
o
66
30
21
53
42
26
26
23
57
32
29
f
n
u
40
31
58
51
j
38
36
35
60
43
41
e
m
67
50
43
61
55
49
46
r
47
64
54
a
d

Fig.50

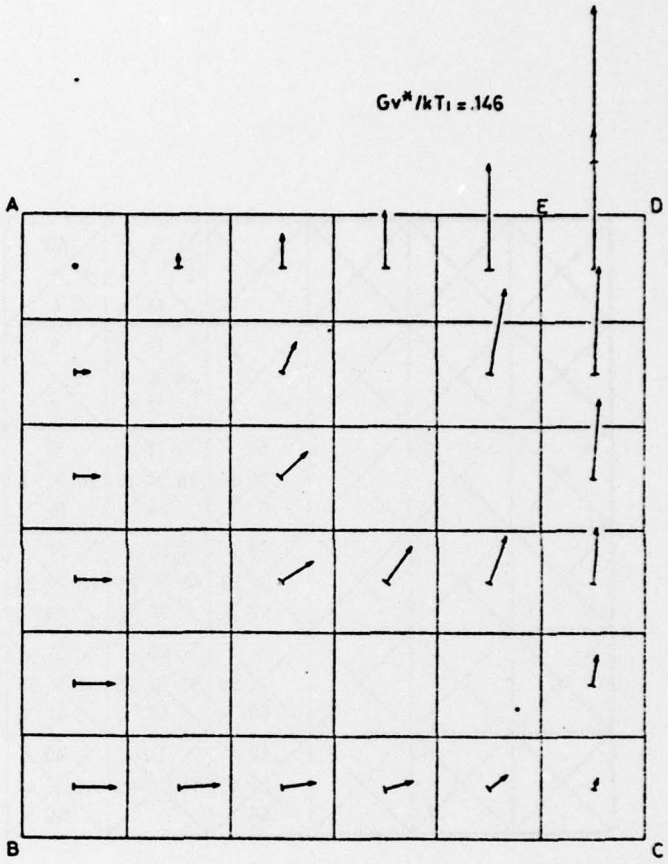
Gv*/kT1 = .146
A
E
D
B
C

Fig.51

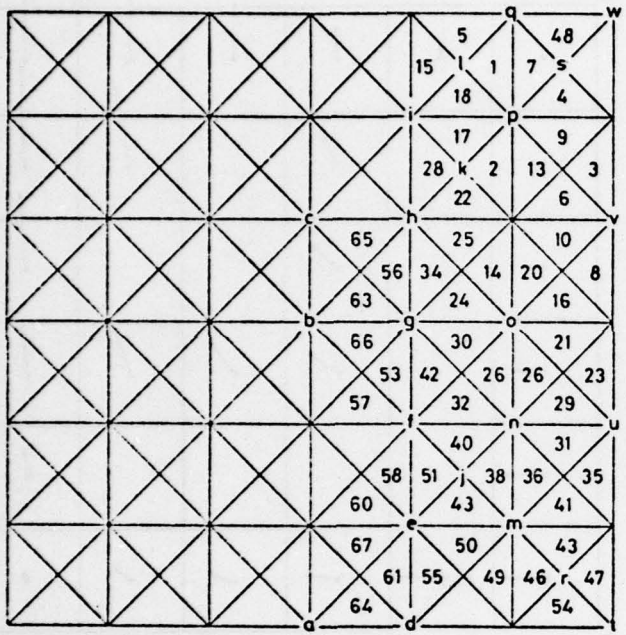
a
w
5
48
15
l
1
7
s
18
4
i
p
17
9
28
k
2
13
3
22
6
c
h
v
65
25
10
56
34
14
20
8
63
24
16
b
g
o
66
30
21
53
42
26
26
23
57
32
29
f
n
u
40
31
58
51
j
38
36
35
60
43
41
e
m
67
50
43
61
55
49
46
r
47
64
54
d

Fig.50

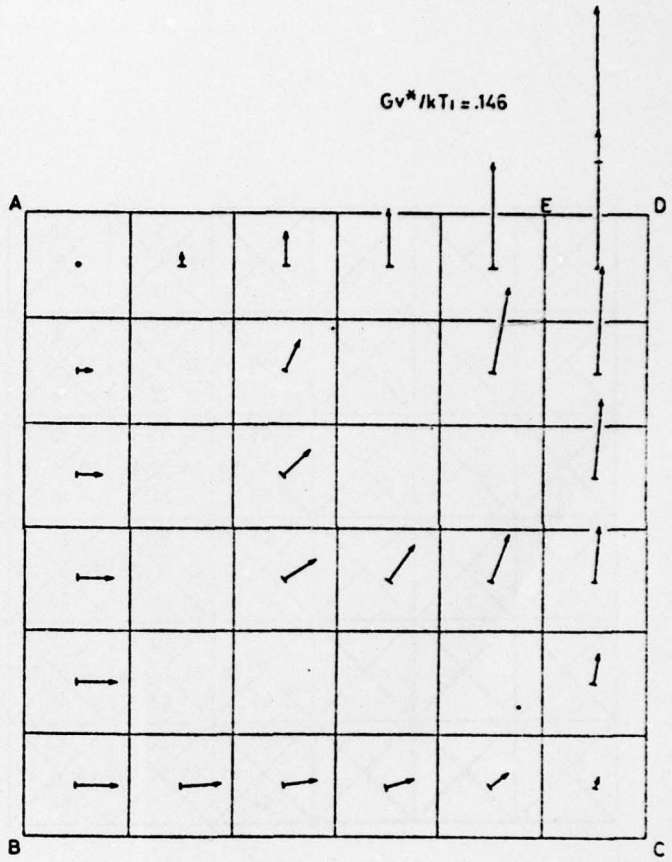
Gv*/kT1 = .146
A
E
D
B
C

Fig.51

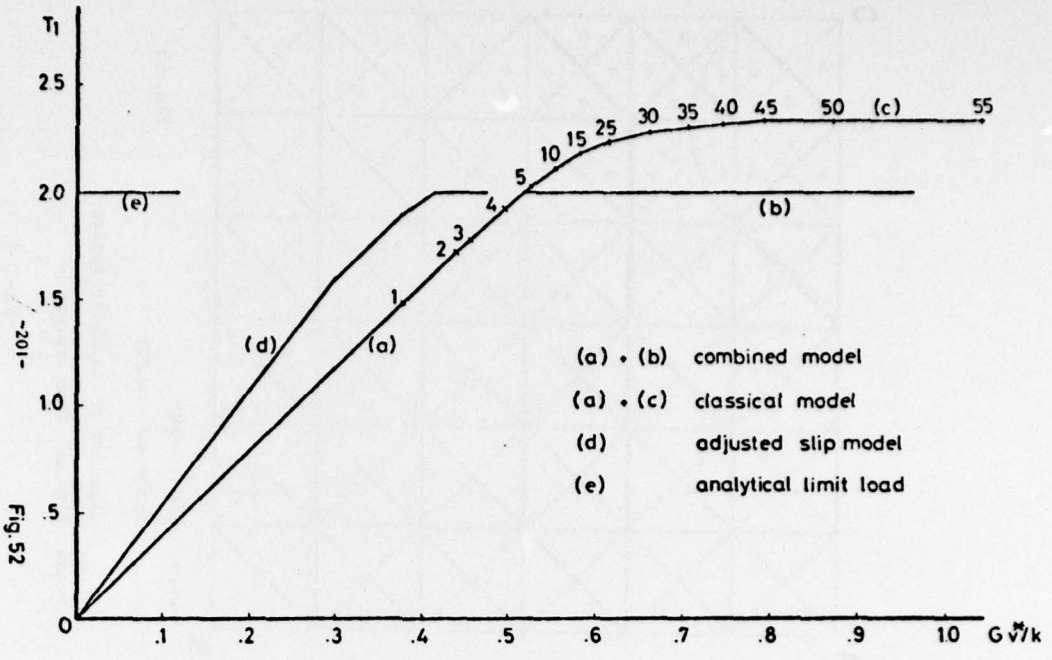
T1
2.5
2.0
1.5
1.0
.5
0
.1
.2
.3
.4
.5
.6
.7
.8
.9
1.0
G√7/k
(a) • (b) combined model
(a) • (c) classical model
(d) adjusted slip model
(e) analytical limit load

Fig. 52

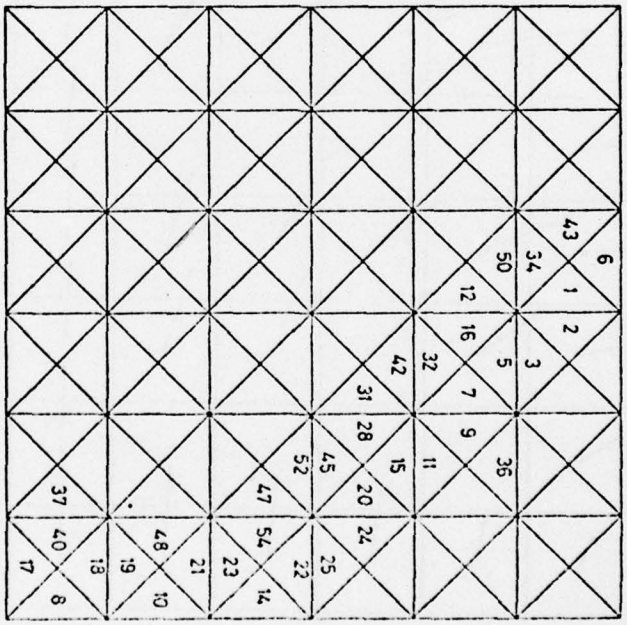

Fig. 53

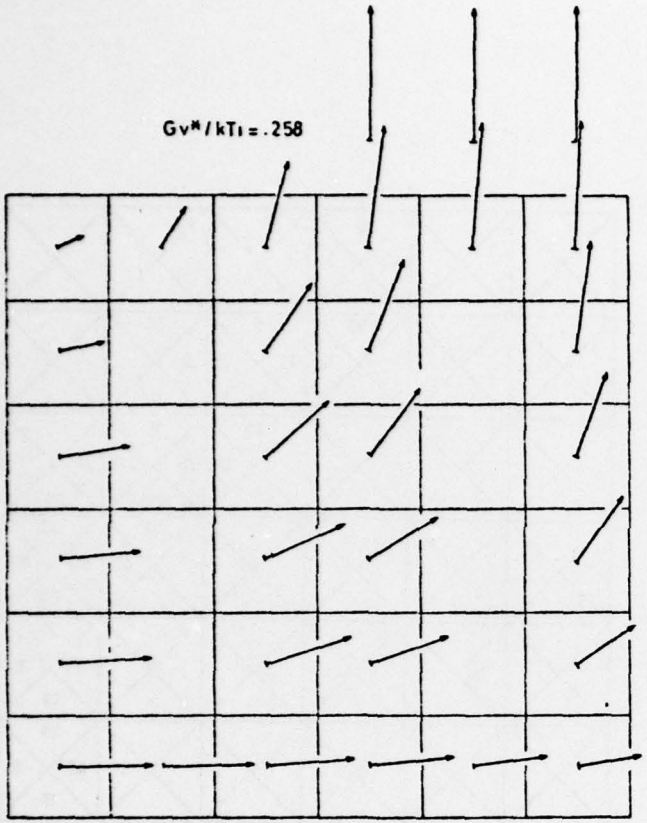
$Gv^{M}/kT_1 = .258$

Fig.54

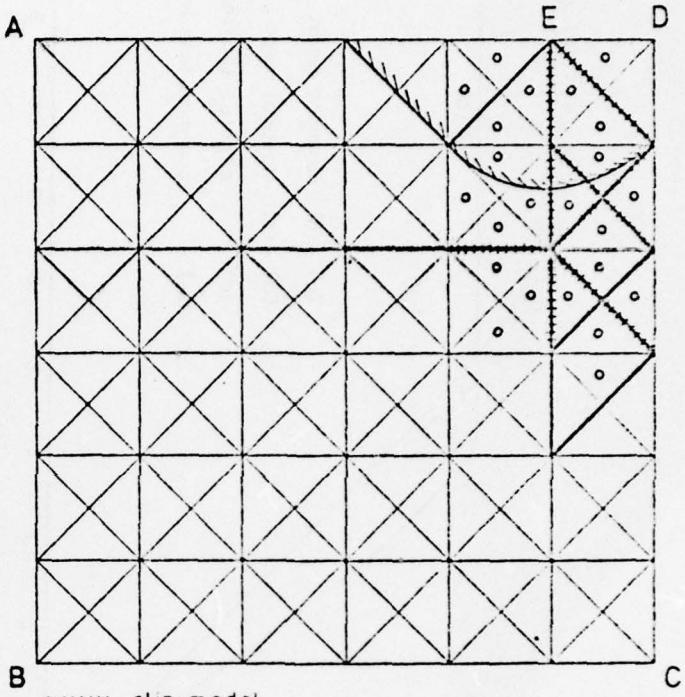
A
E
D
B
C
slip model
combined model
o classical or combined model
Prandtl flow region

Fig 55

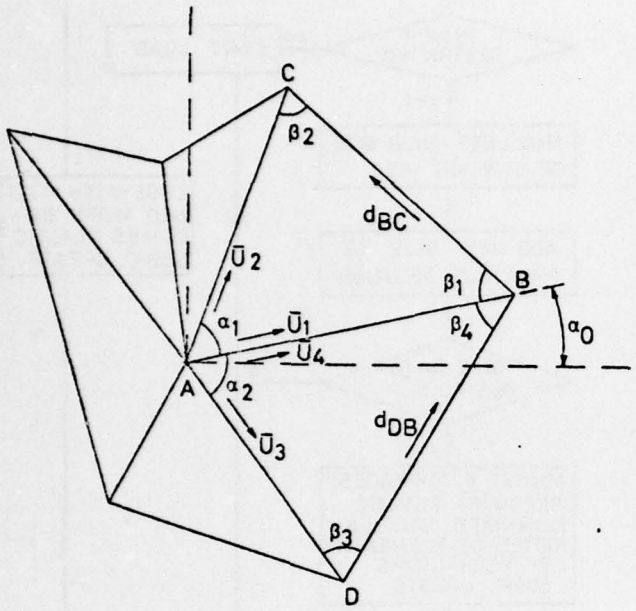

Fig. 56

PROG.: MINDC

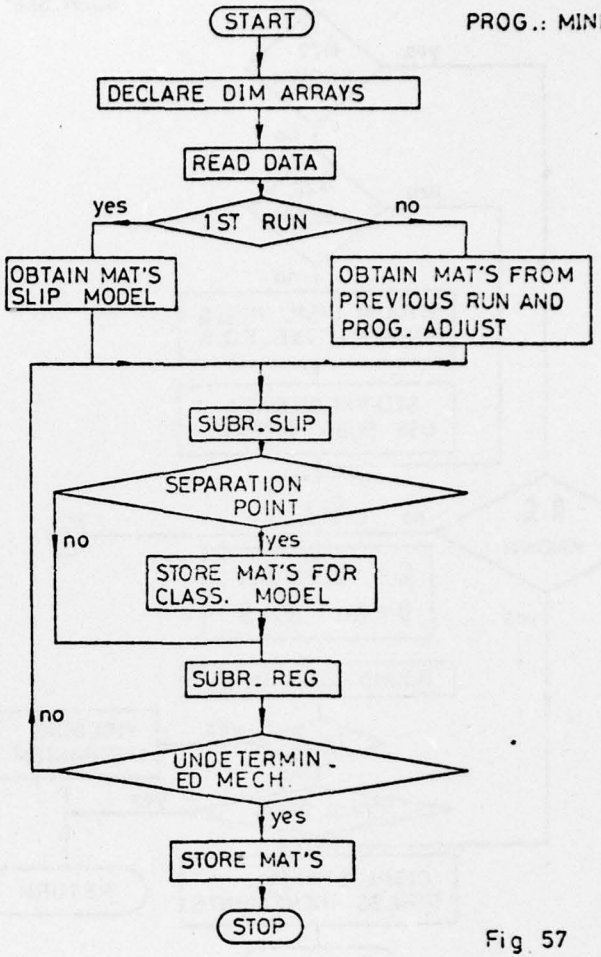

Fig. 57

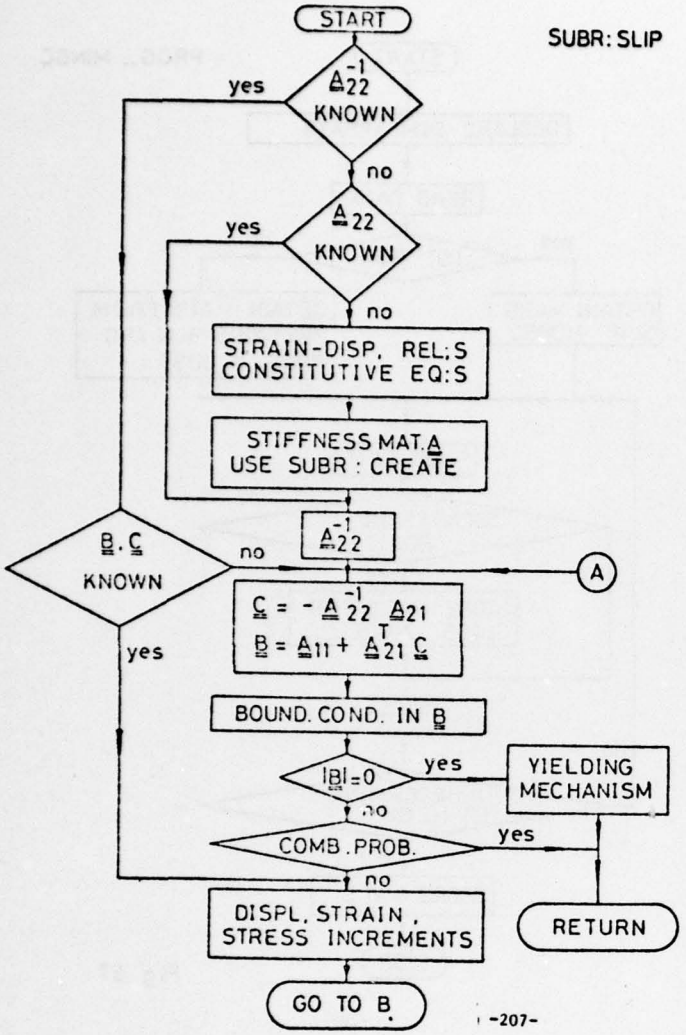

-207-

Fig. 58

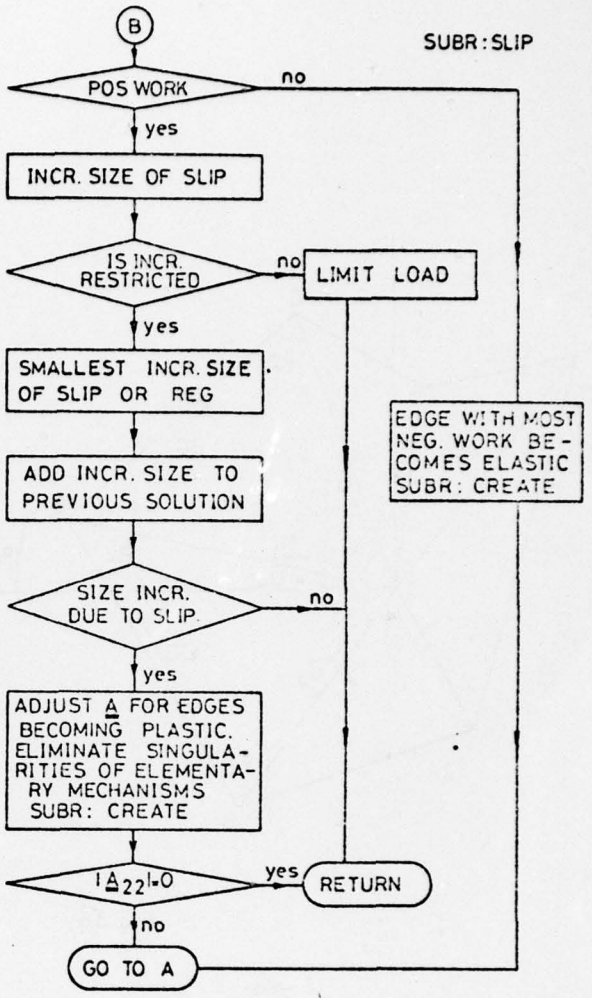

-208-

Fig. 58

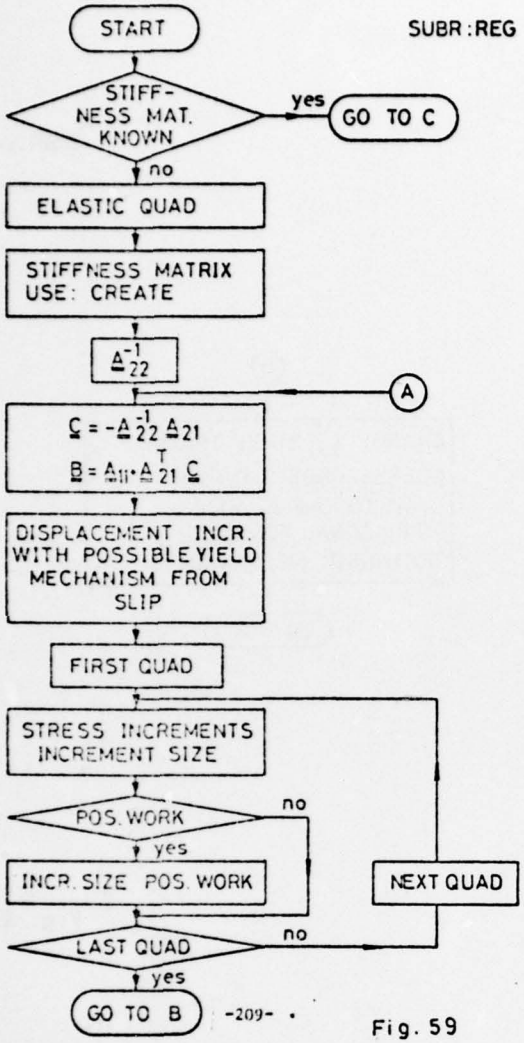

-209-

Fig. 59

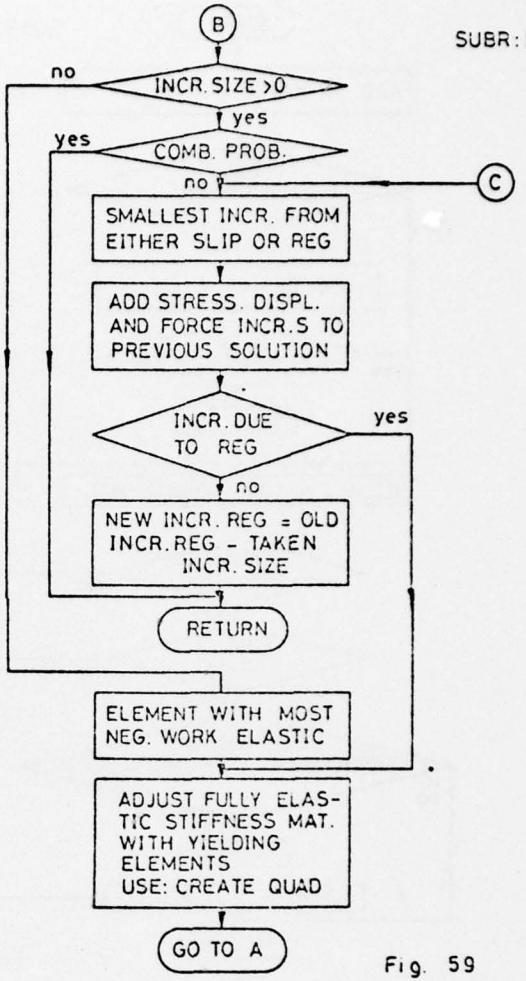

Fig. 59

-210-

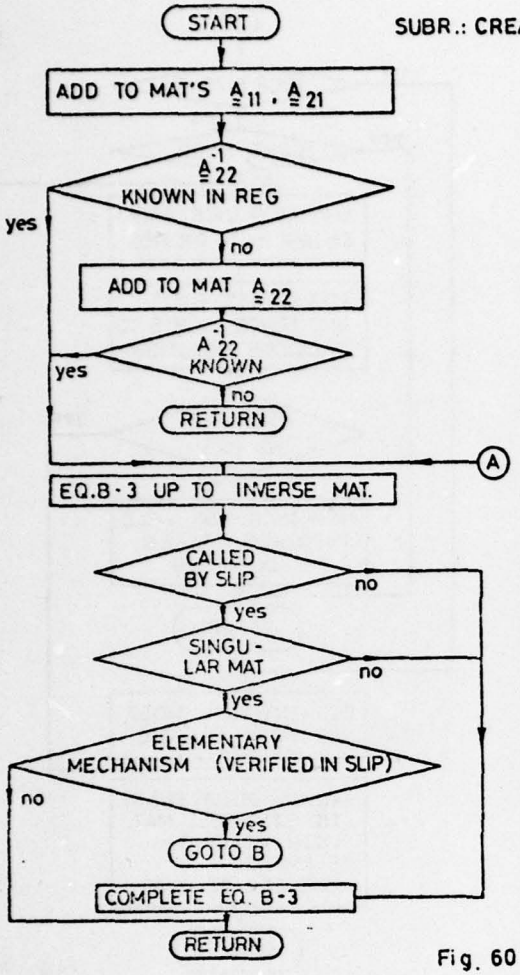
START
SUBR.: CREATE
ADD TO MAT'S $\underline{\underline{A}}_{11}$, $\underline{\underline{A}}_{21}$
$\underline{\underline{A}}^{-1}_{22}$ KNOWN IN REG
yes
no
ADD TO MAT $\underline{\underline{A}}_{22}$
A^{-1}_{22} KNOWN
yes
no
RETURN
A
EQ.B-3 UP TO INVERSE MAT.
CALLED BY SLIP
no
yes
SINGU-LAR MAT
no
yes
ELEMENTARY MECHANISM (VERIFIED IN SLIP)
no
yes
GOTO B
COMPLETE EQ. B-3
RETURN

Fig. 60

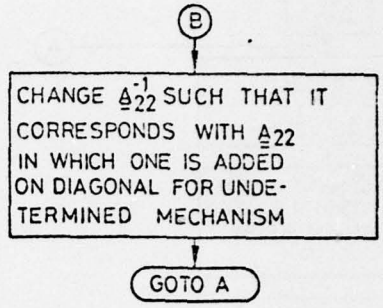
B
CHANGE $\underline{\underline{A}}^{-1}_{22}$ SUCH THAT IT CORRESPONDS WITH $\underline{\underline{A}}_{22}$ IN WHICH ONE IS ADDED ON DIAGONAL FOR UNDE-TERMINED MECHANISM
GOTO A

Fig. 60

PROG.: ADJUST

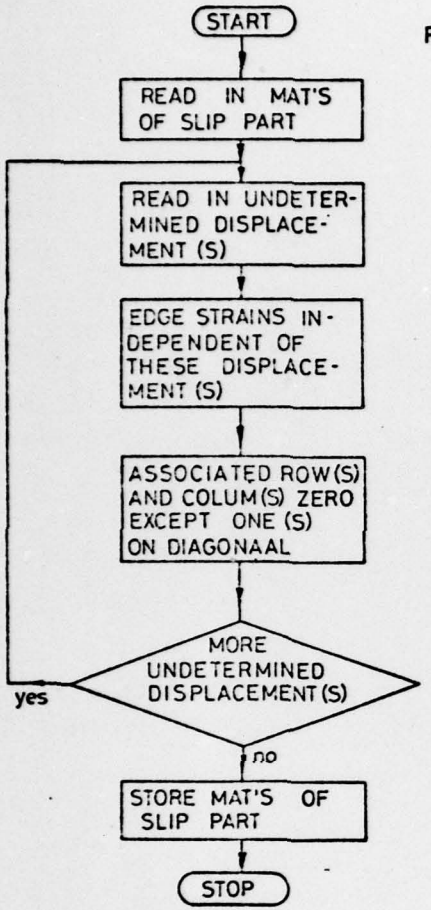

Fig. 61

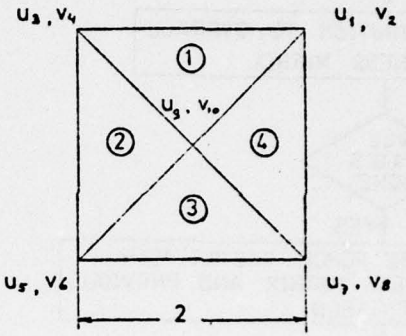

Fig. 62

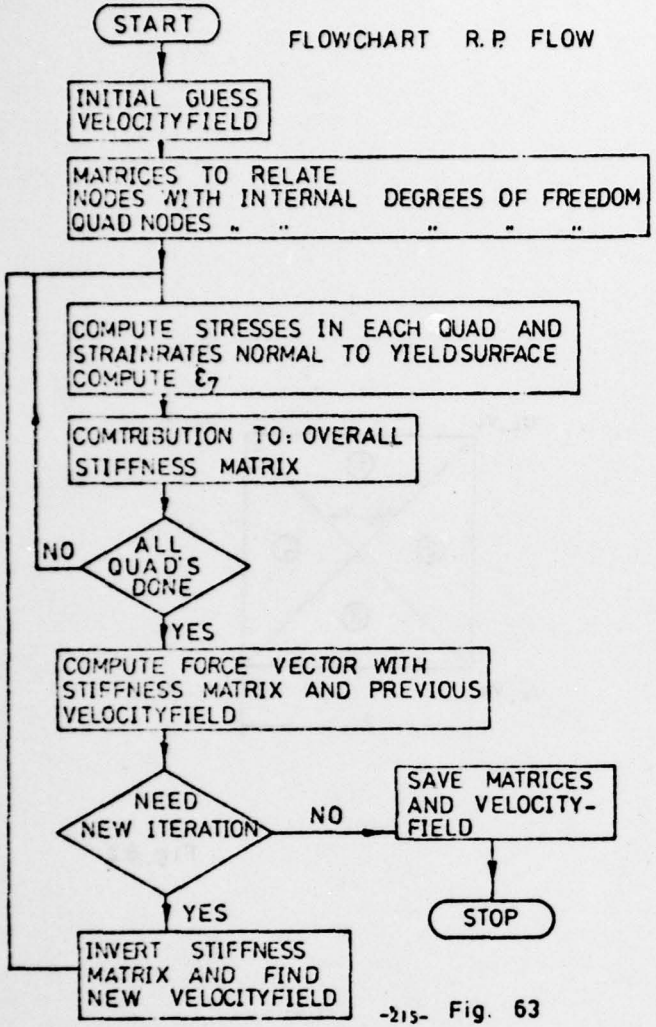
START
FLOWCHART R.P. FLOW
INITIAL GUESS VELOCITYFIELD
MATRICES TO RELATE NODES WITH INTERNAL DEGREES OF FREEDOM QUAD NODES " " " " "
COMPUTE STRESSES IN EACH QUAD AND STRAINRATES NORMAL TO YIELDSURFACE COMPUTE $\dot{\varepsilon}_7$
COMTRIBUTION TO: OVERALL STIFFNESS MATRIX
NO
ALL QUAD'S DONE
YES
COMPUTE FORCE VECTOR WITH STIFFNESS MATRIX AND PREVIOUS VELOCITYFIELD
NEED NEW ITERATION
NO
SAVE MATRICES AND VELOCITY-FIELD
STOP
YES
INVERT STIFFNESS MATRIX AND FIND NEW VELOCITYFIELD

 Fig. 63